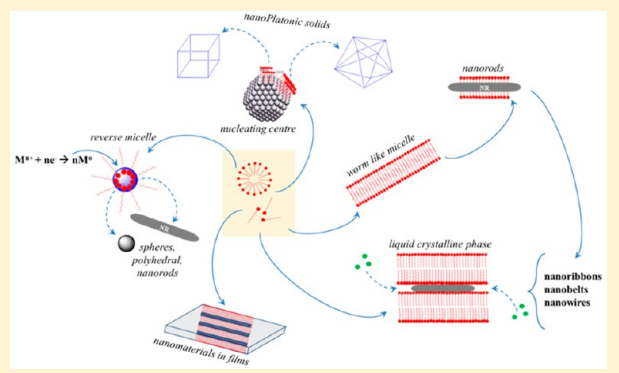


How Surfactants Control Crystal Growth of Nanomaterials

Mandeep Singh Bakshi*

Department of Chemistry and Biochemistry, Wilfrid Laurier University, Science Building, 75 University Avenue West, Waterloo, Ontario N2L 3C5, Canada

ABSTRACT: Exciting characteristic features of nanomaterials in contrast to their bulk phase require shape control of morphologies at the nanometer scale. Surfactants, a unique class of surface active molecules, possess remarkable ability to control crystal growth and direct it in shape and size controlled manner. The fine-tuning of the desired morphologies can be achieved by controlling the surfactant architecture as well as its self-assembly behavior. This review highlights the correlation between the surfactant properties and their ability in designing nanomorphologies. In terms of future perspectives, the methodologies can also be implemented to design biologically sustainable nanomaterials for their possible use in nanomedicine.



1. INTRODUCTION

Since the advancement in nanotechnology, the nanometallic surface with clear atomic packing in different crystal lattice planes has become tremendously important in terms of surface adsorption,^{1–3} surface passivation,^{4–7} shape control effects,^{8–13} and, most importantly, photophysical properties arising from the surface plasmon effects of noble metal nanomaterials.^{14–17} All these properties are dramatically affected in the event of surfactant adsorption. Apart from the micelle forming conventional surfactants, surface active polymers, proteins, and carbohydrates can also influence these properties. However, the effect is more clear and pronounced in the case of surfactants only. Therefore, this review mainly focuses on the shape control effects of surfactants. Nanotechnology requires the synthesis of desired shape and size of the nanomaterials for their appropriate applications. Surfactants have proven to be the best shape directing agents in the synthesis of nanomaterials, which is primarily related to the surface adsorption of surface active molecules on different crystal planes of nucleating centers, thus controlling their overall shape. Different kinds of surfactants have been used for shape controlled synthesis of nanomaterials, while ionic surfactants demonstrate clear shape directing effects.

A typical synthesis of gold nanoparticles (Au NPs) requires a reducing agent to convert Au(III) into Au(0) in order to initiate nucleation. As soon as Au⁰ atoms are produced in the aqueous solution, they generate tiny nucleating centers made up of gold clusters. A stabilizing agent is required at this point to provide colloidal stability and to achieve controlled nucleation. Usually, NaBH₄ is used as a strong reducing agent to convert Au(III) into Au(0) while sodium citrate (NaCit) provides the colloidal stability. But the shape directing effects of NaCit are not that prominent, and hence, it is difficult to obtain well-defined shapes simply by using NaCit.^{18,19} Thus, a surfactant is required for effective shape control to achieve a desired morphology. In an aqueous solution, the surface adsorption of surfactant molecules

takes place through bilayer formation^{20–22} because it is the headgroup of the surfactant molecule that adsorbs on the charged NP surface leaving the hydrocarbon tail insolubilized in the aqueous phase. Another surfactant layer adsorbs on the first one to create the bilayer. The bilayer coating, especially in the case of ionic surfactants, can be quantitatively compared with a concentric diameter comprising double the length of hydrocarbon tail including the surface area of the head groups. This kind of adsorption is usually selective on a specific crystal plane because nucleating centers are mainly tiny polyhedral morphologies, and consequently, such an adsorption leads to an ordered shape evolution.

2. NANORODS, NANORIBBONS, AND NANOBELTS

Preferential adsorption^{23–27} of ionic surfactants usually on the {100} rather than {111} crystal planes allows an ordered anisotropic growth to produce nanorods (NRs) and nanowires, while nanowires or nanoribbons of high aspect ratios require liquid crystalline phase as templates in the bulk.^{28–31} The liquid crystalline phase with marked channels acts as a soft template to allow uniform growth of nanowires or nanoribbons of high aspect ratios, which is usually not that simple to achieve otherwise due to uncontrolled Ostwald ripening effects.^{32–35}

Several solution properties such as density, viscosity, and ionic strength affect the ordered crystal growth in solution. Low density and viscosity are the most preferred bulk environments to allow the growth of colloidal nanoparticles in an ordered fashion, which is sometime hindered by low diffusion under a concentration gradient in a highly viscous medium. Therefore, achieving a liquid crystalline phase at low surfactant concentration is always favorable to have uniform growth of nanowires and nanoribbons of high aspect ratios. Dimethylene bis-

Received: October 13, 2015

Published: December 18, 2015



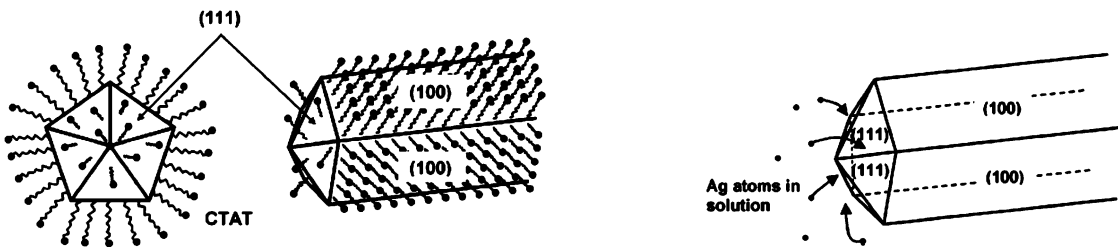


Figure 1. Preferential attachment of CTAT to the lateral (100) planes of the Ag nanorod. Growth of Ag nanorod from preferential transfer of Ag atoms to the end (111) facets. Reproduced from ref 37 with permission. Copyright 2005 American Chemical Society.

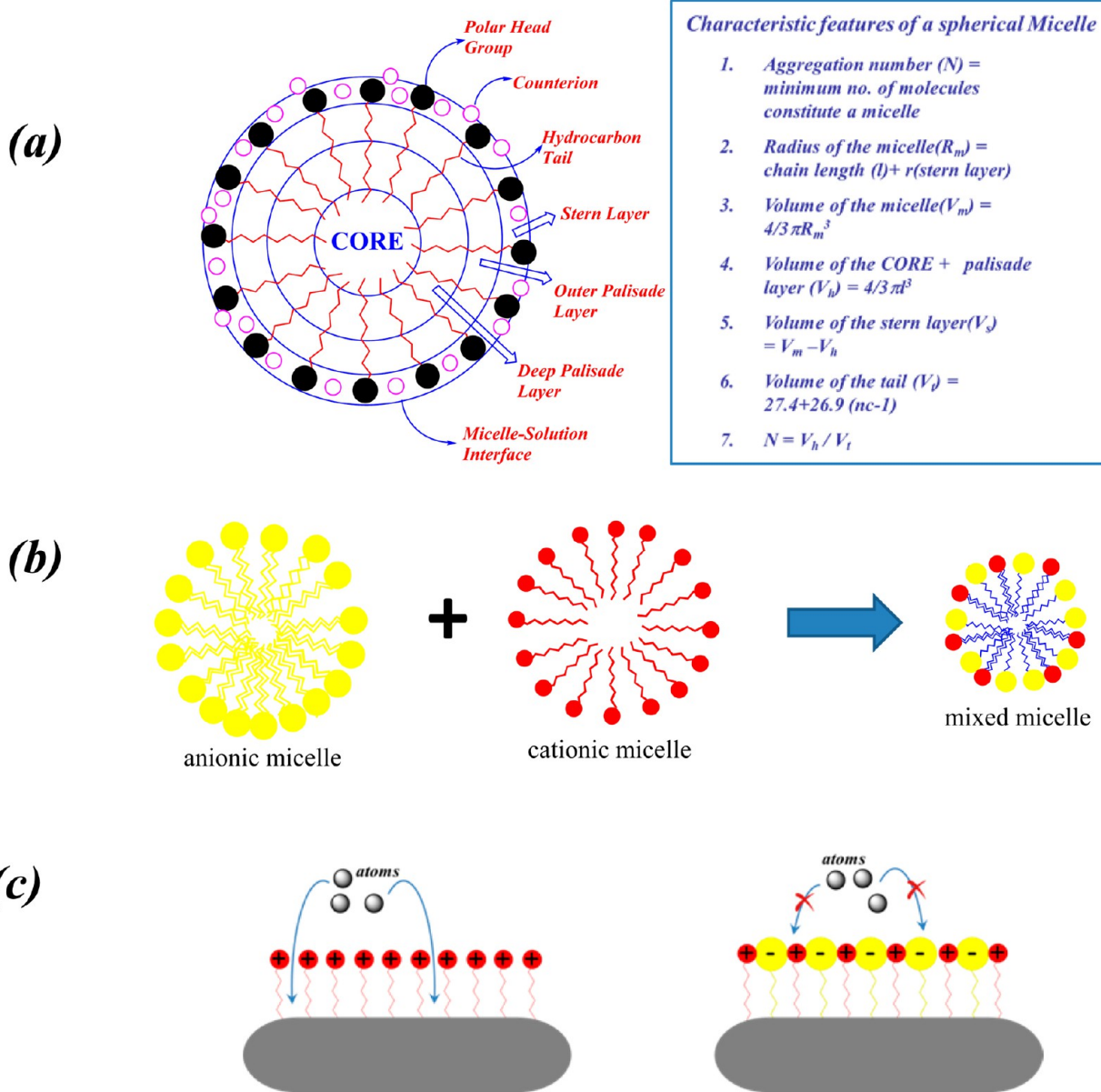


Figure 2. (a) Detailed structure of an ionic micelle and related parameters. (b) Mixed micelle formation from the micelles of oppositely charged individual surfactants. (c) Adsorbed surfactant layer of cationic monomers (left) and mixed oppositely charged monomers (right).

(tetradecyldimethylammonium bromide) (14-2-14) is considered to be the most suitable gemini surfactant to induce the liquid crystalline phase rather than its lower or higher homologues to produce Au nanoribbons.³¹ Higher homologues like dimethylene bis(hexadecyldimethylammonium bromide) (16-2-16) or dimethylene bis(octadecyldimethylammonium bromide) (18-2-

18) dramatically lack aqueous phase solubility and, hence, are not appropriate for the liquid crystalline phase in dilute surfactant solutions.

The liquid crystalline phase produces 1D morphologies of high aspect ratios when a multistep seed-growth method is adopted rather than a single growth process.^{31,36} In the multistep

method, the previous step NPs are used as seeds for the next growth process in a minimum possible time difference between the steps (usually ~ 1 min) in order to use the growing seed particles for a controlled nucleation. In this way, growing seed NPs always have a fresh liquid crystalline phase available for templating, thus generating nanowires of high aspect ratios. Silver nanorods can be very well synthesized by using cetyltrimethylammonium tosylate (CTAT), which is known to form long wormlike micelles in water even at low surfactant concentrations (Figure 1).³⁷ Formation of wormlike micelles is mainly driven by the stronger hydrophobicity as well as headgroup bulkiness of the surfactant molecules, which experience steric hindrance to accommodate spherical micelles and thus prefer to exist in the wormlike or cylindrical micelles rather than conventional spherical micelles. Such surfactant molecules demonstrate a greater affinity to adsorb on a specific crystal plane in the form of a compact monolayer most suitable for surface passivation. Increase in the CTAT concentration leads to an increase in the number of silver nanorods. Nanorod anisotropic growth is promoted by a selective adsorption process involving individual surfactant molecules. The increased formation of nanorods at increased surfactant concentration and the formation of larger aspect ratio nanowires at decreased seed concentration imply that more effective surfactant barrier on the (100) planes is established under these conditions largely due to increased availability of surfactant molecules when an equilibrium between the wormlike micelles and the true surfactant concentration in the solution is maintained. Preferential growth is explained in terms of the unique decahedral nanorod tip geometry, the defect energy that exists between five crystal twining units, and the formation of a CTAT surfactant barrier surrounding the nanorod side planes (Figure 1).

Apart from the wormlike micelles, mixed micelles and vesicles also promote the shape control effect. Mixed micelle and vesicle formation in aqueous phase is usually achieved when two surfactants of the same or different polarities are mixed. The mixed micelles thus produced are generally much smaller in size, compact, and more hydrophobic and have a greater aggregation number due to charge neutralization in the headgroup region (Stern layer) when opposite charged surfactants are mixed (Figure 2).^{38–42} High concentration of oppositely charged surfactants such as CTAB and sodium dodecyl sulfate (SDS) usually leads to the formation of vesicles though vesicles are produced from the shape transformation of the mixed micelles in the first place. The adsorbed layer formation by such oppositely charged surfactants is a highly compact layer due to the expulsion of hydrated water molecules from the Stern layer (headgroup region of the micelle) of the mixed micelles (Figure 2c). Hence, the surface adsorption of such a compact layer provides complete surface passivation leaving no possibility of any penetration by freshly produced atoms to initiate random nucleation. Therefore, a combination of oppositely charged surfactants proves to be the best combination for the shape control process.

Well-defined gold nanobelts are synthesized in this way by taking a mixture of strongly interacting CTAB and SDS surfactants at a low temperature of 4 °C (Figure 3).⁴³ The mixed cationic–anionic surfactants exert a subtle control on the growth of gold nanocrystals in solution due to the cooperative effect. They interact with inorganic nanocrystals in a synergistic way and adsorb on specific crystal surfaces in the form of a mixed surfactant film (Figure 2c).⁴⁴ The packing state of the interfacial mixed film is significantly affected by the temperature and mixing

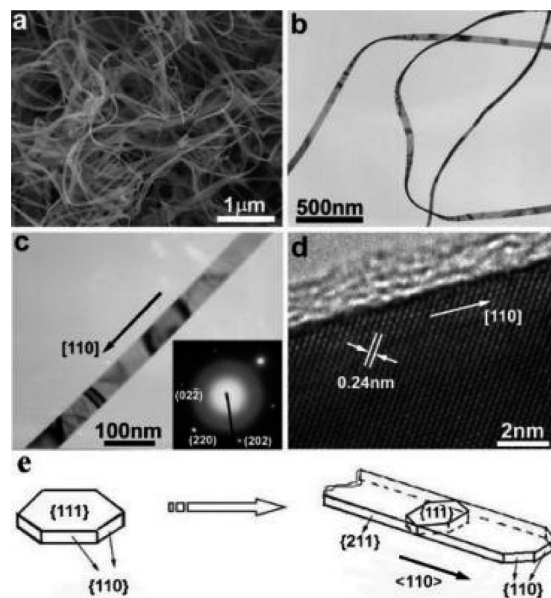


Figure 3. SEM (a), TEM (b,c), and HRTEM (d) images of gold nanobelts obtained at 4 °C. (e) Schematic illustration of the growth direction of gold nanobelts. Reproduced from ref 43 with permission. Copyright 2008 American Chemical Society.

ratio of the surfactants and, hence, largely influences the specific adsorption of the mixed surfactants on the growing nanocrystals.⁴⁵ Temperature decreases the aggregation state of mixed surfactants in solution^{46–49} and consequently affects the specific adsorption of the mixed surfactants on the surfaces of gold nanocrystals. The following discussion will focus on the effect of surfactant architecture on the crystal growth.

2.1. Effect of Surfactant Tail and Headgroup Modifications. Highly hydrophobic surfactants^{50–54} produce wormlike micelles, vesicles, and liquid crystalline phase. These micellar assemblies are suitable templates for the synthesis of long nanorods or wires. This can be evaluated by comparing the relative influence of hydrophobicity of different surfactants on the shape control effect of high aspect ratio nanorods.⁵⁵ For C10TAB with a hydrocarbon chain of C10 carbon atoms, 96% of the gold nanoparticles are spherical with aspect ratio = 1 and only 4% are short rods of aspect ratio = 2–3. For C12TAB, after separation from the spheres, 92% of the nanoparticles are low-aspect ratio nanorods. In the case of C14TAB, the aspect ratio of the resulting gold nanorods after separation from the spheres was 17, while for C16TAB, the aspect ratio is up to 20.⁵⁶ Thus, the length of the nanorods clearly depends on the surfactant alkyl chain length (Figure 4). A longer hydrocarbon chain in fact produces a more compact bilayer due to stronger hydrophobic interactions among the chains that leaves little possibility for the penetration of freshly produced gold atoms to nucleate laterally, and hence, only the ends of the nanorod are available for further crystal growth resulting in the formation of higher aspect ratio. Comparing these results with that of 14-2-14, where the liquid crystalline phase of 14-2-14 promotes the nanoribbon formation, CTAB (C16TAB) is not expected to form the liquid crystalline phase in the dilute concentration range. Therefore, both surfactants promote morphologies with high aspect ratios due to their strong hydrophobic nature; however, the liquid crystalline phase of 14-2-14 facilitates nanoribbons in comparison to nanorods of high aspect ratios in the presence of CTAB.

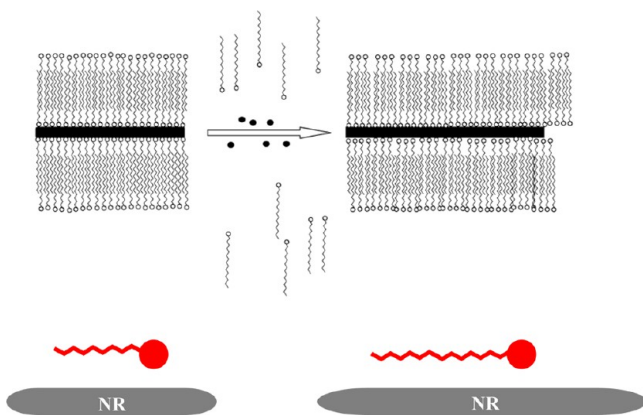


Figure 4. (top) Formation of the bilayer of C_n TAB on the nanorod surface assists nanorod formation as more gold ions (black dots) are introduced. Reproduced from ref 55 with permission. Copyright 2003 American Chemical Society. (bottom) Aspect ratio of the NR depends on the length of the hydrocarbon tail.

Head group modifications^{38,57,58} also influence the overall hydrophobic nature of a surfactant. A surfactant with ionic head groups forms a less compact micelle in comparison to a surfactant with nonionic or zwitterionic surfactant of identical hydrocarbon tails. Head group repulsions among the ionic head groups as well as greater hydration of the Stern layer reduces the magnitude of the nonpolar interactions between the hydrocarbon chains in the core of the micelles (Figure 2). Adding nonpolarity in the headgroup region as of cetyltriethylammonium bromide (CTEAB) in comparison to CTAB⁵⁹ results in a compact bilayer formation in the former where methyl groups are replaced by the ethyl groups. Thus, the use of CTEAB-stabilized seeds produces gold nanorods in high yields in comparison to that in the presence of CTAB.^{59–62}

2.2. Effect of Cosurfactant on the Aspect Ratio of NRs.

In addition to a longer hydrocarbon chains and headgroup modification, altering the growth solution's micellar state in seed-growth method during the epitaxial micellar adsorption and bilayer reconstruction significantly affects the final nanorod morphology.^{63,64} The longitudinal surface plasmon resonance (LSPR) peak can be directly correlated to aspect ratio.⁶⁵

Addition of benzyltrimethylhexadecylammonium chloride (BDAC) in CTAB growth solution in the beginning of reaction promotes the formation of longer and thinner NRs than those produced only in the presence of CTAB micelles (Figure 5).⁶³ But subsequent addition of BDAC at longer periods of time decreases the aspect ratio and increases the diameter of the rod. This contrasting result clearly indicates a large difference in the mixed surfactant surface activity and interfacial adsorption especially on the {100} crystal planes. The mixed micellar structure of the CTAB/BDAC binary surfactant solution⁶⁶ is significantly different from that of the CTAB solution due to the headgroup modification even though they have identical hydrophobic tails. This addition induces an additional nonpolarity in the stern layer due to the benzyl ring and hence, the mixed micelles thus produced are much smaller in size than the size of the CTAB micelles. It results in a dramatic decrease in the relative viscosity of CTAB/BDAC binary mixtures due to the formation of smaller mixed micelles with smaller micelle aggregation number.^{66–70} The smaller mixed micelles possess better surface adsorption ability and better surface passivation because their size is complementary to the growing nucleating centers and, hence, leads to the formation of longer and thinner

NRs by restricting the transverse growth. Preferential mixed micelle adsorption onto the transverse (100) and (110) facets inhibits adatom deposition (Figure 2c) of Au on these facets,^{64,71} and hence, the longitudinal growth is simultaneously promoted. The addition at longer periods of time induces a transition where the effect of BDAC becomes weaker and allows the Cl^- ions to disrupt the favorable state of the mixed micelles and, hence, reduces epitaxial growth, which promotes an increase in the diameter.

2.3. Monodisperse Nanorods and Self-Assembly Behavior.

For successful use of a particular kind of nanomorphology, monodisperse building blocks of the NPs are required.^{72–75} Cell internalization⁷⁶ and the photophysical properties of NPs in terms of biomarkers⁷⁷ need precise shape controlled morphologies. Monodisperse Au NRs can be synthesized by modifying the micellar behavior of CTAB in the presence of nonsurfactant additives. Effective adsorption of CTAB monomers on the crystal planes of growing nucleating centers directs the NR growth leading to the formation of monodisperse particles. Those additives that promote such adsorption certainly help in achieving monodisperse growth. The micellization behavior of CTAB can be modified through the addition of certain aromatic compounds such as sodium salicylate.^{78–80} The nonpolar benzene ring penetrates into the hydrophobic monolayer of CTAB, while the negatively charged COO^- groups interact with aqueous bulk solution.⁷⁸ This changes the micellar packing parameter $p = v/(Al)$, where v is the effective volume of the hydrophobic chain, A is the effective area of the polar headgroup, and l is the length of the hydrocarbon chain.⁸¹ Insertion of the phenyl moiety increases the v of the CTAB micelle. Anion association reduces the micellar surface charge and decreases A by reducing the electrostatic repulsions between the quaternary ammonium groups, promoting the spherical to rod like micellar transitions as templates for a single-crystalline growth in the [001] direction (Figure 6).⁷²

Surfactant coated NRs can be arranged in a self-assembled state of monodisperse nanoscale building blocks of ordered arrays (Figure 7).^{82,83} Such liquid-crystalline-type superstructures or superlattices composed of anisotropic nanocrystals have attracted fast-growing interest due to interesting emergent collective properties.^{84,85} They can be arranged in a large-area nematic liquid crystalline phase above a critical concentration of rods where a net gain in entropy on transition from isotropic random packing to a nematic liquid crystalline phase takes place.⁸⁶ The nematic phase, characterized by a uniaxial orientational order, lacks positional order, usually forms at less concentrated regions, and is more common for NRs of larger aspect ratios. The nematic or smectic ordering can be disrupted through continuous bending of neighboring layers, due to the complex interactions between the NRs. Development of a rigorous framework taking into account not only entropic contributions but also nanoscale forces including van der Waals attractions, electrostatic repulsions, dipole–dipole interactions, and counterion interactions in surfactant coated self-assembling gold nanorods is needed. These are promising substrates for the studies on plasmonic coupling⁸⁷ enhancement of optical signals including Raman and luminescence.^{88,89}

2.4. Role of Ag in Symmetry Breaking for Nanorod Formation.

As discussed above, CTAB is a well-known surfactant for Au nanorod growth, while Ag^+ is an essential component for the formation of single-crystal nanorods.^{90,91} It is not clear what role either Ag^+ or other surfactants play in the embryonic stages of crystal growth. Thus, it is important to know

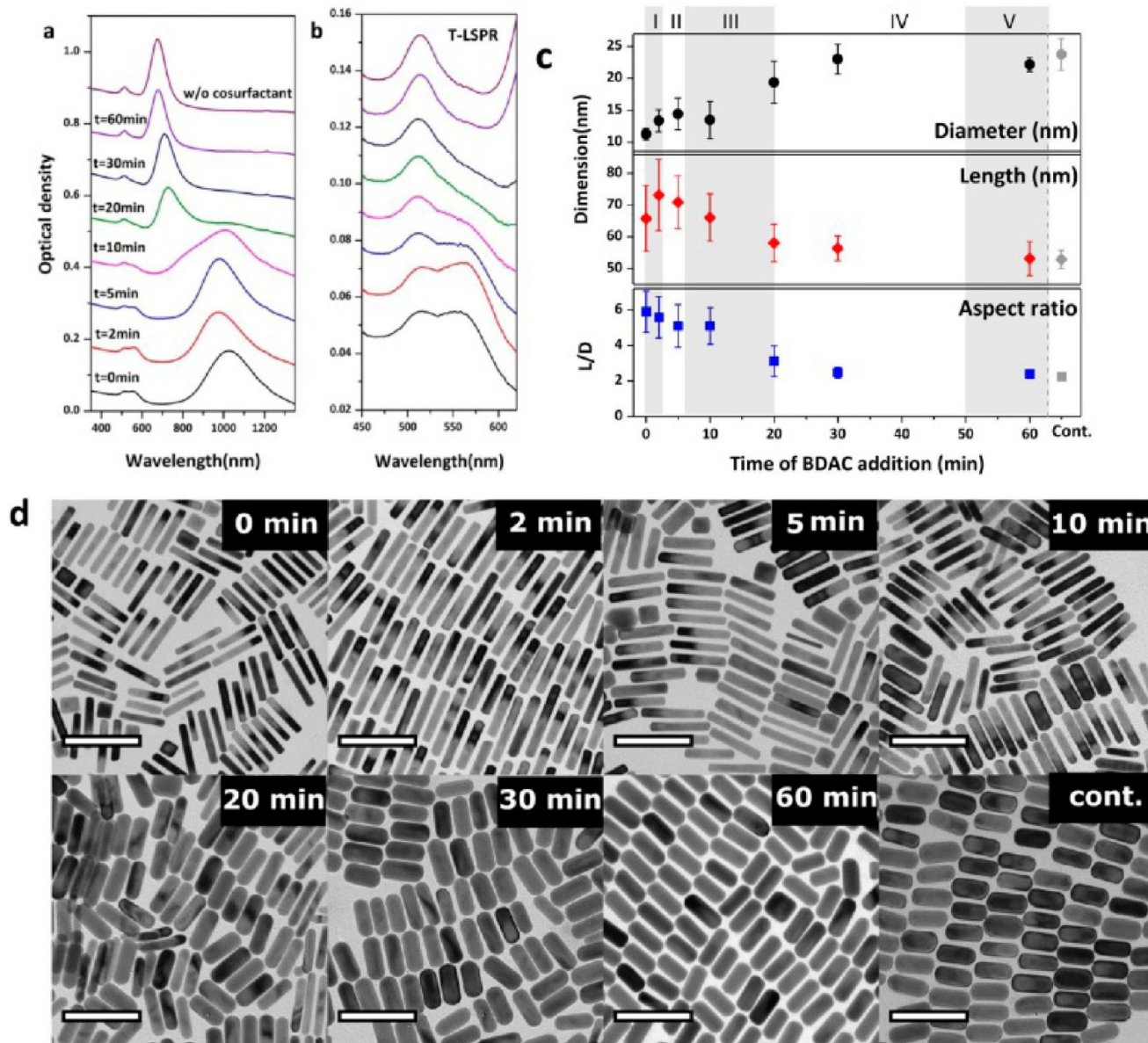


Figure 5. (a) UV–vis–NIR spectra of Au NR solutions after the incremental addition of 0.125 M BDAC subsequent to the initiation of nanorod growth. (b) Change in the transverse plasmon resonance peak. The scale of the y -axis is 5.6 times greater than that of panel a. (c) Time-dependent alteration of nanorod length, diameter, and aspect ratio (L/D). (d) TEM micrographs of Au NRs from the control solution (0.1 M CTAB) and after the addition of 0.125 M BDAC at incremental times. The scale bar is 100 nm. Reproduced from ref 63 with permission. Copyright 2013 American Chemical Society.

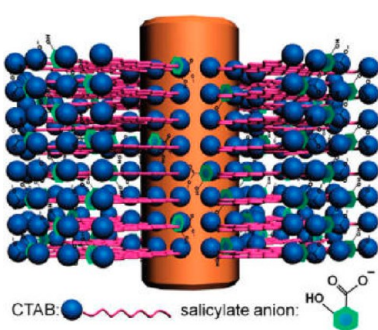


Figure 6. A cartoon illustrating the proposed mechanism to explain the role of aromatic additives (sodium salicylate is shown as an example) in mediating the binding between CTAB bilayers and certain facets of growing gold NRs. Reproduced from ref 72 with permission. Copyright 2012 American Chemical Society.

how to get a uniform crystal shape and growth direction and what is the role of Ag^+ , because silver is essential to break the symmetry of the embryonic nanocrystals and for the subsequent formation of single-crystal Au nanorods.⁹² CTAB adsorbs on certain crystal planes and modifies the surface energetics, causing the minimum energy structure of the particle to differ from that expected based on conventional thermodynamic considerations. The symmetry breaking process that gives rise to anisotropic growth and the resulting single-crystal gold nanorods is proposed through the following steps (Figure 8).⁹² (1) Seed particles synthesized in CTAB are single crystals with a cuboctahedral morphology, bound by symmetrically arranged $\{111\}$ and $\{100\}$ surfaces. (2) Upon introduction to Ag^+ -assisted gold nanorod growth solution, the seed particles initially grow isotropically until they reach a critical particle diameter of 4.6 nm. (3) At this point, small truncating surfaces consisting of a few atoms across form nonuniformly at the intersection of $\{111\}$ facets. These

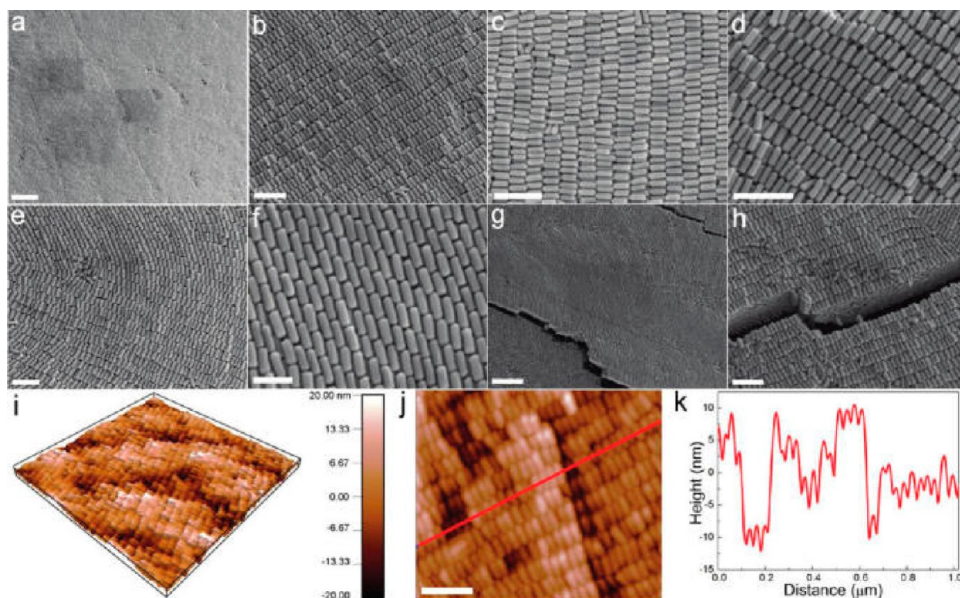


Figure 7. (a–h) SEM images of liquid crystalline assemblies of gold NRs (Aspect ratio = 2.9) synthesized using 5-bromosalicylic acid as the additive except with 0.2 mL of seed solution. (i) AFM three-dimensional topography image and (j) AFM height image of gold NR liquid crystalline assemblies. The scan size in panel i is 2 μm to –2 μm . (k) Height analysis of the line profile indicated in panel j. Scale bars: (a) 1 μm , (b) 200 nm, (c) 200 nm, (d) 200 nm, (e) 200 nm, (f) 100 nm, (g) 500 nm, (h) 200 nm, (j) 200 nm. Reproduced from ref 72 with permission. Copyright 2012 American Chemical Society.

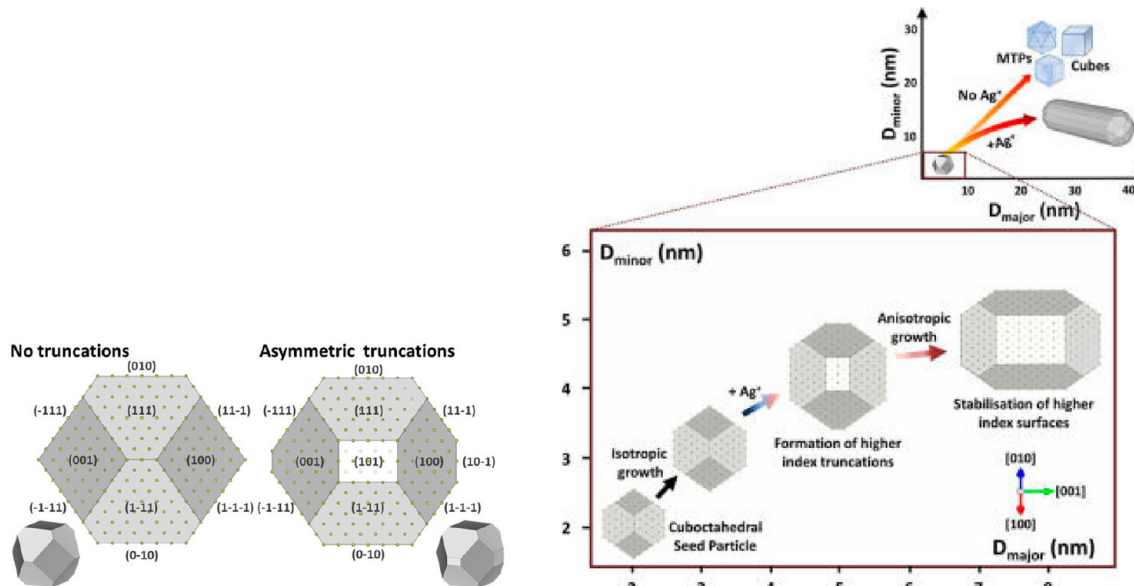


Figure 8. Particle models (left) of a perfect cuboctahedron and a cuboctahedron incorporating asymmetric $\{110\}$ truncations. (right) Schematic representation of the proposed key steps of the symmetry breaking process in single-crystal gold nanorod growth. Reproduced from ref 92 with permission. Copyright 2015 American Chemical Society.

truncations may be atomically rough and lie approximately parallel with $\langle 110 \rangle$. They are more open atomic structures than the comparatively close-packed $\{111\}$ and $\{100\}$ surfaces already present in the nanoparticle and are the preferred sites for Ag underpotential deposition. (4) Stabilization of the higher-index truncations prevents further Au atom deposition. Growth proceeds on the lower-index surfaces, leading to the truncations becoming side facets in the growing embryonic nanorod structure. Thus, small facet truncations develop in the growing seed structure and the stabilization of these truncations in the presence of Ag^+ leads to asymmetry. The participation of the

surfactant molecules in this mechanism is further discussed from theoretical studies using the density functional theory, DFT.

2.5. Theoretical Aspects of Nanorod Formation. DFT can be applied to understand the growth of nanostructured materials^{93–95} in terms of the surface energy of different facets, effect of halide ions, and role of Ag on the thermodynamics of the growth process. The structure of the small Au seeds can be estimated through Wulff construction with a cuboctahedron structure mainly demonstrating $\{111\}$ planes with small contributions from $\{100\}$ (Figure 9).^{96–98} The seed is associated with some adsorbed Br atoms but is not in contact with the CTA⁺ micelle because the radius of the latter is larger at about 2.6 nm.

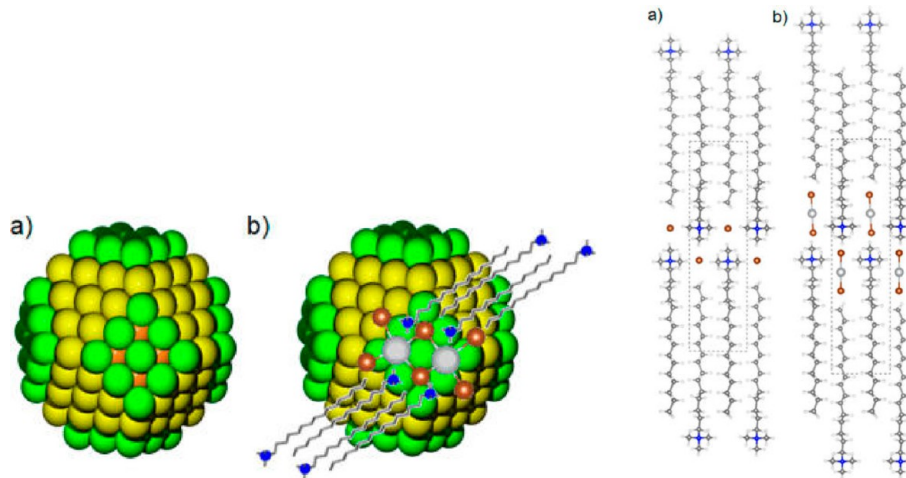


Figure 9. (left, a) Wulff construction of a gold nanoparticle representative of the seed. Yellow planes are {111} and green ones are {100} facets. (left, b) The adsorption of CTAB–AgBr on {100} planes. (right) Crystal lattices of (a) CTAB and (b) CTAB–AgBr (Br, brown; Ag, large light gray spheres; C, gray; H, white; N, blue). Reproduced from ref 96 with permission. Copyright 2014 American Chemical Society.

The seeds enclosed in the soft-template of the micelle, which resemble those in Figure 9a, are then added to the growth mixture that contains AgNO_3 , CTA^+ , Br^- , and the mild reducing agent.⁹⁶ Growth starts by diffusion of the gold atoms into the CTA^+ micelle cavity.⁹⁰

In the growth solution, Ag^+ cations and Br^- anions form $[\text{Br}-\text{Ag}-\text{Br}]^-$ complex on gold surfaces,⁹⁹ which can be entrapped by the CTA^+ cations. AgBr intercalation in the CTAB lattice implies an energy gain of -0.70 eV/ AgBr unit. In this structure, the van der Waals interactions between tails remain, and an ionic interaction takes place between intact ammonium and $[\text{Br}-\text{Ag}-\text{Br}]^-$ to form CTAB–AgBr.¹⁰⁰ This is responsible for the symmetry breaking and nanorod growth¹⁰¹ in view of the preferential adsorption of CTAB–AgBr on {100}. This is not possible on {111} facets because the AgBr crystal shows a rock-salt structure with nonpolar planes of square patterns compatible with the Au {100} surface. This preferential adsorption with subsequent blocking could easily be the origin of symmetry breaking and rod formation. The aspect ratio is controlled by the length of the aliphatic chain of the surfactant as depicted in Figure 4 from experimental studies.⁵⁵ The growth passes through different elementary steps (Figure 10) as follows.⁹⁶ The CTAB–AgBr complex adsorbs on top of the gold surface in step 1 and loses one of the Br atoms in step 2 (CTAB–Ag separated from Br). This leaves a Ag atom on the gold surface still with a Br coordinated to it and with a CTA^+ capping it. The subsequent reaction (step 3) comprises completion of the new facet with incoming Au atoms complexed to CTA^+ that get reduced on the surface. It is also evident that the energy reduction of {520} crystal planes is greater than that of the {100} and {110} facets because the resulting morphologies cannot evolve only from these facets⁹⁷ and, hence, {520} is the most common lateral surface, which provides the best van der Waals interactions in the surfactant crystal structures.

3. NANODUMBBELLS AND THEIR AGGREGATION BEHAVIOR

The gold nanorods prepared by the seed-mediated growth method sometimes contain unreduced gold ions, which can be used as substrates to fine-tune the structure and, therefore, the optical properties of gold nanorods. The structure-directing surfactant CTAB assists in fine-tuning of the shape. CTAB binds

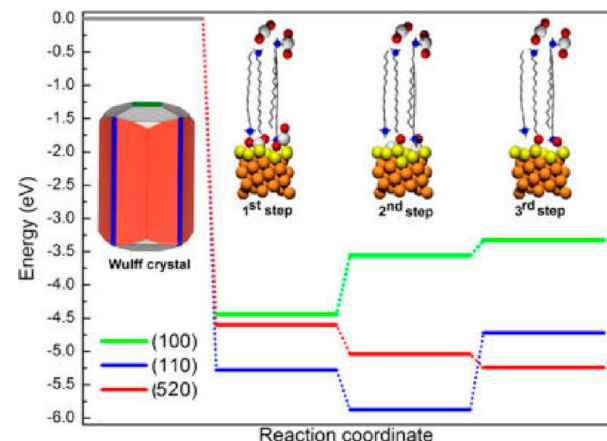


Figure 10. Incorporation and growth of a new Au layer onto a pre-existing structure for different surfaces. Step 1 corresponds to the surface adsorption of the CTAB–AgBr complex, step 2 to the loss of one Br atom, and step 3 to the filling of resting positions in the lattice by Au atoms from the solution. Color code: yellow, surface Au atoms; orange, bulk Au; light gray, Ag; brown, Br; blue, N. The aliphatic skeleton of the CTA^+ surfactant is shown as sticks. The inset shows the final Wulff structure upon CTAB adsorption showing {520} [{520} contains $2\{110\} + 3\{100\}$] planes in red as the most abundant lateral facets and {110} between them in navy. Reproduced from ref 96 with permission. Copyright 2014 American Chemical Society.

preferentially to the middle of the nanorods directing the deposition of more gold preferentially at the ends. The addition of additional ascorbic acid to the unpurified gold nanorod solution causes the reduction of the leftover gold ions. The gold nanorods that are present in solution serve as seeds in the reduction. The assembly of CTAB bilayers along the long gold nanorod faces is preferred, compared with the ends.^{55,102} Therefore, the addition of ascorbic acid causes the reduction of the gold ions at the more accessible ends leading to the formation of dogbone structures (Figure 11).⁶¹ Self-assembly of such dumbbell nanorods is an important way to understand the different ways in which building blocks can be arranged so as to understand the plasmonic behavior.^{103–105} Attractive as well as steric interactions play significant role in achieving the self-assembled state of anisotropic NPs. In the case of CTAB coated

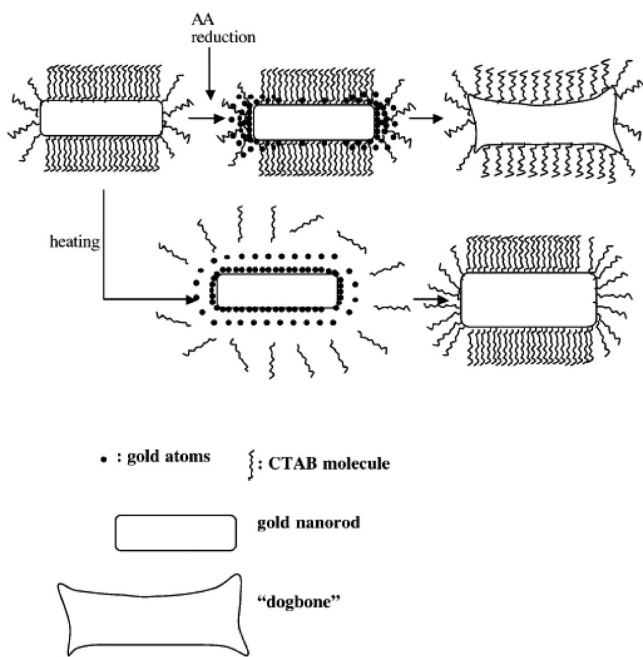


Figure 11. Proposed mechanisms that lead to dogbone structures from gold nanorods upon additional reduction of gold ions by ascorbic acid (top) and that lead to lower-aspect ratio gold nanorods upon heating in the presence of gold ions. Reproduced from ref 61 with permission. Copyright 2005 American Chemical Society.

dumbbell shaped NRs, CTAB molecules are replaced by thiol-terminated polystyrene (PSSH) that selectively adsorbed on the nanorod tips, where the surface reactivity is higher compared with the central part.¹⁰³ An excess amount of ligand exchange causes the particles to aggregate in a random fashion, rather than forming well-defined clusters, because PSSH fully replaces the CTAB bilayer,¹⁰⁶ while a selective addition of five molecules per square nanometer of gold surface provides colloidal stability in tetrahydrofuran/dimethylformamide (THF/DMF) solvent mixture in which addition of water (up to 10 wt %) induces side-to-side clustering (Figure 12).^{103,107} A mixture of THF and DMF (1:3) is a good solvent for the PS block but a bad solvent for CTAB molecules. Initially, the PS ligands are sufficiently long to stabilize the particles by steric repulsions, but in the presence of water, the self-assembly of nanodumbbells is governed by the poor solubility of both PS and CTAB, which promotes the formation of side-to-side dimers (Figure 12). However, addition of PS403-*b*-PAA62 reduces the population of side-to-side arrangement and increases the population of cross-like dimers by promoting hydrophobic interactions from the PS side and hydrophilic interactions from the PAA side to make an organic shell enclosing cross-like dimers (Figure 12).

3.1. Shape Transformation, Nanorod to Spindle. It is also possible to induce shape transformation in nanorods by simply adjusting the rearrangement of surfactant molecules in the presence of other species, which can act as linkers among the nanorods for their end to end arrangement. Glutathione (GSH) is the most abundant thiol species in cells^{108,109} and works in detoxification processes and protection against oxidant injury. It can serve as a trigger for drug release from Au nanoparticle carriers¹¹⁰ and acts as a linker for end-to-end assembly of Au NRs.^{110,111} Its preferential adsorption on the ends of the NRs completely passivates the ends from participation in further nucleation and, hence, causes a dramatic effect on the transverse

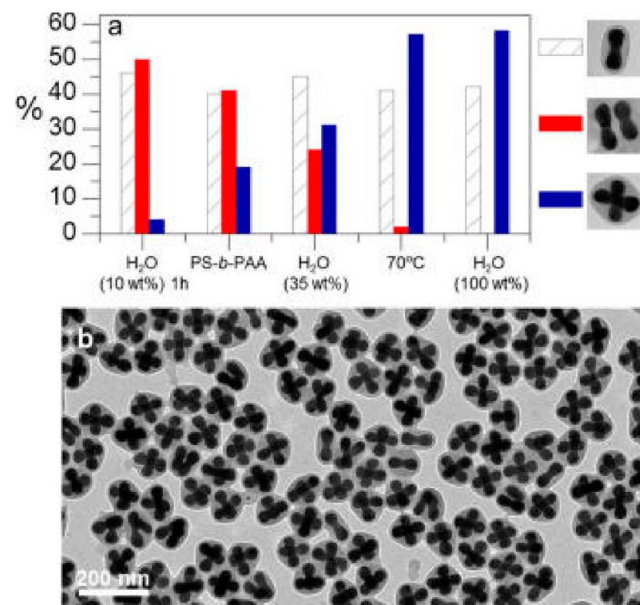


Figure 12. Side-to-side dimers encapsulated inside the polymeric micelles transform into cross-like clusters. (a) Distribution of morphologies at different experimental steps. Addition of PS-*b*-PAA to the mixture increased the fraction of cross-like dimers and decreased the fraction of parallel dimers. (b) TEM image of cross-like dimers. Reproduced from ref 103 with permission. Copyright 2012 American Chemical Society.

overgrowth (Figure 13).¹¹² It leads to spindle shaped NRs and shape transformation from rods, peanuts, and truncated

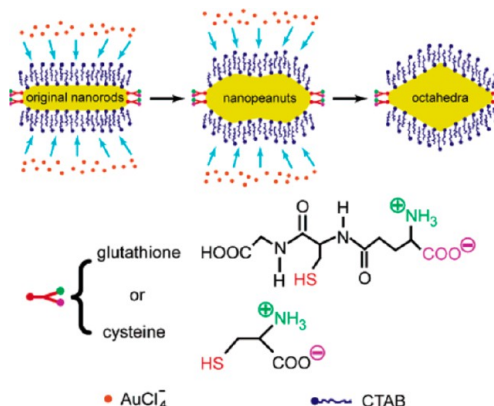


Figure 13. Schematic showing the transverse overgrowth on Au NRs induced by the selective binding of GSH or cysteine to their ends. Reproduced from ref 112 with permission. Copyright 2007 American Chemical Society.

octahedra to faceted spheres as the amount of the Au precursor is increased. In the first step, the original Au NRs are grown using the seed-mediated method in CTAB solution in the presence of AgNO_3 .^{62,113} For transverse overgrowth, a calculated amount of GSH is first added into the as-grown original NR solution. The ligand preferentially adsorbs on the ends of NRs and replaces electrostatically bound CTAB. The resulting mixture is kept at room temperature for 2 h. The original Au NRs have a longitudinal plasmon peak at 778 nm and a transverse one at 513 nm. As the volume of the growth solution is increased, the longitudinal plasmon peak gradually blue shifts and the transverse one slightly red shifts (Figure 14).¹¹² They finally

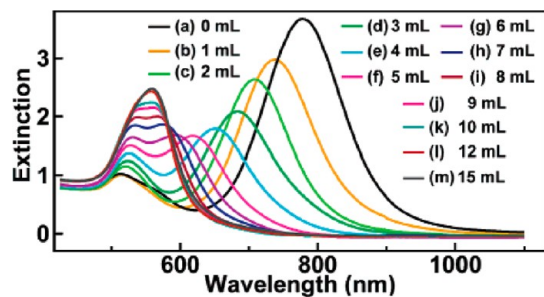


Figure 14. Extinction spectra of the growth products taken 1 day after the addition of varying volumes of the growth solution into 2.5 mL aliquots of the original Au NR solution containing 100 μM GSH. Reproduced from ref 112 with permission. Copyright 2007 American Chemical Society.

merge together at 559 nm. This happens because the lateral adsorption of CTAB cannot completely passivate the {110} and {100} planes and allows them to participate in the nucleation process. Cysteine can also induce transverse overgrowth because cysteine and GSH contain both carboxyl and amino groups.¹¹² The blocking of the longitudinal growth over Au NRs is induced by the bound GSH and cysteine molecules through their zwitterionic groups, which produce stable {111} facets with complete passivation, and hence, the growth shifts to the {110} and {100} facets.

4. CUBES AND CUBE-BASED POLYHEDRA

Apart from the NRs, other geometries can also be produced by selective adsorption of surfactant molecules and are best modeled on the surface area limited (SAL) theory of growth and nanomorphology derived from a kinetic model of shape evolution as a function of time.^{114–117} It is related to surface diffusion, rate of step growth, and surface site availability. This model is applied to show that how the growth of nanorod and truncated octahedron is driven by these factors. Choosing a seed with shape of 50% {100} and 50% {111} surface area equating to 43% of sites distributed evenly on sites on the six {100} facets and

57% of sites distributed evenly on the eight {111} facets, it is possible to select surfactant that will selectively passivate either the {100} or {111} facets, directing the growth on the other planes with entirely different geometries. When {111} facets are blocked by surfactants, the growth is restricted to the {111} direction; consequently, new octahedral corners are formed and the shape is entirely enclosed by {111} facets (Figure 15).¹¹⁴ It is much more rapid at higher temperatures, and thus, temperature variation tailors nanoparticle growth. On the other hand, when {100} planes are blocked, the growth is restricted to the {100} direction. This results in a cube that is entirely enclosed by {100} facets (Figure 16).¹¹⁴ The rate of coarsening in the {100} direction is almost identical to that in the {111} direction and is balanced by the in-plane packing density. A successful implementation of the theory to experimental results needs precise temperature control, stable binding of surfactants to the surface, appropriate time dependence, realistic growth rates,¹¹⁸ and realistic polyhedral morphologies. All these experimental factors can be successfully implemented by choosing an appropriate surfactant along with other shape directing species (discussed in the preceding section), which can completely passivate a particular crystal plane so that entire nucleation is shifted to the other available planes in order to achieve perfect cubes or cube-based polyhedral shapes.

Experimentally, the seed-mediated synthesis^{119–123} produces a vast variety of nanostructures, ranging from Platonic solids, such as octahedra and cubes,^{124–128} to plates and prisms^{129,130} with high-index surface facets.¹³¹ The use of halides in controlling gold nanoparticle shape is the case of the silver assisted syntheses of concave cubes¹²⁸ and tetrahedra,¹³¹ bound with high-index facets. The synthetic conditions for producing these morphologies are nearly identical, except that the {720}-faceted concave cubes¹²⁸ are synthesized in CTACl, while the same synthesis in CTAB results in convex {730}-faceted tetrahedra (Figure 17).¹²⁷ These closely related shapes have either square-pyramidal depressions (concave cubes) or square pyramids (tetrahedra) on each of the six faces. The growth of concave cubes and tetrahedra is favored

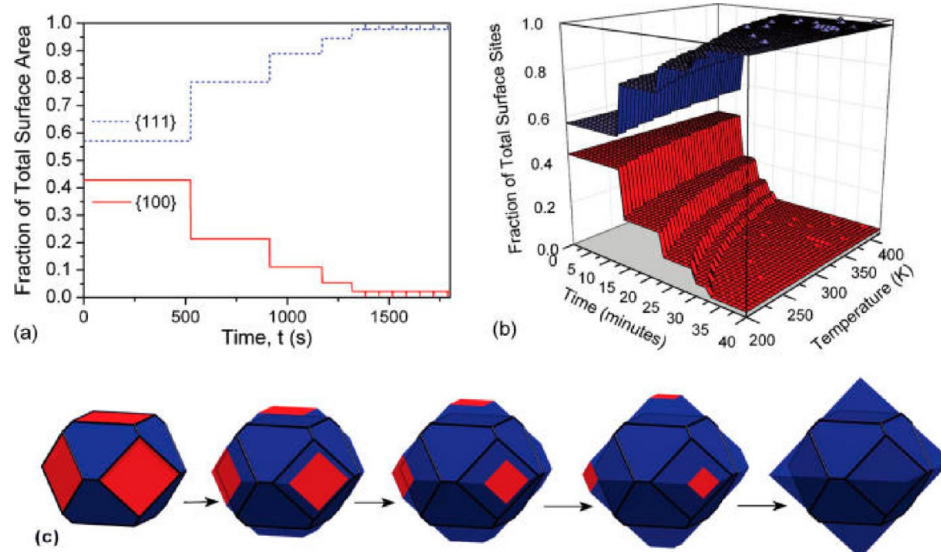


Figure 15. Shape evolution of a gold nanoparticle enclosed by {111} and {100} facets: (a) when {111} facets are blocked by surfactants and coarsening is restricted to the {111} direction at 300 K, (b) the same shape evolution as a function of temperature in the range 200–420 K, and (c) schematic representation of the visual appearance. Reproduced from ref 114 with permission. Copyright 2011 American Chemical Society.

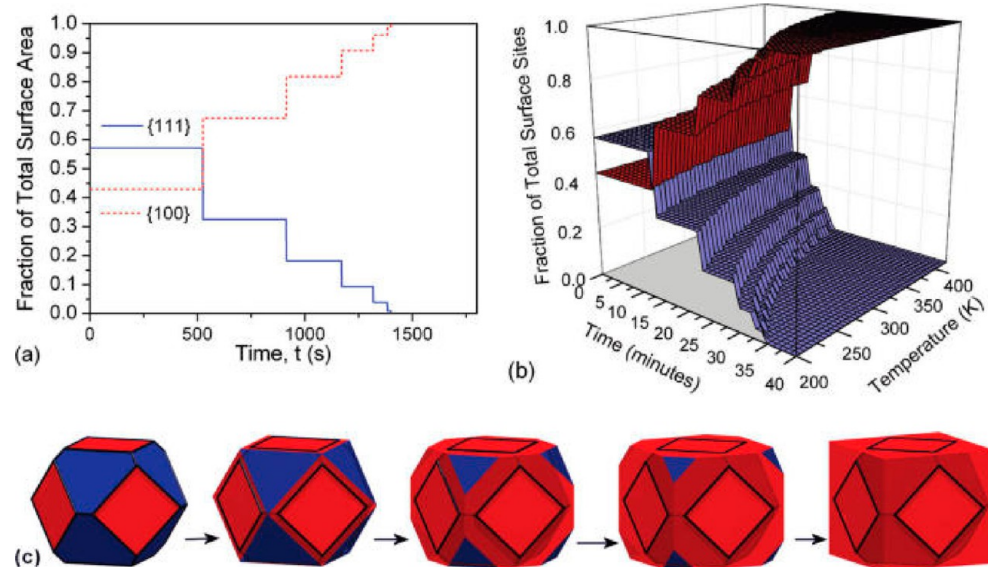


Figure 16. Shape evolution of a gold nanoparticle enclosed by {111} and {100} facets: (a) when {100} facets are blocked by surfactants and coarsening is restricted to the ⟨100⟩ direction at 300 K, (b) the same shape evolution as a function of temperature in the range 200–420 K, and (c) schematic representation of the visual appearance. Reproduced from ref 114 with permission. Copyright 2011 American Chemical Society.

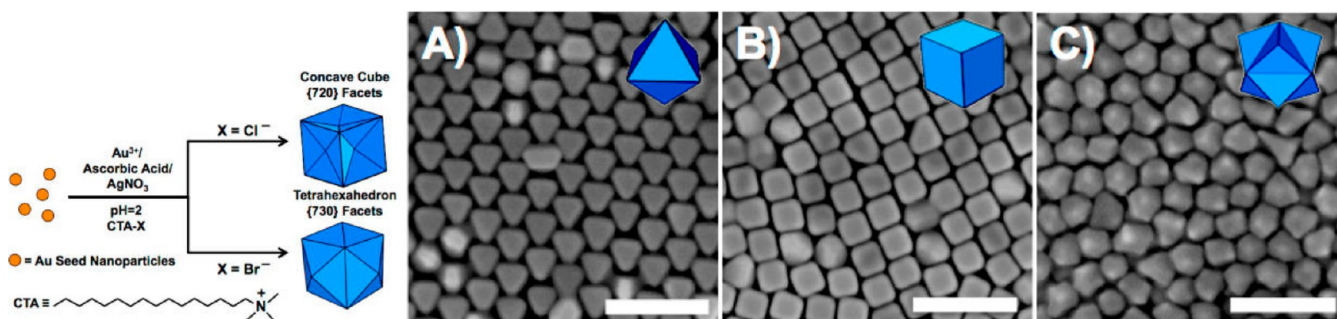


Figure 17. Formation of different morphologies by using CTACl and CTAB surfactants in seed-growth method. SEM images of reaction products from growth solutions containing 10 mM CTAB and (A) 0.5, (B) 2.0, and (C) 10.0 mM ascorbic acid, resulting in the formation of {111}-faceted octahedra, {100}-faceted cubes, and high-index faceted trisoctahedra, respectively. Scale bars: 200 nm. Reproduced from ref 127 with permission. Copyright 2012 American Chemical Society.

in chloride- and bromide-containing surfactants, respectively. Changing the concentration of the reducing agent, ascorbic acid, is a direct way of controlling the particle shape because increasing the amount of reducing agent increases the rate of gold ion reduction, which leads to growth of more kinetically favorable (or less thermodynamically favorable) particle morphologies. For instance, with 0.5 and 2.0 mM ascorbic acid, the reactions generate well-defined {111}-faceted octahedral (Figure 17A) and {100}-faceted cubes (Figure 17B), respectively. However, when the concentration of ascorbic acid is increased to 10 mM, the products form ill-formed trisoctahedra (Figure 17C) bound with high-index facets¹³² due to a poor control of growth in view of a very rapid rate of gold ion reduction. These morphologies are mainly controlled by the nature of halide ions, because the binding strength of the halides to the Au particle surface increases in the order Cl⁻ < Br⁻ < I⁻, as well as the amount of Ag, which deposits epitaxially onto gold and prefers to deposit onto sites where it will have a high coordination number with respect to gold, such as kinks and step edges, and stabilizes high-index facets.¹²⁴ Thus, the role of surfactant is mainly reduced to colloidal stability rather than shape directing agent especially in the kinetically controlled reactions where large amount of

precursor is required to deposit on a particular crystal plane over a period of time. Although, CTACl and CTAB provide the required Cl⁻ and Br⁻ ions depending on the geometry needed, shape is primarily controlled by the surface passivation of halide ions or Ag rather than the surfactant ions.

Contrary to the cubic and cuboctahedral Au NPs discussed above, Pt NPs are entirely synthesized in the presence of TTAB using the benzene hydrogenation activity.¹³³ Although, both CTAB and TTAB have identical head groups, the length of the hydrocarbon tail in the former is C16 in comparison to C14 in the latter case. The purpose of choosing TTAB in comparison to another surfactant with stronger interactions is that, TTAB preserves the surface catalytic nature whereas strongly interacting surfactant completely passivates the surface and renders it unsuitable for catalytic activity. TTAB interacts with the Pt atoms through the alkyl chain rather than the head groups forming C–H···Pt weak bonds. The cubic particles have only (100) crystal planes, whereas the cuboctahedral particles have both (100) and (111) crystal planes (Figure 18).¹³³ IR spectra of pure TTAB and TTAB-stabilized cubic Pt nanoparticles reveal insignificant differences in the C–H rocking (700–740 cm⁻¹), C–H bending (1350–1550 cm⁻¹), and C–N⁺ stretching (880–1000 cm⁻¹)

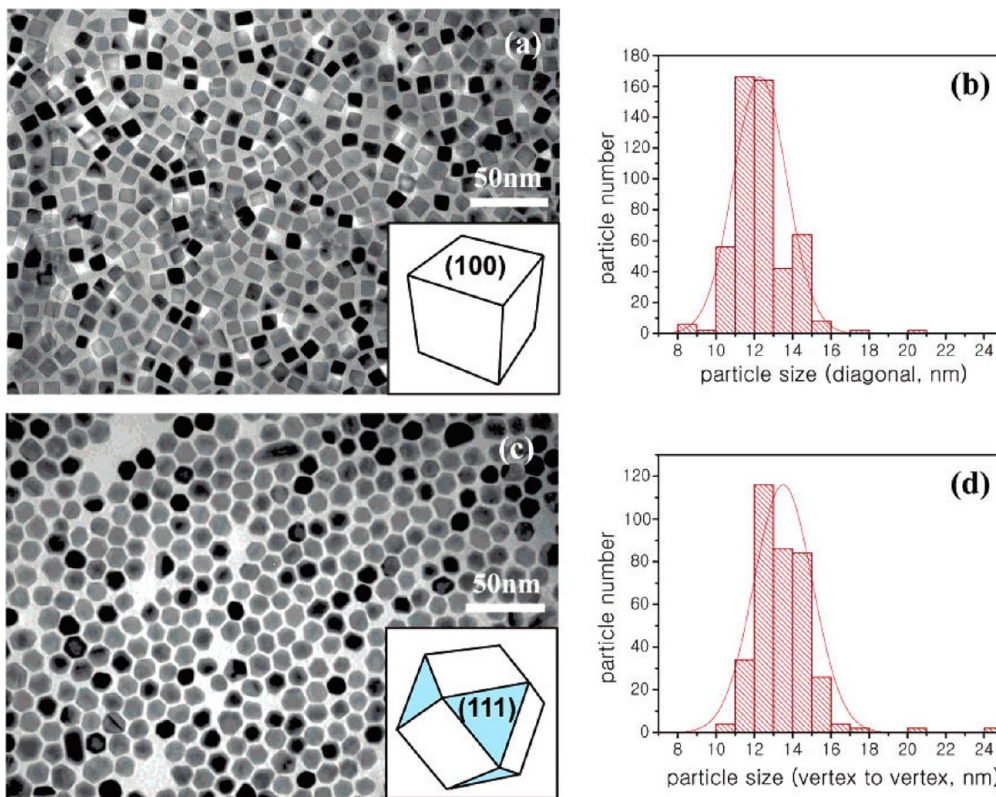


Figure 18. (a) TEM image and (b) size distribution of TTAB-stabilized cubic particles (average size = 12.3 ± 1.4 nm, 79% cubes, 3% triangles, and 18% irregular shapes). (c) TEM image and (d) size distribution of TTAB-stabilized cuboctahedral particles (average size = 13.5 ± 1.5 nm, 90% cuboctahedra and 10% irregular shapes). Reproduced from ref 133 with permission. Copyright 2007 American Chemical Society.

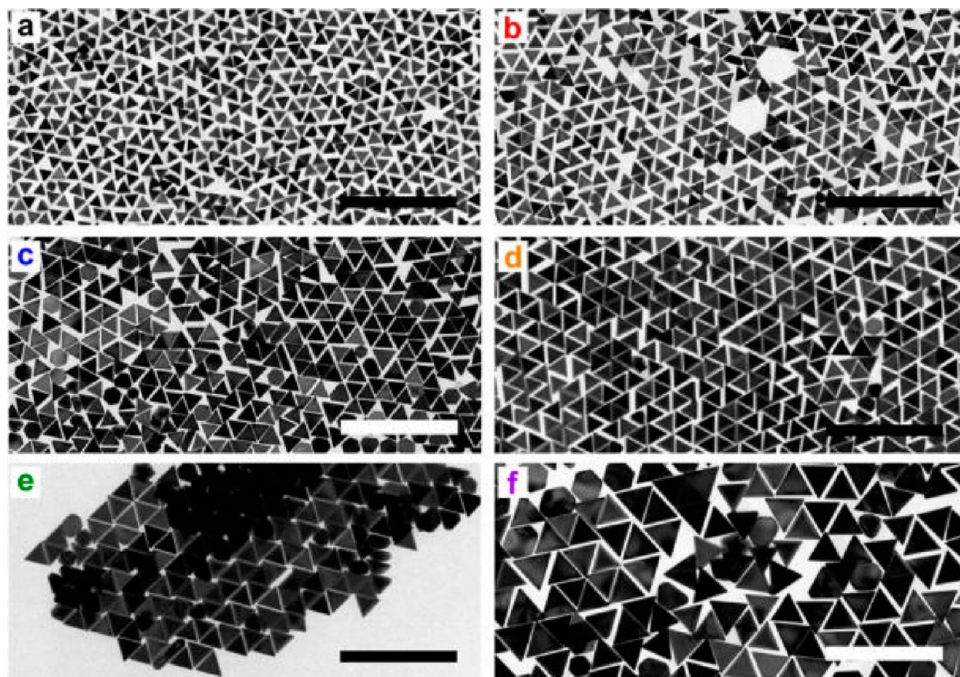


Figure 19. TEM images of Au NTs with increasing edge lengths. Reproduced from ref 135 with permission. Copyright 2014 American Chemical Society.

regions. However, the IR spectra in the C–H stretching region show significant differences in the spectra of pure TTAB and TTAB-stabilized nanoparticles. The IR spectrum of the TTAB-stabilized nanoparticles contains an additional mode at 2783 cm^{-1} , which is attributed to direct C–H···Pt interactions

between Pt atoms on the nanoparticle surfaces and proximal C–H bonds,¹³⁴ and indicates a direct interaction of the alkyl chain with the metal surface. Because the IR spectra of pure TTAB and TTAB-stabilized cubic Pt nanoparticles differ only in the C–H stretching region, TTAB does not interact with the Pt

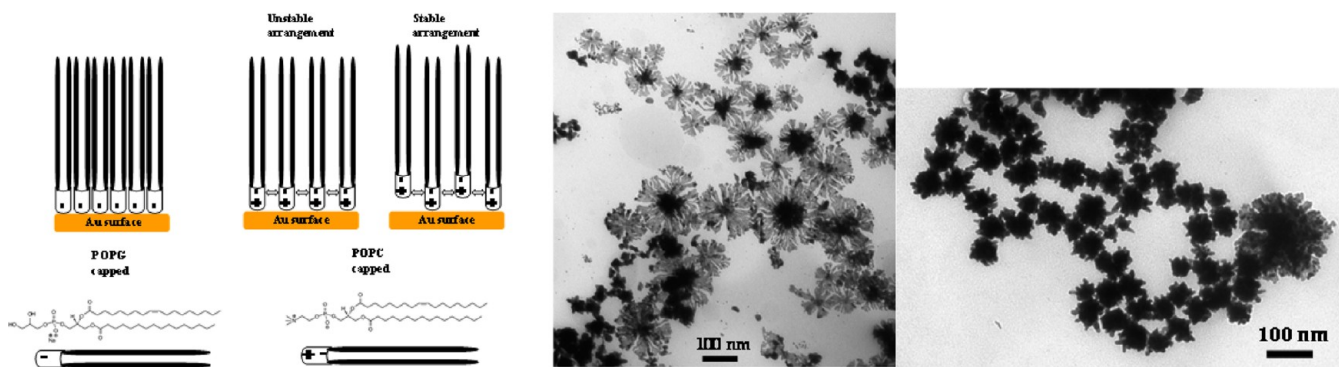


Figure 20. (left) Schematic arrangement of POPG/POPC lipid molecules on the gold surface. (right) TEM images of flower-shaped and predominantly dendritic nanoparticles. All NPs are obtained by using seed at the end of the reaction sequence. Reproduced from ref 120 with permission. Copyright 2007 American Chemical Society.

surface through the trimethylammonium headgroup but rather through the alkyl chain. The different mode of interactions of alkylammonium ions on Pt surfaces in comparison to Au surfaces¹⁰² is due to the difference in atomic density that allows Pt to more readily dehydrogenate alkanes than Au. Benzene hydrogenation studies demonstrate that both cyclohexene and cyclohexane formed on cuboctahedral nanoparticles and only cyclohexane on cubic nanoparticles. This is attributed to an increase of the corner and edge sites on the nanoparticles available for catalysis or changes in the electronic structure of the nanoparticles compared with the Pt single crystals.

5. NANOTRIANGLES

As we have observed for gold cube-based polyhedra that the precise shape control requires the use of halide ions and Ag, nanotriangles (NTs) are another important morphology, which also requires the presence of I⁻ ions to get shape controlled synthesis in the presence of surfactant.¹³⁵ NTs are synthesized by following a seed-mediated growth using CTAC-coated seeds.¹²⁷ The shape yield and monodispersity of the NTs can be significantly improved by overgrowing the seeds in the presence of I⁻ ions to transfer into the final growth solution before the reaction is completed. Usually, it is difficult to get precise shape control in a single step reaction, but an appropriate purification process can be implemented to extract monodisperse NTs of a desired shape and size. Purification can be done by using different CTAC concentrations in which a high purity of precipitate is achieved along with a good purification yield, that is, a large proportion of the initial NTs are precipitated with a color change of the solution from dark blue to indigo. The optimal procedure is found to correspond to a CTAC concentration of 0.15 M, which is well above its cmc, and hence, the surfactant is used here as a stabilizer as well as flocculating agent to extract the NTs of desired shape and size. The size can be varied by decreasing the amount of seed; the NTs' edge length could be increased up to 90 nm (Figure 19).¹³⁵ However, further reduction in seed concentration leads to an increase in polydispersity from less than 6% up to 15%. In the presence of low amounts of I⁻ ions, which can strongly bind to the gold surface and hence significantly affect the growth,^{136,137} the edge length of the NTs can be further increased up to 150 nm. Just like that of cube NPs, it is not easy to attain such morphologies only by using an appropriate surfactant, which can direct the seed growth in a specific direction to obtain NTs. Therefore, the use of appropriate halide ions and Ag concentration are required along with the surfactant to precisely control the morphology.

6. STAR, DENDRITIC, AND FERN SHAPED NANOPARTICLES

6.1. Nanoflower and Dendritic Shapes. Till now, we were discussing the shape control effects of the conventional surfactants like CTAB and its homologues, as well as that of SDS. Biological surfactants^{119,120,138,139} belong to another category of surface active molecules that have attained considerable importance recently in view of their applications in biological systems in terms of biologically sustainable biomaterials. Therefore, their shape control effect and NP surface adsorption is another important aspect to be discussed. Unlike the conventional surfactants, biological surfactants like phospholipids^{119,120} are usually water insoluble, and hence, they directly lead to the formation of vesicles rather than micelles in the aqueous phase but possess inherent surface adsorption ability in the form of bilayers in aqueous phase. Shape control effects of biological (pulmonary) surfactants like 1-palmitoyl-2-oleoyl-sn-glycero-3-[phospho-rac-(1-glycerol)] (sodium salt) (POPG) (16:0–18:1), 1,2-dipalmitoyl-sn-glycero-3-[phospho-rac-(1-glycerol)] (sodium salt) (DPPG) (16:0), and 1,2-dimyristoyl-sn-glycero-3-[phospho-rac-(1-glycerol)] (sodium salt) (DMPG) (14:0) usually results in lipid coated spherical morphologies,^{119,120} which can be converted into a chain like pearl-necklace arrangement with the addition of a slight amount of Ag. However, large flower like morphologies (Figure 20)¹²⁰ of Au and Au–Ag bimetallic NPs are obtained when the seed solution is added at the end of the seed-growth reaction sequence. In relevance to a time-dependent adsorption of phospholipids at immiscible interfaces,^{140–144} the slow adsorption of POPG on the Au surface is surpassed by the fast reduction, which leaves some of the crystal planes uncapped and consequently leads to anisotropic growth. No specific anisotropic shape controlled effects have been observed for phospholipids presumably due to the zwitterionic and bulky nature of the head groups, which are not expected to completely passivate certain crystal planes of growing nucleating centers and hence result in the flower like or dendritic morphologies. In fact, the dislocations and kinks generate active sites for electrostatic adsorption of ionic rather than zwitterionic lipids. Effectiveness of the surface passivation is judged from the membrane forming ability of a phospholipid. A compact membrane produced by an ionic rather than a zwitterionic phospholipid (Figure 20) provides better surface passivation because the interfacial adsorption of the latter arranges the dipolar head groups in an alternative zigzag fashion in order to achieve complete electrical neutrality. This arrangement results in weak electrostatic interactions with poor capping

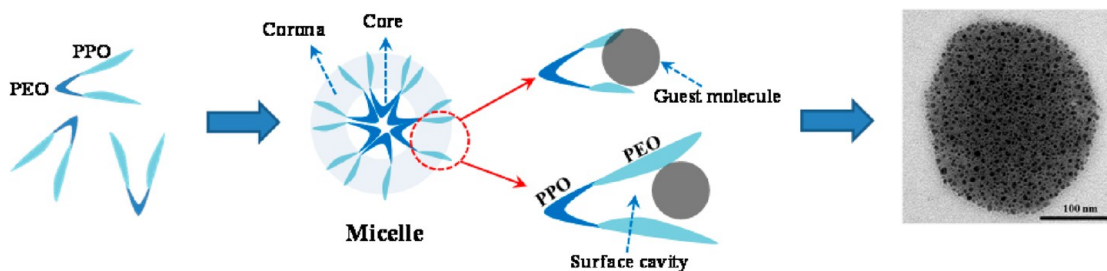


Figure 21. Micelle formation of block polymer and its micellar template.

ability and consequently exposes some of the crystal planes for further nucleation. The secondary nucleation is very hard to control and consequently leads to anisotropic growth.¹²⁰

Flower like or star shaped morphologies are also obtained when pluronic F127 block copolymer ($\text{PEO}_{100}\text{PPO}_{65}\text{PEO}_{100}$) is used as a surfactant.^{145–147} Pluronics are polymeric surfactants, and their micellar behavior is usually much different from that of conventional surfactants because of the large amount of hydration of polymeric monomers in the aqueous phase.^{148–152} Pluronics show micelle formation under the effect of temperature variation and that temperature is known as critical micelle temperature (cmt). The micelle formation is quite prominent because they are well-defined compact micelles usually much larger than conventional micelles under the dehydration effect of temperature rather than concentration. They are relatively less surface active than conventional surfactants, and hence, their shape control effects are not so prominent. The surface cavities of pluronic micelles are used as microreactors for the synthesis of Au NPs, which consequently produce NP loaded micelles (Figure 21).^{53,146} Pluronics have also been used in the synthesis of star shaped Pt NPs (Figure 22)¹⁴⁵ for their versatile catalytic applications. The rich edges and

F127 molecules serve as a structure-directing agent where the PEO group in the PEO–PPO–PEO chain is known to form a crown-ether-like conformation, similar to a cavity structure in aqueous solution.^{146,147} The hydrophobic PPO groups in the pluronic polymer are favorably adsorbed onto the surface of the deposited metal surface. The pluronic chains adsorbed on the Pt surface during Pt deposition in this system could form cavities that facilitate the formation of star shaped NPs; therefore, the concentration of pluronic F127 used should be lower than its cmc.

Nanoscale globular platinum dendrites^{156–158} can also be synthesized by chemical reduction of platinum complexes with ascorbic acid in aqueous micellar solutions. The reduction of aged platinum complex with ascorbic acid in another long chain nonionic aqueous Brij-35 micellar solution under ambient conditions yields a black suspension with some precipitate on the bottom of the glass vessel after 1 h. TEM analysis reveals the presence of the platinum nanostructures that are spherical and porous with each arm of the dendrites bearing a rounded 2–3 nm tip. The diameters of the platinum dendrites range widely from 18 to 102 nm. The size and uniformity of the Pt dendrites can be well controlled either by the addition of Pt nanoparticles as seeds or alternatively by a photocatalytic seeding method. The mechanism for the formation of the platinum dendrites is most likely the reduction of Pt complex and deposition of metal atoms at the surface of the growing dendrite, with surfactant and ascorbic acid playing an interfacial role in producing the dendritic morphology.

6.2. Nanoshells. Gold nanoshells covered with spikes, called spiky nanoshells,^{159–161} can be synthesized by merging templated nanoshell synthesis¹⁶² and the surfactant assisted¹⁶³ seed-growth method (Figure 23).¹⁵⁹ In this approach, polymer

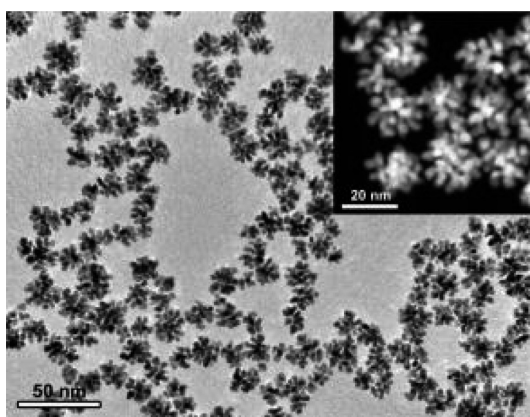


Figure 22. (top right) Micelle formation in a typical triblock polymer and use of its surface cavities for the Au NPs synthesis (tiny black dots in the TEM images are the Au NPs). (bottom) TEM image of the star shaped Pt NPs. Reproduced from ref 145 with permission. Copyright 2010 American Chemical Society.

corner atoms derived from the dendritic structures are highly desired for improving catalytic performance.^{153–155} Low surface activity of pluronic F127 molecules plays an important role in star shaped structure-directing ability for better catalytic performance. However, it is unclear how surface cavities are involved in specific shape control morphologies. The size of the star shaped NPs lies in the range of 13 to 23 nm with an average diameter of 17.4 nm. They are bound with {111} crystal planes. Pluronic

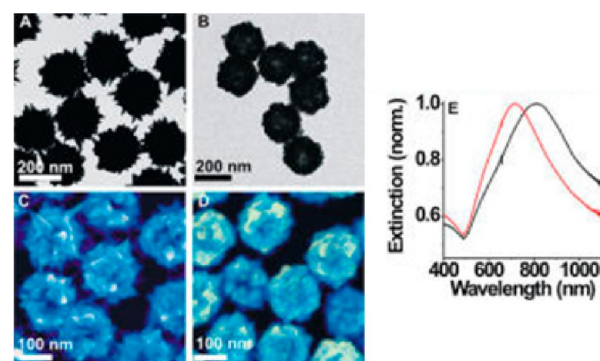


Figure 23. (A,B) TEM images of nanoshells synthesized in (A) CTAB and (B) CTAC. (C, D) SEM images of nanoshells synthesized in (C) CTAB and (D) CTAC. (E) Extinction spectra of nanoshells synthesized in CTAB (black) and CTAC (red). Reproduced from ref 159 with permission. Copyright 2013 American Chemical Society.

beads decorated with small silver seed particles are used as templates to grow gold nanoshells packed with sharp spike shaped particles. Owing to the highly structured surface, spiky nanoshells showed strong far-field and near-field scattering compared with smooth shells.¹⁶¹ The templated surfactant-assisted seed-growth method is used to synthesize gold nanoshells with varying surface topographies by changing the type of surfactants and ions in the growth solution. In typical syntheses of nanoshells, numerous small silver seed particles (2–5 nm in diameter) are first synthesized on negatively charged carboxylate-modified polystyrene (PS) beads (94.5 ± 7.2 nm in diameter). Subsequently, the seed decorated polymer particles are added to a growth solution containing HAuCl₄, ascorbic acid, AgNO₃, and cationic surfactants. The growth solution containing CTAB as the surfactant generates gold nanoshells that are densely covered with sharp spikes (Figure 23A,C). To understand the role of the surfactant in controlling the surface topography, CTAB is replaced in the growth solution with CTAC, which produces gold nanoshells with a relatively smooth surface (Figure 23B,D). In control experiments with isolated gold seed particles, the CTAB growth solution produces rod-shaped particles, whereas the CTAC growth solution generates quasispherical particles.¹⁶⁴ The preferential binding of bromide ions to select facets of gold particles has been found to promote the growth of anisotropic particles in the presence of CTAB.¹⁶⁵ Smooth CTAC nanoshells showed an SPR band at 710 nm, which is blue-shifted from that of typical spiky shells (Figure 23E). Thus, the nanoparticle growth on a polymer template is somewhat different from that in homogeneous synthesis, because the templated synthesis uses silver seed particles instead of commonly used gold seed particles. The highly structured nanoshells are useful for a number of scattering-based applications of nanoshells including surface-enhanced spectroscopy¹⁶⁶ and photothermal therapy.¹⁶⁷

6.3. Ferns. Interesting fern-like morphologies with enhanced surface Raman effects can be synthesized in the presence of β -cyclodextrin (β -CD),¹⁶⁸ a sugar oligomer with inherent ability to complex the hydrophobic molecules in their nonpolar cavities.^{169–171} The hydrocarbon chain of the surfactant molecule can be easily incorporated into the CD cavity to form β -CD–surfactant inclusion complexes. When an inclusion complex of β -CD–DTAB is used, β -CD-to-DTAB molar ratio shows a remarkable effect on the formation of the Au nanostructures. In the absence of β -CD, the product consists of irregular particles exhibiting faceted surfaces with different sizes because DTAB with C12 is obviously much less surface active in comparison to CTAB with C16. In addition, the bilayer required for the surface passivation is less compact with C12 hydrocarbon length than the bilayer formed by C16. Therefore, random anisotropic growth is expected to occur in the presence of DTAB. Under β -CD to DTAB molar ratio of 0.5, flowerlike aggregates consisting of well-defined, symmetric, planar Au dendrites are obtained (Figure 24).¹⁶⁸ In the formation of such morphologies, DTAB/ β -CD inclusion complexes play an important role. It is well-known that CDs are able to form host–guest complexes with most surfactants with high binding constants by including surfactants into CD cavities.^{172,173} When 2.5 mM 1-adamantanol is added to the mixed DTAB/ β -CD solutions, Au nanodendrites could not be obtained anymore because adamantanol has a very high binding ability with the β -CD cavity and it does not allow the DTAB molecule to complex with the CD cavity.¹⁷⁴ Thus, the specific adsorption of the DTAB/ β -CD inclusion complexes on Au crystal surfaces is

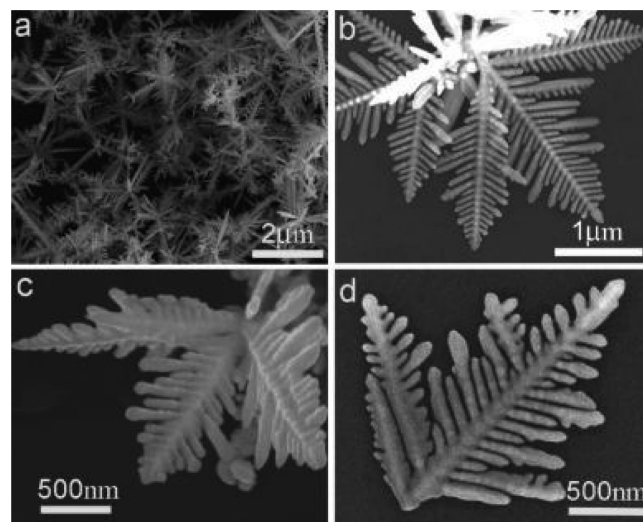


Figure 24. SEM images of Au nanodendrites grown in mixed DTAB/ β -CD solution: [DTAB] = 5.0 mM; [β -CD]/[DTAB] = 0.5. Reproduced from ref 168 with permission. Copyright 2010 American Chemical Society.

considered to contribute to the formation of planar Au nanodendrites.

7. SHAPE CONTROL IN SEMICONDUCTOR NANOPARTICLES

Conventional surfactants have also been widely used for morphology control of chalcogenide nanomaterials just like that of noble metal NPs.^{175–177} The overall role of surfactants in shape control of semiconductor nanomaterials is quite similar to that we have discussed for the noble metal NPs in the previous section. In comparison to the single tail surfactants, double tail surfactants demonstrate high potential for shape control effects because of their greater interfacial adsorption ability, and hence, didodecyl dimethylammonium bromide (12-0-12, critical micelle concentration, cmc = 0.2 mM), dimethylene bis-(dodecyldimethylammonium bromide) (12-2-12, cmc = 0.84 mM), and dimethylene bis(hexadecyldimethylammonium bromide) (16-2-16, cmc = 0.02 mM) have been successfully used as shape directing agents for the synthesis of PbS NPs.¹⁷⁵ They show remarkable control over crystal growth at nanoscale and produce well-defined morphologies. Double tail surfactants^{176–179} are more hydrophobic as well as surface active in comparison to their monomeric homologues, and hence, they are considered to be even better shape directing agents due to a better surface passivation ability. When DTAB is used as a shape directing agent for the synthesis of PbS NPs, large fern like morphologies are produced with an average size distribution close to 5 μ m (Figure 25). However, when DTAB is replaced with 12-0-12 with double hydrocarbon chains of same length, it results in the formation of fine cubes (Figure 26a). Introduction of two methylene groups in the headgroup region of 12-0-12 to convert it into 12-2-12 produces monodisperse hexagons (Figure 26b), while increasing the length of hydrocarbon chain as in the case of 14-2-14 again produces fine cubes (Figure 26c). One would observe a clear correlation between the hydrophobicity of the surfactant and shape evolution of the final morphology. A cube enclosed with {100} crystal planes is generated when a surfactant is highly hydrophobic as in the case of 12-0-12 and 14-2-14; otherwise we will get hexagons bound with {111} crystal planes. Thus, stronger hydrophobicity passivates the {100}

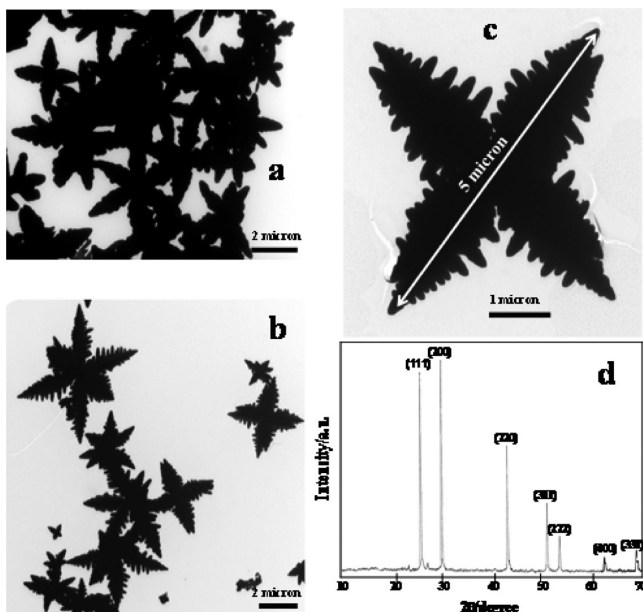


Figure 25. TEM micrographs of PbS MC in the presence of DTAB: (a) $[DTAB] = 0.1\text{ mM}$; (b) $[DTAB] = 1\text{ mM}$; (c) magnified view of single PbS star-shaped MC with an approximate size of $5\text{ }\mu\text{m}$; (d) XRD pattern of PbS MC in the presence of DTAB ($[DTAB] = 5\text{ mM}$). Reproduced from ref 175 with permission. Copyright 2007 American Chemical Society.

crystal planes, and weaker hydrophobicity preserves $\{111\}$ crystal planes of fcc PbS. The latter is due to the greater atomic density of PbS (Pb^+/S^-) on $\{111\}$ facets; hence, they attract relatively lower hydrophobic surfactants. The appearance of large fern like morphologies in the presence of DTAB is also due to the preferential adsorption of surfactant ions on the $\{111\}$ facets. In order to check the surfactant specific shape control behavior, the addition of SDS in a reaction controlled by 12-0-12 or 14-2-14 leads to the formation of large star shaped microcrystals with little shape control effects. Strong electrostatic interactions between the anionic SDS and cationic 12-0-12 or 14-2-14 produce aqueous insoluble salts or large vesicles that have little interfacial adsorption. Hence, the effective concentration of 12-0-12 or 14-2-14 required for the passivation of the $\{100\}$ crystal planes reduces, which in turn allows these planes to further participate in the nucleation and, thus, produces large micrometer sized morphologies. Therefore, shape control effects of

highly hydrophobic surfactants are very specific just like those observed in the Au NPs and can be selectively used for the synthesis of desired morphologies.

Similar morphologies can be obtained for PbSe NPs when cationic surfactants are used for their synthesis.^{176,180–183} Shape controlled reaction of 12-0-12 cationic surfactant produces mostly cubic crystalline geometries of $39.1 \pm 9.1\text{ nm}$ with fine shell of 12-0-12 around each NP. One can find a surfactant monolayer $\sim 1.5\text{ nm}$ thick corresponding to the tail length of C12 (Figure 27). This value is in good agreement with the radius of

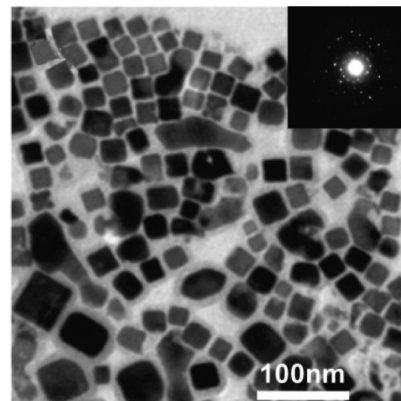


Figure 27. Plate-like core–shell morphologies of predominantly cubic geometries of PbSe particles with a clear surfactant coating of a sample synthesized in the presence of 12-0-12 = 16 mM. Reproduced with permission from ref 176. Copyright 2010 American Chemical Society.

DTAB micelle with C12 carbon tail length, 1.8 nm.¹⁸⁴ A slightly larger latter value can be attributed to the hydrated state of the micelle in comparison to the dried monolayer on the surface of NP. The presence of surfactant monolayer around each NP is further confirmed from the gel electrophoresis. All samples show displacement toward the negatively charged electrode indicating the fact that PbSe NPs are positively charged due to the presence of the monolayer of cationic surfactants.

If the reactions are conducted at high temperature using the growth technique of dynamic injection, fine PbSe nanocubes are produced (Figure 28).¹⁸⁵ This is done by rapidly injecting a phenyl ether solution of lead acetate and trioctylphosphine selenide into a vigorously stirred hot phenyl ether at 180 or 230 °C in the presence of oleic acid, which is a vesicle forming surface

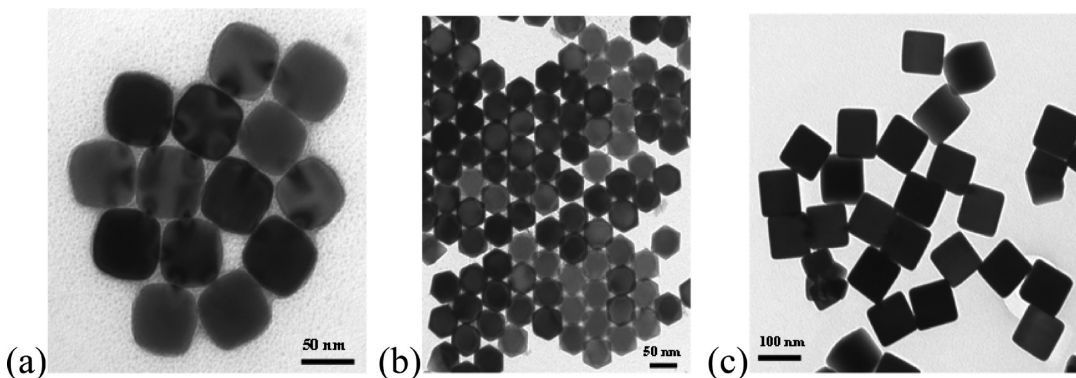


Figure 26. TEM micrographs of PbS NC in the presence of different surfactants: fine monodispersed cubic crystalline NPs prepared (a) with $[12\text{-}0\text{-}12] = 0.5\text{ mM}$, (b) with $[12\text{-}2\text{-}12] = 0.5\text{ mM}$, and (c) with $[14\text{-}2\text{-}14] = 0.5\text{ mM}$. Reproduced from ref 175 with permission. Copyright 2007 American Chemical Society.

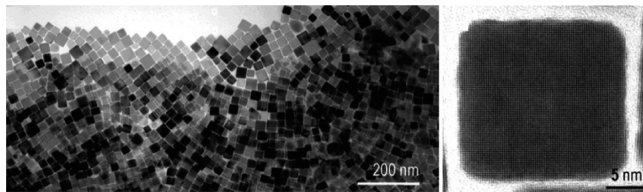


Figure 28. TEM images of a size-selected PbSe nanocube assembly and HRTEM image of a single PbSe nanocube. Reproduced with permission from ref 185. Copyright 2005 American Chemical Society.

active molecule and is aqueous insoluble. Therefore, it is the best stabilizing as well as shape directing agent when the synthesis is carried out in nonaqueous phase. Small PbSe clusters immediately form and grow with stabilization provided by the capping ligands. The shape evolution of PbSe NPs is dependent on the growth time, whereas the NP size can be tuned by varying the growth temperature. The higher growth rate in the $\langle 111 \rangle$ direction compared with that in the $\langle 100 \rangle$ direction results in the formation of nanocubes.

In contrast, the reactions of CuSe NP synthesis in the presence of 16-2-16 generate entirely different shapes.¹⁷⁶ All particles are single crystal and thin nanoplates of polyhedral geometries with size 116 ± 33 nm and thickness $\sim 5\text{--}8$ nm (Figure 29a,b). The EDS spectrum (Figure 29c,d) confirms the presence of Cu and Se in 1:1 atom %. Each single NP has a clear bright shell of surfactant monolayer, which is ~ 2.5 nm thick, corresponding to the radius of the CTAB micelle,¹⁸⁴ with an identical chain length of C16 of 16-2-16. Interestingly, almost all NPs show

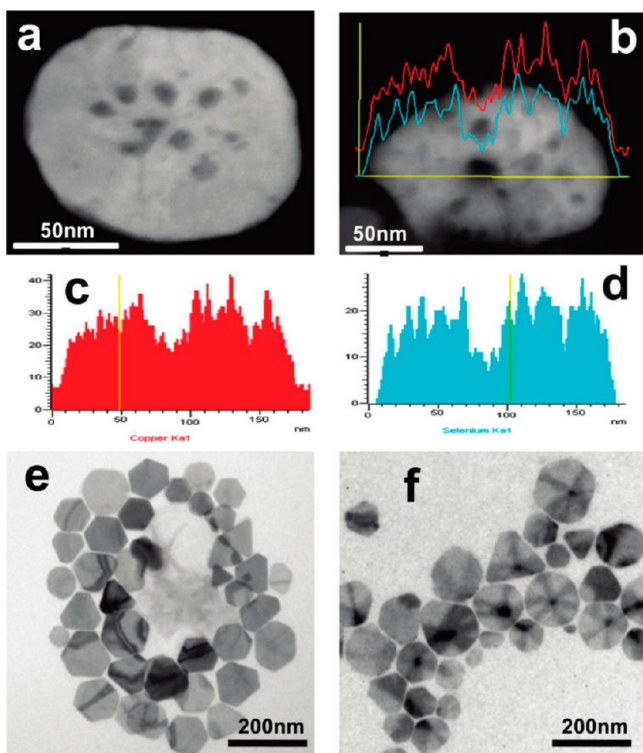


Figure 29. (a) HAADF image of a single nanoplate showing dark perforations. (b) EDX line spectrum confirming the presence of perforations as well as 1:1 composition of Cu (c) and Se (d). Several nanoplates without perforations synthesized in the presence of 12-2-12 = 16 mM (e) and 12-0-12 = 16 mM (f). Reproduced with permission from ref 175. Copyright 2007 American Chemical Society.

perforations (Figure 29a), and the EDS line spectrum confirms this (Figure 29b). However, no perforated NPs are produced in the presence of 12-2-12 and 12-0-12 (Figure 29e,f) with lower hydrophobicity than that of 16-2-16 under similar reaction conditions. This demonstrates that the stronger hydrophobicity influences the thickness of the plates. A thinner nanoplate is prone to perforations due to crystal defects. Since the CuSe colloidal particles are stabilized in aqueous phase, cationic gemini surfactant head groups are in contact with water in order to maintain the colloidal stability, while hydrophobic tails are surface adsorbed on CuSe NPs. This is only possible if the NPs have zero dipole moment.^{186–188} Zero dipole moment is primarily associated with the lattice structure. The {100} crystal facets are made up of both Cu and Se atoms, and hence, they are without any charge polarization. Contrary to this, {111} crystal planes are predominantly occupied by either Cu or Se atoms and, hence, lead to an overall charge separation and establish a dipole. Therefore, the zero dipole moment provides nonpolar properties to {100} crystal planes, which will in turn act as suitable platforms for surfactant adsorption. The nonpolar interactions attract the surfactant hydrophobic tails to have a monolayer formation, while head groups are in contact with the aqueous phase. This arrangement protects the {100} facets from further growth and hence, directs the growth at {110} or {111} crystal planes. Since the {111} facets possess higher surface energy, they are eliminated during the growth in the presence of surfactant. This mechanism has been observed for PbSe nanowire formation.¹⁸⁸ A more tightly packed surfactant layer is more effective in reducing the participation of {100} planes in the crystal growth and, thus, produces flat geometries. The 16-2-16 provides better and tighter surface coverage compared with 12-2-12/12-0-12 and, hence, results in even thinner NP formation. The thinner NPs are more prone to crystal defects, which lead to surface perforations.

Conventional surfactants are used for the synthesis of Se–Te alloy nanomaterials,^{177,189} which demonstrate versatile applications in nanoelectronics. Their synthesis over the whole mole fraction range of Se + Te mixtures is carried out in an aqueous micellar phase of CTAB by simultaneous reduction of sodium selenite and tellurite with hydrazine, which produces different Se–Te alloy nanomorphologies. A drastic change in the shape, structure, and composition of nanomorphologies is observed. At high hydrazine concentrations, Se–Te alloy NPs are always made up of a much greater amount of Te even in the Se-rich region of the mixture. Figure 30 shows a phase diagram of solid nanoalloy solution in which straight dotted lines represent the ideal mixing between elemental Se and Te in Se–Te alloy. Although, both Se and Te undergo spiral trigonal hexagonal atomic arrangement, Se is largely considered as nonmetal with smaller atomic radius (117 pm) than Te (143 pm). Thus, Te possesses greater tendency to show metallic properties than Se^{190–192} with a greater tendency to crystallize in the form of 1D morphologies.^{193–195} A greater aqueous solubility preference of Se nucleating centers leaves a much greater amount of Te in heterogeneous crystalline phase even in the Se-rich region of the mixture. A greater amount of Se produces polyhedral morphologies, while a lesser amount of Se than Te generates rhombohedral NPs, which transform into spindles and finally long needles to ribbons for pure Te. The right-hand side (Se-rich region) of the phase diagram prefers polyhedral or rhombohedral shape, while left-hand side (Te-rich region) favors 1D nanomorphologies. The equimolar region of the mixtures clearly identifies the transitions between the two extremes. All

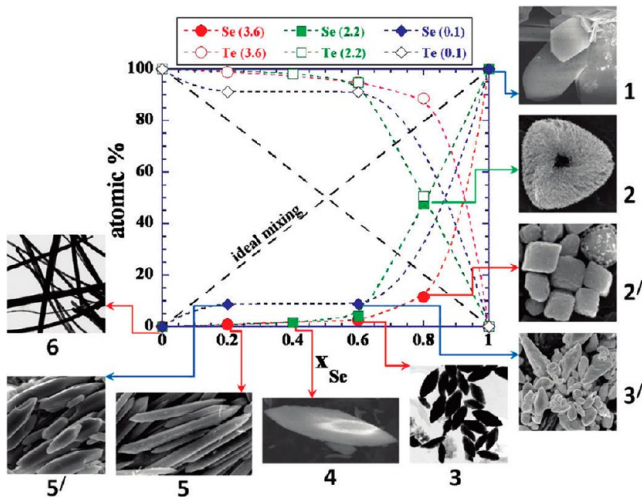


Figure 30. A plot of atom % of Se and Te in Se–Te alloy NCs versus stoichiometric mole fraction of Se over the whole composition range of Se + Te. Reproduced with permission from ref 177. Copyright 2010 American Chemical Society.

morphologies show a complete homogeneous mixing between elemental Se and Te in Se–Te alloy but with a marked nonideal behavior with respect to their stoichiometric mole fractions over the total mixing range. This sequence of phase diagram demonstrates that the shape and size of different morphologies are primarily related to the amount of the Se and Te in the alloy and fully controlled by the CTAB. In fact, the concentration of CTAB decides the overall shape of especially Se NPs. A concentration greater than 0.1 M leads to the formation of nanowires or nanotubes of Se because the reaction is considered to be driven by the micellar template effects. A lower concentration than this usually produces spherical Se NPs. Since all mole ratios are rich in Te, the final morphologies show gradual transformation from nanowires to long needles and then spindles as the amount of Te is increased. However, all morphologies over the entire mole fraction range are well-defined and fully controlled by the stabilizing as well as the shape directing effect of CTAB. A marked difference in the surface adsorption is observed from pure Te to Se as the mole fraction of Se is increased. The formation of the 1D morphologies in the Te-rich region demonstrates the preservation of {100} crystal planes, and growth is mainly directed at the {111} crystal planes, while the opposite is observed in the Se-rich region. The metallic nature of Te allows the preferential adsorption of CTAB on {100} crystal planes that passivates them from further participating in the nucleation process, and hence, the growth is directed at the {111} crystal planes.

Apart from CTAB, nonionic surfactants such as $C_{18}EO_{20}$ and $C_{12}EO_{10}$ are used for the synthesis of Se nanowires and

nanobelts.^{196–198} The extended polar shell of nonionic micelles containing poly(oxyethylene) chains and entrapped water solubilizes amorphous selenium (a-Se)¹⁹⁹ and catalyzes its transition to trigonal (t-Se). The growth of t-Se nanowires proceeds through the continuous addition of Se atoms to the t-Se seeds at the circumferential edges of hexagonally or trigonally faceted seeds. $C_{18}EO_{20}$ micelles are much larger than $C_{12}EO_{10}$ with a larger nonpolar core and a thicker polar shell resulting in a slower diffusion rate of a-Se and favoring the preferential growth of t-Se nanobelts, whereas the smaller $C_{12}EO_{10}$ micelles favor the formation of t-Se nanowires with pseudohexagonal cross sections. In comparison to the CTAB micelles, nonionic micelles are still considered to be better solubilization sites for a-Se because of their hydrated poly(oxyethylene) chains, which provide the required amount of amphiphilicity for favorable solubilization of a-Se. This is obviously not possible for an entirely hydrophobic core of CTAB just above the cmc. But as the concentration of CTAB exceeds 0.1 M, there are large micelle transitions resulting in the formation of wormlike micelles or vesicles entrapping the required amount of water necessary for the diffusion of a-Se in the core during the growth process of 1D morphologies of t-Se.

8. SURFACTANT ASSISTED GROWTH OF NANOPARTICLES IN FILMS

In addition to solution phase, surfactants possess the inherent ability to control the shape and size of nanomaterials in thin films.²⁰⁰ ZnO nanostructured films are prepared in a soft chemical synthesis route by using ZnO seeds in the presence of alkyl sulfate surfactants of different chain lengths, which act as structure-directing agents. These films²⁰¹ find their applications in photocatalysis, photovoltaics,^{202,203} optoelectronic devices,²⁰⁴ biosensors, and gas sensors.^{205,206} Structural properties of the surfactant influence size and morphology of the hybrid surfactant/ZnO lamellar films, thickness, and arrangements. Depending on the hydrocarbon chain length of the alkyl sulfate, well-aligned nanorods or ordered lamellar hybrid structures are obtained. Nanorods are obtained when alkyl sulfate of C8 chain length is used. They are converted into nanoplates when chain length of C10–C18 is selected. SDS (C12) induces much bigger plates with a length of up to 20 μm and a width up to 5 μm . The lamellar structures of nanoplates exhibit alternative layers of ZnO and surfactants. The growth of specific ZnO 1D or 2D nanostructures can be controlled by tuning the length of the surfactant chain. In the absence of surfactants, only ZnO nanorods are obtained, but their growth is inhibited upon the adsorption of alkyl chains on the (00.1) face, which has a higher energy than the lateral and nonpolar faces (Figure 31).²⁰⁰ Both C6 and C8 exhibit no cmc and do not form micelles; therefore, their concentration tends to increase locally when they adsorb onto crystal surfaces.²⁰⁷ This causes a growth inhibition of the

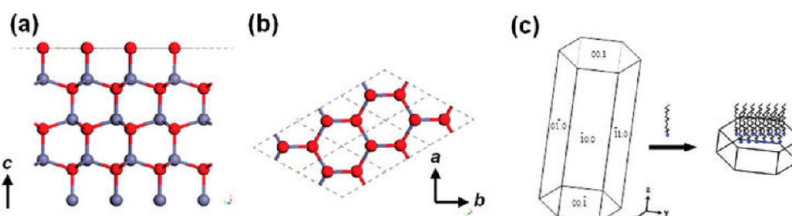


Figure 31. Computational model of ZnO crystal structure: (a) view along the c axis, (b) top view of the (00.1) plane, and (c) growth of ZnO hexagonal crystal in the presence of surfactant. Reproduced with permission from ref 200. Copyright 2011 American Chemical Society.

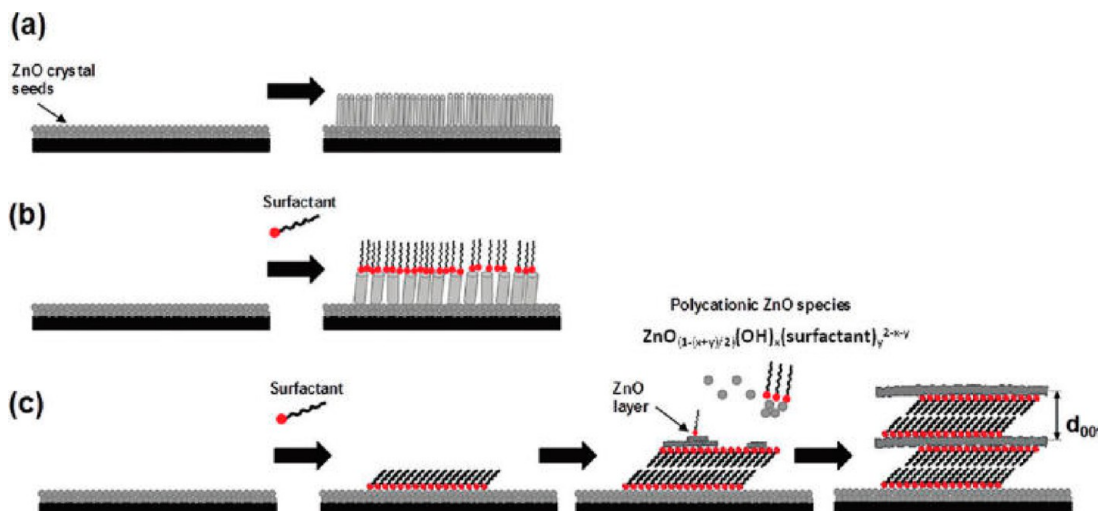


Figure 32. Growth of ZnO nanostructures: (a) nanorods without additive; (b) nanorods in the presence of alkyl sulfates C6 and C8, and (c) lamellar nanostructures in the presence of alkyl sulfates C12–18. Reproduced with permission from ref 200. Copyright 2011 American Chemical Society.

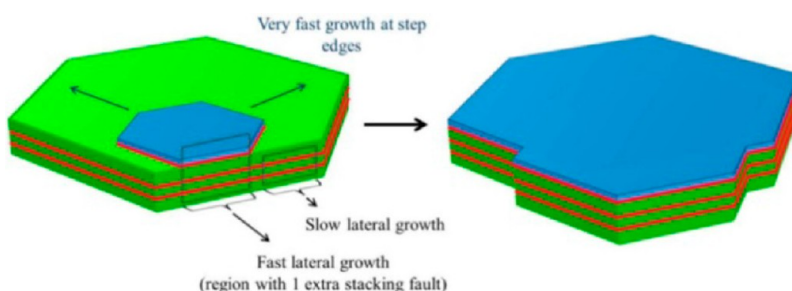


Figure 33. A representation of the proposed mechanism for irregular polygonal plate growth. A new layer (blue) nucleates forming a stacking fault (highlighted in red) with the original plate (green). Where the new layer meets the perimeter of the underlying plate, lateral plate growth is accelerated due to the presence of an additional stacking fault (left). The new layer quickly covers the entire original plate, resulting in a smooth surface and uniform plate thickness (right). Reproduced with permission from ref 208. Copyright 2015 American Chemical Society.

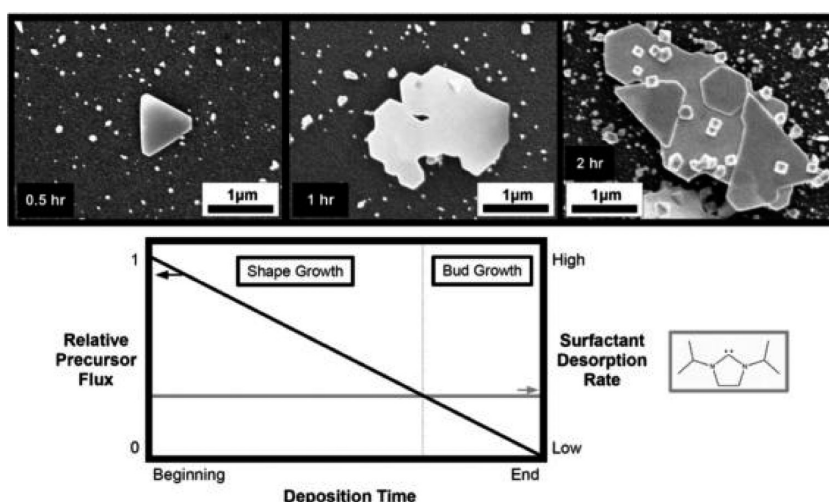


Figure 34. Time-dependent depositions using $[\text{AuN}(\text{SiMe}_3)_2\text{NHC}]$ at 430 °C at 0.5, 1, and 2 h points. A hypothetical plot of both observed growth regimes is shown below. As precursor is depleted from the source, the influx of surfactant also decreases. Plate and wire growth occurs while there is an excess of surface-bound surfactant. Eventually, the rate of surfactant adsorption to the surface is overtaken by the rate of surfactant desorption, and budding occurs. Reproduced with permission from ref 208. Copyright 2015 American Chemical Society.

nanorods, and nanorods of lower aspect ratio are obtained. On the other hand, when the surfactants with hydrocarbon chain length of C10–C18 are used, the growth inhibition is much more because of the greater surface activity with longer hydrocarbon

chain, and hence, nanoplates are formed. The alkyl chains are adsorbed in the form of bilayers onto the (001) plane of the ZnO crystal seeds with long-range order, and the anionic head groups of the second layer are exposed to the solution where they

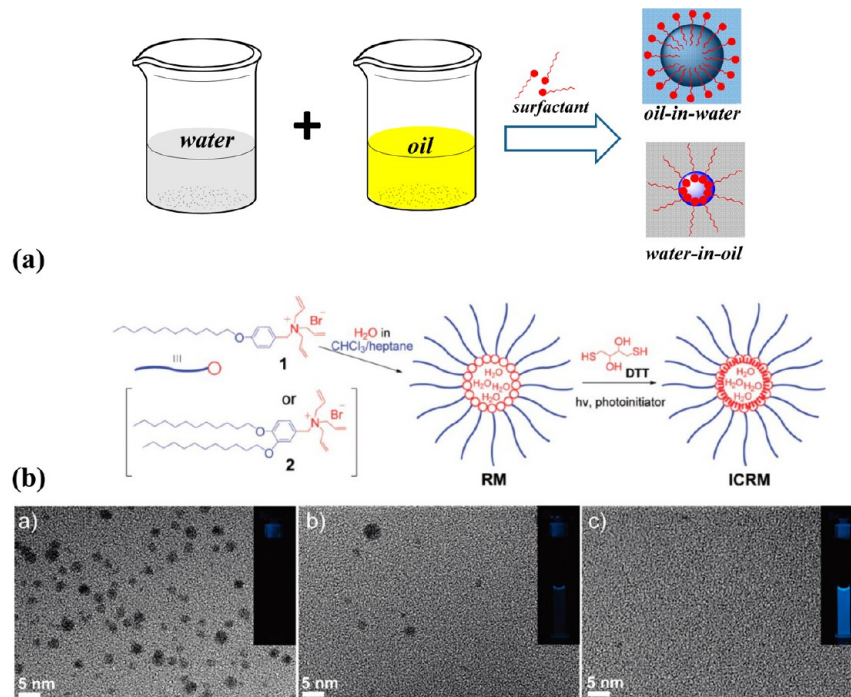


Figure 35. (a) Preparation of emulsion or microemulsion. (b) Preparation of interfacially cross-linked reverse micelles (ICRM) by the thiol–ene addition (upper reaction). TEM micrographs of Au–ICRMs with (a) 1:1, (b) 0.1:1, and (c) 0.02:1 $[\text{HAuCl}_4]/[1]$. The gold nanoparticles appear as dark spots due to their high electron density. Reproduced with permission from ref 217. Copyright 2011 American Chemical Society.

interact with polycationic zinc oxide species leading to the formation of surfactant–Zn hybrid assemblies (Figure 32).²⁰⁰

Thus, the length of the alkylene chain influences the morphology of the plates grown onto the film of ZnO nanoparticles. C12 and C14 surfactants are the most efficient surfactants to form lamellar structures and produce large nanoplates. The results are consistent with the self-assembly behavior of alkyl sulfates in solution and account for the different cmc and solubility in water.

Chemical vapor deposition (CVD) is a widely used technique for the synthesis of thin films.^{208,209} N-Heterocyclic carbenes (NHCs)^{210,211} and trialkylphosphines^{212,213} are chemically similar ligands to surfactants and capping agents, which are used in the synthesis of Au nanocrystals because of their strong coordination to gold. They are used in thermal decomposition and CVD. Two gold precursors, $[\text{AuN}(\text{SiMe}_3)_2\text{NHC}]$ (NHC = 1,3-diisopropyl-imidazolidin-2-ylidene) and $[\text{AuN}-(\text{SiMe}_3)_2(\text{PMe}_3)]$,²¹⁴ for single-source CVD of gold have been used to synthesize various morphologies where the coordinative ligands participate as transient surfactants. Among various morphologies, plates are often obtained compared with hexagons or triangles between 370 and 460 °C due to layer-by-layer growth promoted by stacking faults because gold and silver are known to have low stacking fault energies compared with other metals, which promote plate growth (Figure 33).²⁰⁸ A time-dependent growth profile (Figure 34)²⁰⁸ indicates that the diminished surfactant surface concentration promotes the secondary nucleation sites on all gold surfaces. This makes the nanoparticulate layer dense through secondary nucleation on existing nanoparticles and results in the formation of irregularly shaped plates. The gold surface is assumed to be saturated with surfactant ligand, and the rate of desorption of this surfactant species remains constant at a given temperature. At high temperatures, phosphines are labile when coordinated to gold nanoparticles²¹⁵ and thus more easily dissociate than NHCs and lead to the formation of nanoparticles. However, plate formation

at lower temperatures occurs when precursor flux is reduced or a ligand more readily desorbs.

9. SHAPE CONTROL IN MICROEMULSIONS

An emulsion is obtained when an emulsifier is added in an oil–water immiscible system. The emulsifier has a dual affinity to simultaneously interact with the oil and water phases, and surfactants are the best emulsifiers. Usually emulsions are opaque because the size of the dispersed phase is much larger than the wavelength of visible light; however, transparent or translucent emulsions can be obtained by carefully controlling the concentration of every ingredient of an emulsion so as to achieve tiny droplets with size comparable to the wavelength of visible light.²¹⁶ Reverse micelles (RMs) are formed when a surfactant forms micelles in organic solvent by entrapping aqueous phase in the core of the micelle surrounded by hydrophilic groups in which the arrangement of surfactant molecules is reversed to that in conventional micelles in aqueous phase. RMs are widely utilized as media for catalysis and templates to prepare inorganic nanomaterials in nonaqueous phase,^{217,218} where the dimensions may or may not correspond to the size of the templates because several factors affect the size and morphology of the final nanomaterials.^{219–222} Usually, when a reaction is conducted inside the aqueous pool of an emulsion droplet where preferential adsorption of surfactant onto certain facets of the growing nanocrystals influences the resulting morphology, much different shape and size of the NPs from the actual size of the droplet are obtained.^{223,224} Crystal growth in reverse microemulsions is a complex process that involves the interplay of crystal growth kinetics and thermodynamics in the multiphase system.²²⁵ A precise shape and size of the resulting morphology can be tailored by carefully inducing cross-linking of the surfactant head groups inside the RMs by free radical polymerization (Figure 35).^{217,226,227}

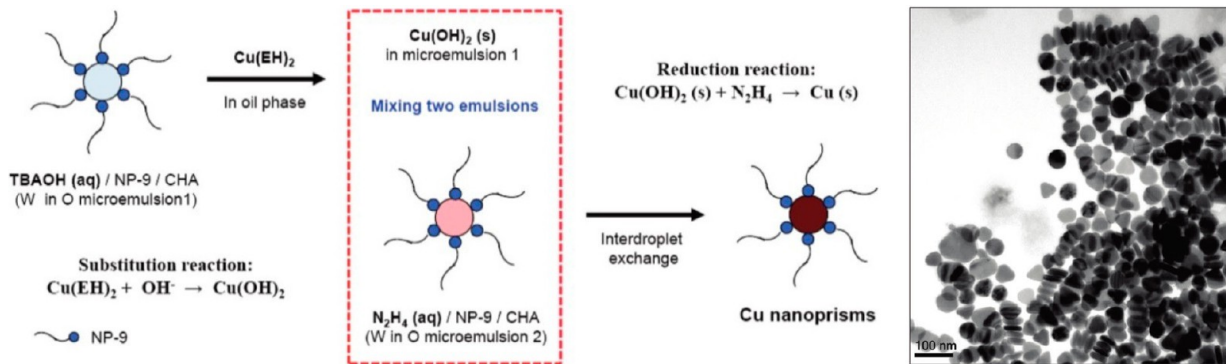


Figure 36. Two-step reaction processed in nonionic W-in-O microemulsions by mixing two microemulsions [2-ethyl hexanoate ($\text{Cu}(\text{EH})_2$); cyclohexene (CHE)]. TEM image of truncated triangular nanoplates prepared in NP-5 microemulsion of $R = 2.0$. Reproduced with permission from ref 228. Copyright 2010 American Chemical Society.

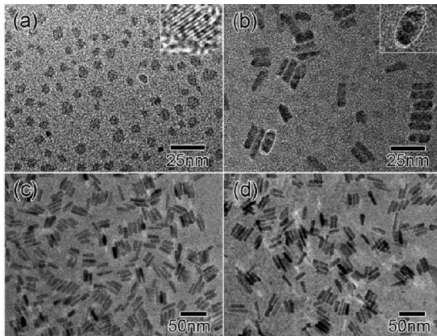
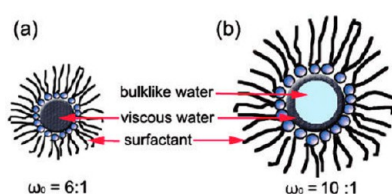


Figure 37. (a) Rigid reverse micelle containing viscous water and (b) soft reverse micelle containing viscous and bulk-like water. TEM images of ZnO nanorods at different reaction times: (a) 0.5, (b) 1.5, (c) 5, and (d) 60 min. Reproduced with permission from ref 229. Copyright 2010 American Chemical Society.

Nanoalloys are obtained by combining two metal precursors in such reactions. Both the structure of the cross-linkable surfactant as well as the cross-linking reaction are critical to the covalent capture of RMs with minimal disturbance to the packing of the surfactants in the RM. A single- and a double-tailed cationic surfactant with the triallylammonium headgroup forms RMs in heptane/chloroform containing a small amount of water. The RMs are cross-linked at the interface upon UV irradiation in the presence of a water-soluble dithiol cross-linker and a photoinitiator (Figure 35). The resulting interfacially cross-linked RMs extract gold chloride and platinum chloride ions from water into the organic phase and convert them into highly luminescent Au and Pt metal nanoparticles, respectively, using a reducing agent with size complementary to that of the RM. Thus, cross-linked RMs can extract metal salts easily into their hydrophilic core, making them ideal templates for nanoparticle synthesis.

Nonionic water in oil (W-in-O) microemulsion is used for the synthesis and geometric control of colloidal truncated triangular copper nanoplates in the presence of tetrabutylammonium (TBA) and alkyl carboxylates (Figure 36).²²⁸ The resulting geometries are strongly influenced by the molar ratio of the two reactants. The same reactions using the identical ionic stabilizers lead to the common production of truncated triangular nanoplates in three different nonionic microemulsions prepared with different lengths of polyoxyethylene groups of polyoxyethylene (POE) nonyl phenyl ethers. Manipulation of size and corresponding optical response are done by altering the type of nonionic surfactants. The average size in nonionic microemulsions is around 50 nm with Igepal CO-520 (NP-5) (hydrophilic–lipophilic balance (HLB) = 10), 60 nm with

Tergitol NP-9 (HLB = 12.9), and 70 nm with Igepal CO-720 (NP-12) (HLB = 14). The morphology of nanoplates is controlled by the tetrabutylammonium alkyl carboxylate salts, while the size is influenced by the water phases stabilized by different POE blocks of nonionic surfactants because the size of nanoplates increases as the length of hydrophilic chains increases. In W-in-O emulsion, the reaction is controlled by the water pool in the droplet, the magnitude of which is related to the degree of hydration of hydrophilic chains. Longer hydrophilic chains obviously possess greater hydration (Figure 36). Thus, the growth of the nucleating centers in the aqueous pool is influenced by the amount of water-soluble precursors, and hence, larger morphologies are expected when a larger aqueous pool is present. In this way, one can have precise control over the size of the NPs simply by controlling length of the hydrophilic chain of polyoxyethylene nonyl phenyl ether nonionic surfactants.

ZnO nanotetrahedra and nanorods are synthesized in a W-in-O microemulsion system using bis(2-ethylhexyl) sulfosuccinate sodium salt (AOT) and carbon tetrachloride (CCl_4).²²⁹ $\text{Zn}(\text{NO}_3)_2$ and monoethanol amine (MEA) are used as precursors to produce ZnO nanostructures. The RMs containing different precursors are first mixed and then kept at room temperature or heated to high temperature for reaction²²¹ to achieve desired growth. If the synthesis is conducted by using a hot mixing method, the RMs are first heated and then mixed, producing monodisperse nanoparticles. At a low ratio of water to surfactant concentration ($w_0 = 6:1$), many ZnO tetrahedra are formed because the RMs are expected to be smaller and most of the water molecules interact with surfactants and exist in the form

of “viscous water”²³⁰ (Figure 37)²²⁹ present at the interface between the pool of water and hydrocarbon layer constituted by the surfactant tails. ZnO nanocrystals formed in viscous water interact with surfactant molecules directly at the interface. The surfactant molecules are absorbed onto the high-energy {110} and {101} planes, thus depressing their preferential growth and leading to the formation of ZnO tetrahedra. As the ratio of water to surfactant increases, the equilibrium size of RMs becomes larger with a large water pool in the center of the droplet producing ZnO nanorods over a period of time (Figure 37).²²⁹ In the hot mixing, several ZnO nuclei are formed simultaneously in a reverse micelle with polar features due to the positively charged {001} planes composed of Zn atoms and negatively charged {001̄} planes composed of O atoms. They undergo oriental attachment due to Ostwald ripening^{32–35} and eventually convert into perfect ZnO nanorods. Thus, the morphology and optical properties of ZnO nanostructures can be easily tuned by adjusting the ratio of water to surfactant concentration. The hot mixing of RMs is not limited to the synthesis of ZnO nanostructures and can be applied in other reaction systems for various products with high uniformity and tunable properties.

Likewise, one-dimensional CdSe nanoparticles are synthesized by using a combination of the RMs of AOT and the hydrothermal method.²³¹ AOT forms cylindrical RMs with hydrazine hydrate when a mixture of hydrazine hydrate and aqueous Na₂SeO₃ solution is added with constant stirring into the AOT and Cd²⁺ solution. The solution is transferred to an autoclave and heated to initiate nucleation and growth. A mixture of small spherical and short rod-like nanoparticles is produced. Slowly, cylindrical RMs are gradually destroyed due to the elevated temperature and pressure in the autoclave. The larger rod-like nanoparticles settle at the bottom of the autoclave, and this morphology is controlled by the amount of AOT, the amount of hydrazine hydrate, and the reaction temperature. AOT restricts the growth of the length and hydrazine hydrate controls the growth of the CdSe nanorods. The mechanism consists of various steps (Figure 38).²³¹ Initially RM solubilized

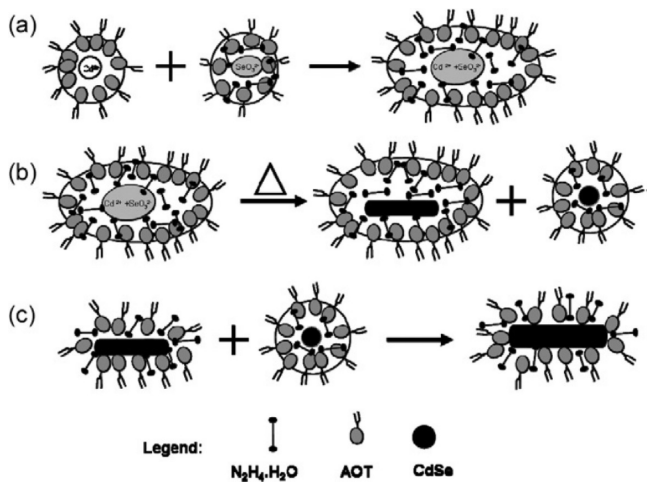


Figure 38. Proposed model of the process of nanoparticle formation in RMs assisted by the hydrothermal method: (a) fusion and exchange of the contents within the cores and redispersion of the RMs before heating; (b) nucleation and growth of spherical and rodlike nanoparticles with heating and pressure before micelles collapse; (c) further growth of nanorods provided by directional aggregation of smaller particles including shorter rods and nuclei after micelles collapse. Reproduced with permission from ref 231. Copyright 2008 Elsevier.

Cd²⁺ and SeO₃²⁻ ions merge to initiate the formation of CdSe nucleating centers in the presence of hydrazine. These nucleating centers grow under hydrothermal treatment, and the morphology control is carried out by the AOT surfactant molecules to produce small CdSe nanorods. RMs cannot be stabilized at elevated temperature due to the increasing Brownian motions and decreasing amphiphilic interactions among the surfactant molecules with the result that the confinement of the nanorods cannot be restricted anymore in the micelle cages and, hence, small NPs further fuse and grow into the large nanorods.

A similar method has been used to synthesize the magnetic cobalt nanocrystals in RMs followed by hydrothermal treatment.²³² The synthesis is carried out by first mixing an aqueous solution containing cobalt chloride and poly(sodium 4-styrenesulfonate) (PSS) with an organic mixture containing CTAB to form RMs. Cobalt ions are reduced with sodium borohydride, which produces well-dispersed CTAB/PSS-encapsulated cobalt nanocrystals of 3.5 nm. Didodecyldimethylammonium bromide (DDAB)/toluene RMs solution,²³³ as well as cobalt(II) bis(2-ethylhexyl) sulfosuccinate [Co(AOT)₂] RMs,²³⁴ are used for the synthesis of cobalt NPs. PSS is a water-soluble polymer that complexes electrostatically at the interface with the cationic CTAB head groups in the RMs creating an electric double layer, which entraps the aqueous pool in the revered micelle (Figure 39).²¹² The Co²⁺ ions solubilized in the aqueous pool adsorb electrostatically onto the backbone of polyanionic PSS. In this way, the electrical double layer acts as an oxygen impermeable shell to protect cobalt nanocrystals from oxidation. It is followed by the hydrothermal treatment at high temperature and pressure. The cobalt nanoparticles usually have low crystallinity, while CTAB/PSS-encapsulated nanoparticles can remain intact at high temperature and pressure during the hydrothermal treatment, thus allowing the cobalt nanoparticles to nucleate and recrystallize without agglomeration. Thus, the shape and the size of the Co NPs synthesized in this way are usually complementary to that of the size of the RMs.

α -Calcium sulfate hemihydrate (α -HH) is a very important class of cementitious material, which is widely applied in molding, special binder systems, and the construction industry due to its high strength.²³⁵ It is also found in a number of orthopedic applications, including bone cement and bone graft substitutes.^{236–238} The α -HH crystals with a spherical shape or a low aspect ratio are preferable for use in bone cement because they are easy to inject and have preferable mechanical properties.²³⁹ Therefore, their morphological control is an important aspect for their appropriate performance in these applications. α -HH NPs are synthesized by mixing two microemulsions containing aqueous CTAB as dispersed and n-hexanol as the continuous oil phase in the presence of CaCl₂ and H₂SO₄ separately in these microemulsions and maintained at 95.0 °C for 1.0 h, which leads to the formation of calcium sulfate particles.²⁴⁰ The same reactions are also performed in the mixed CTAB and SDS microemulsions. Both CTAB and SDS and their ratio play a key roles in controlling the morphology of α -HH nanomaterials (Figure 40). The crystal lattice of α -HH consists of repeating –Ca– and –SO₄– in chains of –Ca–SO₄–Ca–SO₄– in which each S atom is covalently bonded to four O atoms that form a tetrahedral corner.²⁴¹ This provides a greater distribution of SO₄²⁻ ions on the side facets of {110} and {100} and a greater distribution of Ca²⁺ ions on the top facets of {111}.²⁴² Thus, the {110} and {100} facets of the α -HH crystal are negatively charged and interact strongly with CTAB, while positively charged {111} facets interact with anionic SDS. The

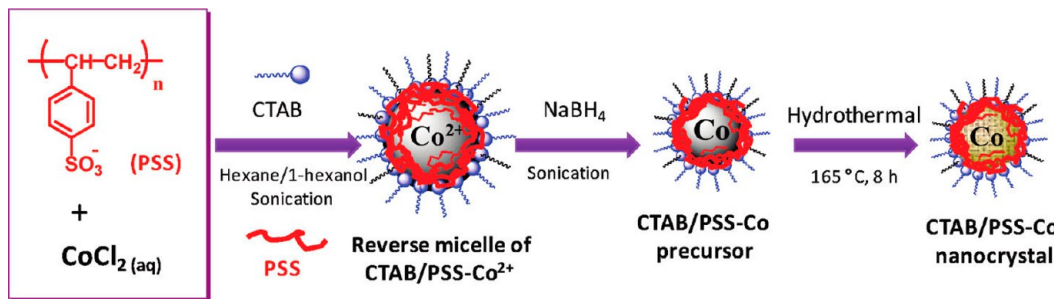


Figure 39. Synthesis of cobalt nanocrystals with surfactant/polymer complex coatings. Reproduced with permission from ref 232. Copyright 2010 American Chemical Society.

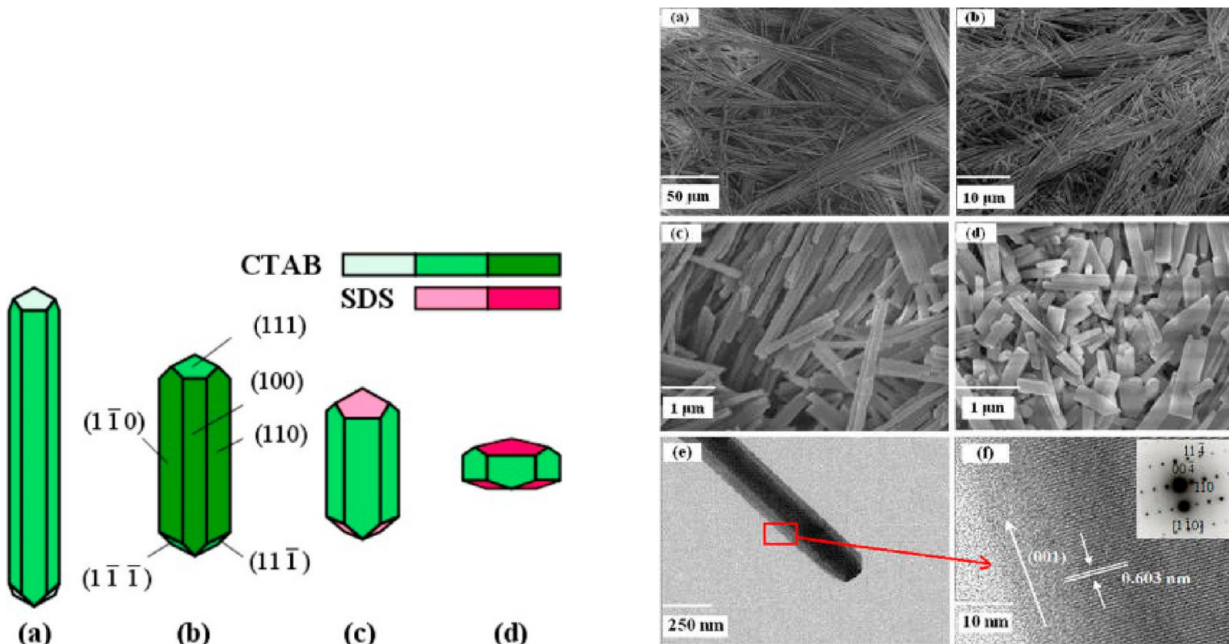


Figure 40. Schematic representation of α -HH growth in the CTAB stabilized reverse microemulsion with or without SDS. SEM images of α -HH synthesized at the mass ratio of CTAB/ H_2O (a) 1.3, (b) 2.0, (c) 3.5, and (d) 4.5. (e, f) TEM and HRTEM images and SAED pattern. Reproduced with permission from ref 240. Copyright 2012 American Chemical Society.

preferential adsorption of CTAB molecules to the $\{110\}$ and $\{100\}$ facets of α -HH directs the crystal growth on $\{111\}$ facet resulting in the formation of rod-shaped crystals^{243,244} (Figure 40), the size of which is much larger than that of the microemulsion droplet.²⁴⁵ The aspect ratio of α -HH nanorods is controlled by the mass ratio of CTAB/ H_2O , and the interactions between the microemulsion droplets and the surfaces of the growing crystals. Unlike CTAB, SDS adsorbs more strongly on the positively charged $\{111\}$ facets and, hence, blocks the crystal growth along the *c* axis. This induces transitions from rods to hexagonal plates and eventually to nanograins with increase in the amount of SDS. Thus, a preferential adsorption of CTAB and SDS controls the overall morphology of the nanocrystal.

To develop heterogeneous catalytic materials with a stable active metal surface area and high selectivity, coated materials with catalytically active metal surfaces covered by porous oxides have drawn attention for their unique advantages in various catalytic reactions.^{245–249} Several synthetic strategies have emerged for encapsulation of metal particles in cavities to prepare coated catalysts. SiO_2 nanotubes containing Ni nanoparticles can be synthesized in a nonionic surfactant W-in-O microemulsion (Figure 41).²⁵⁰ Cyclohexane (C_6H_{12}) is used to

form the oil phase, and polyoxyethylene (10) cetyl ether ($\text{C}_{16}\text{E}_{10}$) is used as the nonionic surfactant, while tetraethyl orthosilicate (TEOS, $\text{Si}(\text{OCH}_2\text{CH}_3)_4$) and $\text{Ni}(\text{NO}_3)_2$ are the silica and Ni precursors, respectively, to produce Ni@SiO_2 particles. This reaction creates a gas phase that remains entrained in RMs and effects the elongation and agglomeration of silica species, thus leading to the formation of a cavity. The cavity length strongly depends on aging time before silica precursor addition, hydrazine concentration, and synthesis temperature. Formation of the elongated rodlike or cylindrical micelles is attributed to the suppression of electrostatic repulsions between hydrophilic head groups and favorable interactions between the hydrophobic tail groups,^{251,252} while electrostatic repulsions between the charged hydrophilic surfactant groups produce spherical micelles. The elongation of RMs is produced by nonionic surfactant when the hydrophobic groups become less miscible with the continuous oil phase due to shorter alkyl chain length.^{253–255} The degree of elongation increases with temperature and leads to a gas phase formation in the micelles that is the driving force for the cavity formation (Figure 41). Such micelle templates are responsible for the formation of nanotubes.

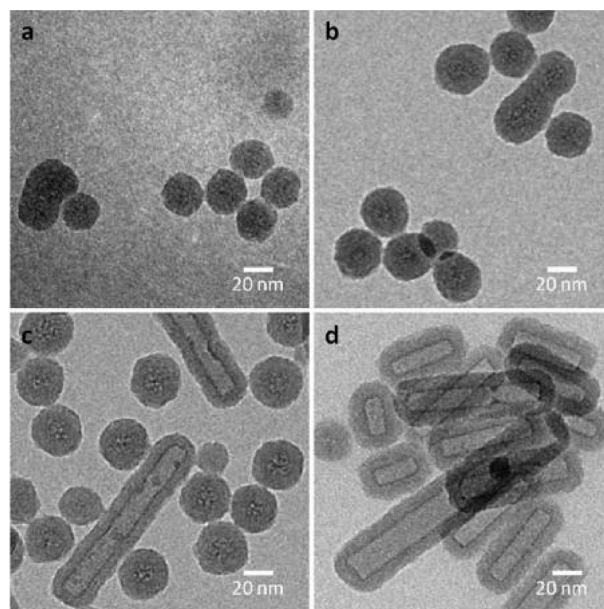
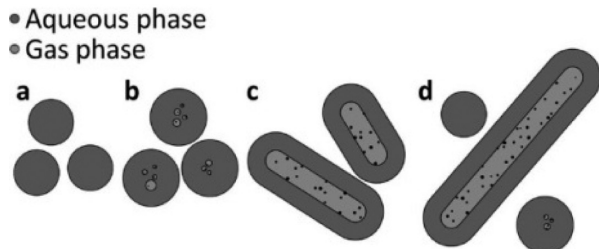


Figure 41. Schematic illustration (left) of gas-induced elongation profile of RMs over time: (a) initial spherical RMs containing Ni^{2+} and N_2H_4 ; (b) larger spherical micelles containing small amounts of entrained gas; (c) elongated micelles with distinct gas phases; (d) further elongated micelles with reformed spherical micelles. TEM images (right) of calcined $\text{Ni}@\text{SiO}_2$ samples synthesized with varying $\text{N}_2\text{H}_4/\text{Ni}$ concentration: (a) $\text{N}_2\text{H}_4/\text{Ni} = 3$; (b) $\text{N}_2\text{H}_4/\text{Ni} = 12$; (c) $\text{N}_2\text{H}_4/\text{Ni} = 24$; (d) $\text{N}_2\text{H}_4/\text{Ni} = 45$. (Reproduced with permission from ref 250).

10. CONCLUDING REMARKS AND FUTURE PERSPECTIVES

This review summarizes the comprehensive details of shape control effects of surfactants on the synthesis of nanomaterials. Surfactants in their monomeric, micellar, vesicular, wormlike, and microemulsion forms possess inherent ability to control the crystal growth of nanomaterials to achieve desired morphologies (Figure 42). Although some studies have reported shape controlled morphologies of different nanomaterials in the absence of surfactants,^{256–259} surfactants with their unique ability of interfacial adsorption still enjoy the status of the best shape directing agents. The review mainly focuses on conventional surfactants, though there are many other categories of surface active species such as surface active polymers, proteins, carbohydrates, and lipids that can be used for shape controlled synthesis. In terms of biological sustainable materials and their exciting biological applications in nanomedicine, the shape control behavior of surface active biomolecules needs to be exploited (Figure 42). Surface active biomolecules can be used in the shape controlled synthesis of nanomaterials though there are few studies in this direction.^{259–263} Robust conventional pharmaceutically important proteins such as BSA and zein can be used in the shape control reactions even at moderately high temperature of $\sim 100^\circ\text{C}$ where protein acts as a weak reducing as well as stabilizing agent^{260,261,263} in the synthesis of especially bioactive Au NPs, which can act as biomarkers or drug release vehicles in systemic circulation. For a quantitative drug release in systemic circulation, monodisperse biomolecule coated NPs with little hemolysis are needed. This is only possible when the NPs are completely passivated by surface active proteins such as BSA to minimize their interactions with blood cells. Thus, well-known shape control strategies can be easily extended to biomaterials of desired shape and size for biomedical applications and implementation as devices in biological systems where shape and size are the most important characteristic features for miniature device implantation.

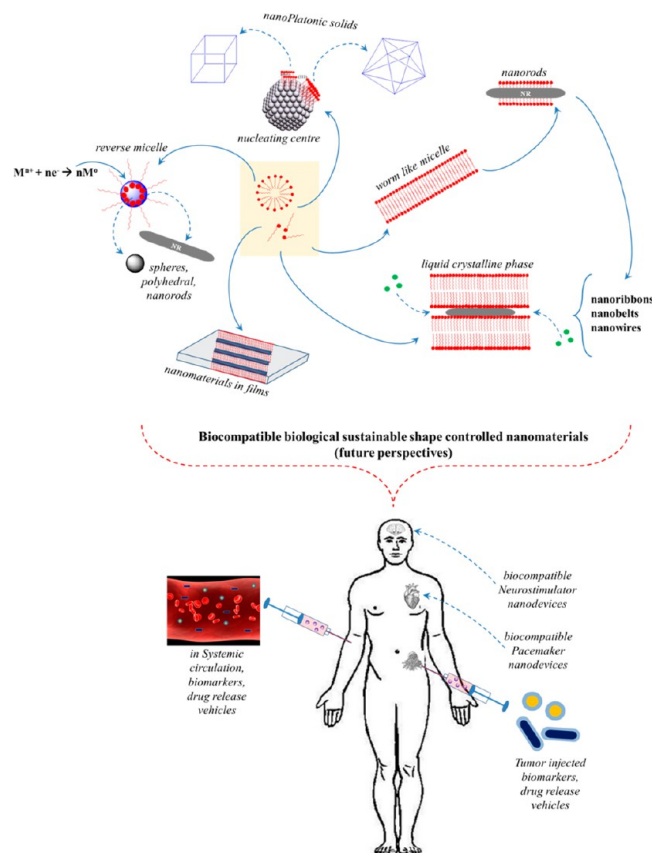


Figure 42. A summary of shape control behavior of surfactant in its different self-assembled templating states to produce morphologies of desired shape and size (upper flow diagram). Similar strategies can be employed to achieve biologically sustainable materials for several important biological applications in nanomedicine (lower flow diagram).

AUTHOR INFORMATION

Corresponding Author

*E-mail: ms_bakshi@yahoo.com.

Notes

The authors declare no competing financial interest.

ACKNOWLEDGMENTS

These studies were partially supported by financial assistance under Article 28.8 of the CAS agreement of WLU, Waterloo.

REFERENCES

- (1) Kawai, T.; Neivandt, D. J.; Davies, P. B. Sum Frequency Generation on Surfactant-Coated Gold Nanoparticles. *J. Am. Chem. Soc.* **2000**, *122*, 12031–12032.
- (2) Barhoum, A.; Rahier, H.; Abou-Zaied, R. E.; Rehan, M.; Dufour, T.; Hill, G.; Dufresne, A. Effect of Cationic and Anionic Surfactants on the Application of Calcium Carbonate Nanoparticles in Paper Coating. *ACS Appl. Mater. Interfaces* **2014**, *6*, 2734–2744.
- (3) Dalfovo, M. C.; Salvarezza, R. C.; Ibanez, F. J. Improved Vapor Selectivity and Stability of Localized Surface Plasmon Resonance With a Surfactant-Coated Au Nanoparticles Film. *Anal. Chem.* **2012**, *84*, 4886–4892.
- (4) Csik, I.; Russo, S. P.; Mulvaney, P. Density Functional Study of Surface Passivation of Nonpolar Wurtzite CdSe Surfaces. *J. Phys. Chem. C* **2008**, *112*, 20413–20417.
- (5) Manna, L.; Wang, Cingolani, R.; Alivisatos, A. P. First-Principles Modeling of Unpassivated and Surfactant-Passivated Bulk Facets of Wurtzite CdSe: A Model System for Studying the Anisotropic Growth of CdSe Nanocrystals. *J. Phys. Chem. B* **2005**, *109*, 6183–6192.
- (6) Zanella, M.; Maserati, L.; Pernia Leal, M.; Prato, M.; Lavieille, R.; Povia, M.; Krahne, R.; Manna, L. Atomic Ligand Passivation of Colloidal Nanocrystal Films Via Their Reaction With Propyltrichlorosilane. *Chem. Mater.* **2013**, *25*, 1423–1429.
- (7) Usui, H. Influence of Surfactant Micelles on Morphology and Photoluminescence of Zinc Oxide Nanorods Prepared by One-Step Chemical Synthesis in Aqueous Solution. *J. Phys. Chem. C* **2007**, *111*, 9060–9065.
- (8) Watt, J.; Cheong, S.; Tilley, R. D. How to Control the Shape of Metal Nanostructures in Organic Solution Phase Synthesis for Plasmonics and Catalysis. *Nano Today* **2013**, *8*, 198–215.
- (9) Zhang, J. W.; Hou, C. P.; Huang, H.; Zhang, L.; Jiang, Z. Y.; Chen, G. X.; Jia, Y. Y.; Kuang, Q.; Xie, Z. X.; Zheng, L. S. Surfactant-Concentration-Dependent Shape Evolution of AuPd Alloy Nanocrystals From Rhombic Dodecahedron to Trisoctahedron and Hexoctahedron. *Small* **2013**, *9*, 538–544.
- (10) Dong, H. P.; Wang, Y. J.; Tao, F. F.; Wang, L. X. Electrochemical Fabrication of Shape-Controlled Copper Hierarchical Structures Assisted by Surfactants. *J. Nanomater.* **2012**, *2012*, 901842.
- (11) Xiao, J. Y.; Qi, L. M. Surfactant-Assisted, Shape-Controlled Synthesis of Gold Nanocrystals. *Nanoscale* **2011**, *3*, 1383–1396.
- (12) Xing, R.; Lehmler, H. J.; Knutson, B. L.; Rankin, S. E. Demixed Micelle Morphology Control in Hydrocarbon/Huorocarbon Cationic Surfactant Templating of Mesoporous Silica. *J. Phys. Chem. C* **2010**, *114*, 17390–17400.
- (13) Zhao, N.; Qi, L. M. Low-Temperature Synthesis of Star-Shaped PbS Nanocrystals in Aqueous Solutions of Mixed Cationic/Anionic Surfactants. *Adv. Mater.* **2006**, *18*, 359–362.
- (14) Yang, Y. C.; Wang, H. J.; Whang, J.; Huang, J. S.; Lyu, L. M.; Lin, P. H.; Gwo, S.; Huang, M. H. Facet-Dependent Optical Properties of Polyhedral Au-Cu₂O Core-Shell Nanocrystals. *Nanoscale* **2014**, *6*, 4316–4324.
- (15) Ghosh, S. K.; Nath, S.; Kundu, S.; Esumi, K.; Pal, T. Solvent and Ligand Effects on the Localized Surface Plasmon Resonance (LSPR) of Gold Colloids. *J. Phys. Chem. B* **2004**, *108*, 13963–13971.
- (16) Dalfovo, M. C.; Salvarezza, R. C.; Ibanez, F. J. Improved Vapor Selectivity and Stability of Localized Surface Plasmon Resonance With a Surfactant-Coated Au Nanoparticles Film. *Anal. Chem.* **2012**, *84*, 4886–4892.
- (17) Matthews, J. R.; Payne, C.; Hafner, J. H. Analysis of Phospholipid Bilayers on Gold Nanorods by Plasmon Resonance Sensing and Surface-Enhanced Raman Scattering. *Langmuir* **2015**, *31*, 9893–9900.
- (18) Bastus, N. G.; Comenge, J.; Puntes, V. Kinetically Controlled Seeded Growth Synthesis of Citrate-Stabilized Gold Nanoparticles of Up to 200 nm: Size Focusing Versus Ostwald Ripening. *Langmuir* **2011**, *27*, 11098–11105.
- (19) Henglein, A.; Giersig, M. Formation of Colloidal Silver Nanoparticles: Capping Action of Citrate. *J. Phys. Chem. B* **1999**, *103*, 9533–9539.
- (20) Wang, W.; Gu, B.; Liang, L.; Hamilton, W. A. Adsorption and Structural Arrangement of Cetyltrimethylammonium Cations at the Silica Nanoparticle–Water Interface. *J. Phys. Chem. B* **2004**, *108*, 17477–17483.
- (21) Sau, T. K.; Murphy, C. J. Self-Assembly Patterns Formed Upon Solvent Evaporation of Aqueous Cetyltrimethylammonium Bromide-Coated Gold Nanoparticles of Various Shapes. *Langmuir* **2005**, *21*, 2923–2929.
- (22) Bakshi, M. S.; Zhao, L.; Smith, R.; Possmayer, F.; Petersen, N. O. Metal Nanoparticle Pollutants Interfere With Pulmonary Surfactant Function In Vitro. *Biophys. J.* **2008**, *94*, 855–868.
- (23) Zhu, T. J.; Chen, X.; Meng, X. Y.; Zhao, X. B.; He, J. Anisotropic Growth of Cubic PbTe Nanoparticles to Nanosheets: Controlled Synthesis and Growth Mechanisms. *Cryst. Growth Des.* **2010**, *10*, 3727–3731.
- (24) Lee, I.; Zaera, F. Catalytic Conversion of Olefins on Supported Cubic Platinum Nanoparticles: Selectivity of (100) Versus (111) Surfaces. *J. Catal.* **2010**, *269*, 359–366.
- (25) Bhattacharya, S.; Biswas, J. Role of Spacer Lengths of Gemini Surfactants in the Synthesis of Silver Nanorods in Micellar Media. *Nanoscale* **2011**, *3*, 2924–2930.
- (26) Tian, G. R.; Sun, S. X.; Song, X. Y.; Zhao, W.; You, T. Catanionic Surfactants Assisted Synthesis of Dilead Pentaoxochromate Nanorods. *Cryst. Res. Technol.* **2008**, *43*, 817–822.
- (27) Yoshida, K.; Jiu, J.; Nagamatsu, D.; Nemoto, T.; Kurata, H.; Adachi, M.; Isoda, S. Structure of TiO₂ Nanorods Formed With Double Surfactants. *Mol. Cryst. Liq. Cryst.* **2008**, *491*, 14–20.
- (28) De Sio, L.; Annesi, F.; Placido, T.; Comparelli, R.; Bruno, V.; Pane, A.; Palermo, G.; Curri, M. L.; Umeton, C.; Bartolino, R. Templating Gold Nanorods With Liquid Crystalline DNA. *J. Opt.* **2015**, *17*, 025001.
- (29) Meuer, S.; Oberle, P.; Theato, P.; Tremel, W.; Zentel, R. Liquid Crystalline Phases From Polymer-Functionalized TiO₂ Nanorods. *Adv. Mater.* **2007**, *19*, 2073–2078.
- (30) Bu, W. B.; Hua, Z. L.; Zhang, L. X.; Chen, H. R.; Huang, W. M.; Shi, J. L. Surfactant-Assisted Synthesis of Lanthanide Phosphates Single-Crystalline Nanowires/Nanorods. *J. Mater. Res.* **2004**, *19*, 2807–2811.
- (31) Bakshi, M. S.; Possmayer, F.; Petersen, N. O. Aqueous-Phase Room-Temperature Synthesis of Gold Nanoribbons: Soft Template Effect of a Gemini Surfactant. *J. Phys. Chem. C* **2008**, *112*, 8259–8265.
- (32) Sahu, P.; Prasad, B. L. V. Time and Temperature Effects on the Digestive Ripening of Gold Nanoparticles: Is There a Crossover From Digestive Ripening to Ostwald Ripening? *Langmuir* **2014**, *30*, 10143–10150.
- (33) Zong, R. L.; Wang, X. L.; Shi, S. K.; Zhu, Y. F. Kinetically Controlled Seed-Mediated Growth of Narrow Dispersed Silver Nanoparticles Up to 120 nm: Secondary Nucleation, Size Focusing, and Ostwald Ripening. *Phys. Chem. Chem. Phys.* **2014**, *16*, 4236–4241.
- (34) Zhang, W. Z.; Qiao, X. L.; Qiu, X. L.; Chen, Q. Y.; Cai, Y. C.; Chen, H. Q. Controllable Synthesis and Ostwald Ripening of Silver Nanoparticles. *Curr. Nanosci.* **2013**, *9*, 753–758.
- (35) Bastus, N. G.; Comenge, J.; Puntes, V. Kinetically Controlled Seeded Growth Synthesis of Citrate-Stabilized Gold Nanoparticles of Up to 200 nm: Size Focusing Versus Ostwald Ripening. *Langmuir* **2011**, *27*, 11098–11105.

- (36) Bakshi, M. S. Room Temperature Surfactant Assisted Crystal Growth of Silver Nanoparticles to Nanoribbons. *J. Nanosci. Nanotechnol.* **2010**, *10*, 1757–1765.
- (37) Ni, C.; Hassan, P. A.; Kaler, E. W. Structural Characteristics and Growth of Pentagonal Silver Nanorods Prepared by a Surfactant Method. *Langmuir* **2005**, *21*, 3334–3337.
- (38) Bakshi, M. S.; Singh, J.; Singh, K.; Kaur, G. Mixed Micelles of Cationic Gemini With Tetraalkyl Ammonium and Phosphonium Surfactants: the Head Group and Hydrophobic Tail Contributions. *Colloids Surf., A* **2004**, *234*, 77–84.
- (39) Bakshi, M. S.; Singh, J.; Singh, K.; Kaur, G. Mixed Micelles of Cationic 12-2-12 Gemini With Conventional Surfactants: the Head Group and Counter ion Effects. *Colloids Surf., A* **2004**, *237*, 61–71.
- (40) Bakshi, M. S.; Singh, K. Synergistic Interactions in the Mixed Micelles of Cationic Gemini With Zwitterionic Surfactants: Fluorescence and Krafft Temperature Studies. *J. Colloid Interface Sci.* **2005**, *287*, 288–297.
- (41) Bakshi, M. S.; Singh, K.; Kaur, G.; Yoshimura, T.; Esumi, K. Spectroscopic Investigation on the Hydrophobicity in the Mixtures of Nonionic Plus Twin Tail Alkylammonium Bromide Surfactants. *Colloids Surf., A* **2006**, *278*, 129–139.
- (42) Bakshi, M. S.; Kaur, G.; Yoshimura, T.; Esumi, K. Azeotropic Mixing of C₁₆peLac With Different Surfactants of Monomeric and Dimeric Nature Under the Effect of Temperature. *Colloids Surf., A* **2006**, *281*, 163–170.
- (43) Zhao, N.; Wei, Y.; Sun, N.; Chen, Q.; Bai, J.; Zhou, L.; Qin, Y.; Li, M.; Qi, L. Controlled Synthesis of Gold Nanobelts and Nanocombs in Aqueous Mixed Surfactant Solutions. *Langmuir* **2008**, *24*, 991–998.
- (44) Shi, H.; Qi, L.; Ma, J.; Cheng, H.; Zhu, B. Synthesis of Hierarchical Superstructures Consisting of BaCrO₄ Nanobelts in Cationic Reverse Micelles. *Adv. Mater.* **2003**, *15*, 1647–1651.
- (45) Shi, H.; Qi, L.; Ma, J.; Wu, N. Architectural Control of Hierarchical Nanobelt Superstructures in Cationic Reverse Micelles. *Adv. Funct. Mater.* **2005**, *15*, 442–450.
- (46) Bakshi, M. S.; Kaura, A.; Kaur, G. Effect of Temperature on the Unfavorable Mixing Between Tetraethylene Glycol Dodecyl Ether and Pluronic P103. *J. Colloid Interface Sci.* **2006**, *296*, 370–373.
- (47) Bakshi, M. S.; Sharma, P.; Kaur, G.; Sachar, S.; Banipal, T. S. Synergistic Mixing of L64 With Various Surfactants of Identical Hydrophobicity Under the Effect of Temperature. *Colloids Surf., A* **2006**, *278*, 218–228.
- (48) Bakshi, M. S.; Bhandari, P. Fluorescence Studies on the Non-Ideal Mixing in Triblock Copolymer Binary Mixtures Under the Effect of Temperature: A Block Hydration Effect. *J. Photochem. Photobiol., A* **2007**, *186*, 166–172.
- (49) Bakshi, M. S.; Kaur, N.; Mahajan, R. K. Photophysical Evaluation of Synergism From Critical Micelle Temperature of Mixed Triblock Polymer Micelles. *J. Photochem. Photobiol., A* **2007**, *186*, 349–356.
- (50) O'Connor, A. J.; Hatton, T. A.; Bose, A. Dynamics of Micelle–Vesicle Transitions in Aqueous Anionic/Cationic Surfactant Mixtures. *Langmuir* **1997**, *13*, 6931–6940.
- (51) Silva, B. F. B.; Marques, E. F.; Olsson, U. Unusual Vesicle–Micelle Transitions in a Salt-Free Catanionic Surfactant: Temperature and Concentration Effects. *Langmuir* **2008**, *24*, 10746–10754.
- (52) Mendes, E.; Narayanan, J.; Oda, R.; Kern, F.; Candau, S. J.; Manohar, C. Shear-Induced Vesicle to Wormlike Micelle Transition. *J. Phys. Chem. B* **1997**, *101*, 2256–2258.
- (53) Khullar, P.; Singh, V.; Mahal, A.; Kaur, H.; Singh, V.; Banipal, T. S.; Kaur, G.; Bakshi, M. S. Tuning the Shape and Size of Gold Nanoparticles With Triblock Polymer Micelle Structure Transitions and Environments. *J. Phys. Chem. C* **2011**, *115*, 10442–10454.
- (54) Rharbi, Y.; Winnik, M. A. Salt Effects on Solute Exchange and Micelle Fission in Sodium Dodecyl Sulfate Micelles Below the Micelle-to-Rod Transition. *J. Phys. Chem. B* **2003**, *107*, 1491–1501.
- (55) Gao, J.; Bender, C. M.; Murphy, C. J. Dependence of the Gold Nanorod Aspect Ratio on the Nature of the Directing Surfactant in Aqueous Solution. *Langmuir* **2003**, *19*, 9065–9070.
- (56) Johnson, C. J.; Dujardin, E.; Davis, S. A.; Murphy, C. J.; Mann, S. J. *Mater. Chem.* **2002**, *12*, 1765–1770.
- (57) Bakshi, M. S.; Kaur, I. Aggregates of Cationic Surfactants and Anionic Polyelectrolytes Influenced by Bulky Head Group Modifications. *Colloids Surf., A* **2003**, *224*, 185–197.
- (58) Bakshi, M. S.; Sood, R. Head Group Controlled Specific Interactions of Aliphatic- and Aromatic-Polyester Dendrimers With Cationic Surfactants of Identical Hydrophobic Tails. *Colloids Surf., A* **2004**, *244*, 159–168.
- (59) Gole, A.; Murphy, C. J. Seed-Mediated Synthesis of Gold Nanorods: Role of the Size and Nature of the Seed. *Chem. Mater.* **2004**, *16*, 3633.
- (60) Huang, C.-C.; Yang, Z. S.; Chang, H.-T. Synthesis of Dumbbell-Shaped Au-Ag Core-Shell Nanorods by Seed-Mediated Growth under Alkaline Conditions. *Langmuir* **2004**, *20*, 6089.
- (61) Gou, L.; Murphy, C. J. Fine-Tuning the Shape of Gold Nanorods. *Chem. Mater.* **2005**, *17*, 3668–3672.
- (62) Tsung, C.-K.; Kou, X. S.; Shi, Q. H.; Zhang, J. P.; Yeung, M. H.; Wang, J. F.; Stucky, G. D. Selective Shortening of Single-Crystalline Gold Nanorods by Mild Oxidation. *J. Am. Chem. Soc.* **2006**, *128*, 5352.
- (63) Wadams, R. C.; Fabris, L.; Vaia, R. A.; Park, K. Time-Dependent Susceptibility of the Growth of Gold Nanorods to the Addition of a Cosurfactant. *Chem. Mater.* **2013**, *25*, 4772–4780.
- (64) Park, K.; Drummy, L. F.; Wadams, R. C.; Koerner, H.; Nepal, D.; Fabris, L.; Vaia, R. A. Growth Mechanism of Gold Nanorods. *Chem. Mater.* **2013**, *25*, 555–563.
- (65) Link, S.; Mohamed, M. B.; El-Sayed, M. A. Simulation of Optical Absorption Spectra of Gold Nanorods as a Function of Their Aspect Ratio and Effect of the Medium Dielectric Constant. *J. Phys. Chem. B* **1999**, *103*, 3073.
- (66) Bakshi, M. S.; Kaur, I.; Sood, R.; Singh, J.; Singh, K.; Sachar, S.; Singh, K. J.; Kaur, G. Mixed Micelles of Benzyltrimethyltetradecylammonium Chloride With Tetradecyltrimethylammonium and Tetradecyltriphenylphosphonium Bromides: a Head Group Contribution. *J. Colloid Interface Sci.* **2004**, *271*, 227–231.
- (67) Alargova, R. G.; Kochiashky, I. I.; Sierra, M. L.; Zana, R. Micelle Aggregation Numbers of Surfactants in Aqueous Solutions: A Comparison between the Results from Steady-State and Time-Resolved Fluorescence Quenching. *Langmuir* **1998**, *14*, 5412–5418.
- (68) Bakshi, M.; Kaur, I. Head-Group-Induced Structural Micellar Transitions in Mixed Cationic Surfactants With Identical Hydrophobic Tails. *Colloid Polym. Sci.* **2003**, *281*, 10–18.
- (69) Bakshi, M.; Kaur, I. Benzylic and Pyridinium Head Groups Controlled Surfactant-Polymer Aggregates of Mixed Cationic Micelles and Anionic Polyelectrolytes. *Colloid Polym. Sci.* **2004**, *282*, 476–485.
- (70) Bakshi, M.; Kaur, I. Head-Group-Modification-Controlled Mixing Behavior of Binary Cationic Surfactants: Conductometric, Viscometric, and NMR Studies. *Colloid Polym. Sci.* **2003**, *281*, 935–944.
- (71) Grochola, G.; Snook, I. K.; Russo, S. P. Computational modeling of nanorod growth. *J. Chem. Phys.* **2007**, *127*, 194707.
- (72) Ye, X.; Jin, L.; Caglayan, H.; Chen, J.; Xing, G.; Zheng, C.; Doan-Nguyen, V.; Kang, Y.; Engheta, N.; Kagan, C. R.; Murray, C. B. Improved Size-Tunable Synthesis of Monodisperse Gold Nanorods Through the Use of Aromatic Additives. *ACS Nano* **2012**, *6*, 2804–2817.
- (73) Murphy, C. J.; Sau, T. K.; Gole, A. M.; Orendorff, C. J.; Gao, J. X.; Gou, L.; Hunyadi, S. E.; Li, T. Anisotropic Metal Nanoparticles: Synthesis, Assembly, and Optical Applications. *J. Phys. Chem. B* **2005**, *109*, 13857–13870.
- (74) Jones, M. R.; Osberg, K. D.; Macfarlane, R. J.; Langille, M. R.; Mirkin, C. A. Templated Techniques for the Synthesis and Assembly of Plasmonic Nanostructures. *Chem. Rev.* **2011**, *111*, 3736–3827.
- (75) Rycenga, M.; Cobley, C. M.; Zeng, J.; Li, W.; Moran, C. H.; Zhang, Q.; Qin, D.; Xia, Y. Controlling the Synthesis and Assembly of Silver Nanostructures for Plasmonic Applications. *Chem. Rev.* **2011**, *111*, 3669–3712.
- (76) Huang, X.; Peng, X.; Wang, Y.; Wang, Y.; Shin, D. M.; El Sayed, M. A.; Nie, S. A. Reexamination of Active and Passive Tumor Targeting by Using Rod-Shaped Gold Nanocrystals and Covalently Conjugated Peptide Ligands. *ACS Nano* **2010**, *4*, 5887–5896.

- (77) Khouri, L. R.; Goldbart, R.; Traitel, T.; Enden, G.; Kost, J. Harvesting Low Molecular Weight Biomarkers Using Gold Nanoparticles. *ACS Nano* **2015**, *9*, 5750–5759.
- (78) Lin, Z.; Cai, J. J.; Scriven, L. E.; Davis, H. T. Spherical-to-Wormlike Micelle Transition in CTAB Solutions. *J. Phys. Chem. B* **1994**, *98*, 5984–5993.
- (79) Aswal, V. K.; Goyal, P. S.; Thiagarajan, P. Small-Angle Neutron-Scattering and Viscosity Studies of CTAB/NaSal Viscoelastic Micellar Solutions. *J. Phys. Chem. B* **1998**, *102*, 2469–2473.
- (80) Yoo, H.; Sharma, J.; Yeh, H.-C.; Martinez, J. S. Solution-Phase Synthesis of Au Fibers Using Rod-Shaped Micelles as Shape Directing Agents. *Chem. Commun.* **2010**, *46*, 6813–6815.
- (81) Israelachvili, J. N.; Mitchell, D. J.; Ninham, B. W. Theory of Self-Assembly of Hydrocarbon Amphiphiles into Micelles and Bilayers. *J. Chem. Soc., Faraday Trans. 2* **1976**, *72*, 1525–1568.
- (82) Nie, Z.; Petukhova, A.; Kumacheva, E. Properties and Emerging Applications of Self-Assembled Structures Made from Inorganic Nanoparticles. *Nat. Nanotechnol.* **2010**, *5*, 15–25.
- (83) Nie, Z. H.; Fava, D.; Kumacheva, E.; Zou, S.; Walker, G. C.; Rubinstein, M. Self-Assembly of Metal-Polymer Analogues of Amphiphilic Triblock Copolymers. *Nat. Mater.* **2007**, *6*, 609–614.
- (84) Glotzer, S. C.; Solomon, M. J. Anisotropy of Building Blocks and Their Assembly into Complex Structures. *Nat. Mater.* **2007**, *6*, 557–562.
- (85) Tao, A.; Sinsermsuksakul, P.; Yang, P. Tunable Plasmonic Lattices of Silver Nanocrystals. *Nat. Nanotechnol.* **2007**, *2*, 435–440.
- (86) Onsager, L. The Effects of Shape on the Interaction of Colloidal Particles. *Ann. N. Y. Acad. Sci.* **1949**, *51*, 627–659.
- (87) Halas, N. J.; Lal, S.; Chang, W.-S.; Link, S.; Nordlander, P. Plasmons in Strongly Coupled Metallic Nanostructures. *Chem. Rev.* **2011**, *111*, 3913–3961.
- (88) Tao, A.; Kim, F.; Hess, C.; Goldberger, J.; He, R.; Sun, Y. G.; Xia, Y.; Yang, P. Langmuir-Blodgett Silver Nanowire Monolayers for Molecular Sensing Using Surface-Enhanced Raman Spectroscopy. *Nano Lett.* **2003**, *3*, 1229–1233.
- (89) Lal, S.; Grady, N. K.; Kundu, J.; Levin, C. S.; Lassiter, J. B.; Halas, N. J. Tailoring Plasmonic Substrates for Surface Enhanced Spectroscopies. *Chem. Soc. Rev.* **2008**, *37*, 898–911.
- (90) Nikoobakht, B.; El-Sayed, M. A. Preparation and Growth Mechanism of Gold Nanorods (NRs) Using Seed-Mediated Growth Method. *Chem. Mater.* **2003**, *15*, 1957–1962.
- (91) Jana, N. R. Gram-Scale Synthesis of Soluble, Near-Monodisperse Gold Nanorods and Other Anisotropic Nanoparticles. *Small* **2005**, *1*, 875–882.
- (92) Walsh, M. J.; Barrow, S. J.; Tong, W.; Funston, A. M.; Etheridge, J. Symmetry Breaking and Silver in Gold Nanorod Growth. *ACS Nano* **2015**, *9*, 715–724.
- (93) Parker, J. F.; Fields-Zinna, C. A.; Murray, R. W. The Story of a Monodisperse Gold Nanoparticle: $\text{Au}_{25}\text{L}_{18}$. *Acc. Chem. Res.* **2010**, *43*, 1289–1296.
- (94) Mpourmpakis, G.; Caratzoulas, S.; Vlachos, D. G. What Controls Au Nanoparticle Dispersity During Growth? *Nano Lett.* **2010**, *10*, 3408–3413.
- (95) Zhang, Z.; Nenoff, T. M.; Leung, K.; Ferreira, S. R.; Huang, J. Y.; Berry, D. T.; Provencio, P. P.; Stumpf, R. Room-Temperature Synthesis of Ag-Ni and Pd-Ni Alloy Nanoparticles. *J. Phys. Chem. C* **2010**, *114*, 14309–14318.
- (96) Almora-Barrios, N.; Novell-Leruth, G.; Whiting, P.; Liz-Marzan, L. M.; Lopez, N. Theoretical Description of the Role of Halides, Silver, and Surfactants on the Structure of Gold Nanorods. *Nano Lett.* **2014**, *14*, 871–875.
- (97) Barmparis, G. D.; Remediakis, I. N. Dependence on CO adsorption of the shapes of multifaceted gold nanoparticles: A density functional theory. *Phys. Rev. B: Condens. Matter Mater. Phys.* **2012**, *86*, 085457.
- (98) Cleveland, C. L.; Landman, U.; Shafiqullin, M. N.; Stephens, P. W.; Whetten, R. L. *Z. Phys. D: At., Mol. Clusters* **1997**, *40*, 503–508.
- (99) Niidome, Y.; Nakamura, Y.; Honda, K.; Akiyama, Y.; Nishioka, K.; Kawasaki, H.; Nakashima, N. Characterization of silver ions adsorbed on gold nanorods: surface analysis by using surface-assisted laser desorption/ionization time-of-flight mass spectrometry. *Chem. Commun.* **2009**, 1754–1756.
- (100) Liu, X. H.; Luo, X. H.; Lu, S. X.; Zhang, J. C.; Cao, W. L. J. A novel cetyltrimethyl ammonium silver bromide complex and silver bromide nanoparticles obtained by the surfactant counterion. *J. Colloid Interface Sci.* **2007**, *307*, 94–100.
- (101) Hubert, F.; Testard, F.; Spalla, O. Cetyltrimethylammonium Bromide Silver Bromide Complex as the Capping Agent of Gold Nanorods. *Langmuir* **2008**, *24*, 9219–9222.
- (102) Nikoobakht, B.; El-Sayed, M. A. Evidence for Bilayer Assembly of Cationic Surfactants on the Surface of Gold Nanorods. *Langmuir* **2001**, *17*, 6368–6374.
- (103) Grzelczak, M.; Sanchez-Iglesias, A.; Mezherji, H. H.; Bals, S.; Perez-Juste, J.; Liz-Marzan, L. M. Steric Hindrance Induces Crosslike Self-Assembly of Gold Nanodumbbells. *Nano Lett.* **2012**, *12*, 4380–4384.
- (104) Zerrouki, D.; Baudry, J.; Pine, D.; Chaikin, P.; Bibette, J. Chiral colloidal clusters. *Nature* **2008**, *455*, 380–382.
- (105) Wei, Y.; Bishop, K. J. M.; Kim, J.; Soh, S.; Grzybowski, B. A. Making Use of Bond Strength and Steric Hindrance in Nanoscale Synthesis. *Angew. Chem., Int. Ed.* **2009**, *48*, 9477–9480.
- (106) Petukhova, A.; Greener, J.; Liu, K.; Nykypanchuk, D.; Nicolay, R.; Matyjaszewski, K.; Kumacheva, E. Standing arrays of gold nanorods end-tethered with polymer ligands. *Small* **2012**, *8*, 731–737.
- (107) Fava, D.; Nie, Z.; Winnik, M. A.; Kumacheva, E. Evolution of self-assembled structures of polymer-terminated gold nanorods in selective solvents. *Adv. Mater.* **2008**, *20*, 4318–4322.
- (108) Smith, C. V.; Jones, D. P.; Guenther, T. M.; Lash, L. H.; Lauterburg, B. H. Compartmentation of glutathione: implications for the study of toxicity and disease. *Toxicol. Appl. Pharmacol.* **1996**, *140*, 1–12.
- (109) Schafer, F. Q.; Buettner, G. R. Redox environment of the cell as viewed through the redox state of the glutathione disulfide/glutathione couple. *Free Radical Biol. Med.* **2001**, *30*, 1191–1212.
- (110) Verma, A.; Simard, J. M.; Worrall, J. W. E.; Rotello, V. M. Tunable Reactivation of Nanoparticle-Inhibited β -Galactosidase by Glutathione at Intracellular Concentrations. *J. Am. Chem. Soc.* **2004**, *126*, 13987–13991.
- (111) Hong, R.; Han, G.; Fernandez, J. M.; Kim, B.-J.; Forbes, N. S.; Rotello, V. M. Glutathione-mediated delivery and Release Using Monolayer Protected Nanoparticle Carriers. *J. Am. Chem. Soc.* **2006**, *128*, 1078–1079.
- (112) Kou, X.; Zhang, S.; Yang, Z.; Tsung, C. K.; Stucky, G. D.; Sun, L.; Wang, J.; Yan, C. Glutathione- and Cysteine-Induced Transverse Overgrowth on Gold Nanorods. *J. Am. Chem. Soc.* **2007**, *129*, 6402–6404.
- (113) Sau, T. K.; Murphy, C. J. Seeded High Yield Synthesis of Short Au Nanorods in Aqueous Solution. *Langmuir* **2004**, *20*, 6414–6420.
- (114) Seyed-Razavi, A.; Snook, I. K.; Barnard, A. S. Surface Area Limited Model for Predicting Anisotropic Coarsening of Faceted Nanoparticles. *Cryst. Growth Des.* **2011**, *11*, 158–165.
- (115) Barnard, A. S. Modeling the Impact of Alkanethiol SAMs on the Morphology of Gold Nanocrystals. *Cryst. Growth Des.* **2013**, *13*, 5433–5441.
- (116) Barnard, A. S. Shape-Dependent Confinement of the Nano-diamond Band Gap. *Cryst. Growth Des.* **2009**, *9*, 4860–4863.
- (117) Wilson, H. F.; Barnard, A. S. Thermodynamic Control of Halogen-Terminated Silicon Nanoparticle Morphology. *Cryst. Growth Des.* **2014**, *14*, 4468–4474.
- (118) Henkel, A.; Schubert, O.; Plech, A.; Sonnichsen, C. Growth Kinetic of a Rod-Shaped Metal Nanocrystal. *J. Phys. Chem. C* **2009**, *113*, 10390–10394.
- (119) Bakshi, M. S.; Kaur, G.; Thakur, P.; Banipal, T. S.; Possmayer, F.; Petersen, N. O. Surfactant Selective Synthesis of Gold Nanowires by Using a DPPC–Surfactant Mixture As a Capping Agent at Ambient Conditions. *J. Phys. Chem. C* **2007**, *111*, 5932–5940.
- (120) Bakshi, M. S.; Possmayer, F.; Petersen, N. O. Role of Different Phospholipids in the Synthesis of Pearl-Necklace-Type Gold–Silver

- Bimetallic Nanoparticles As Bioconjugate Materials. *J. Phys. Chem. C* **2007**, *111*, 14113–14124.
- (121) Bakshi, M. S.; Sachar, S.; Kaur, G.; Bhandari, P.; Kaur, G.; Biesinger, M. C.; Possmayer, F.; Petersen, N. O. Dependence of Crystal Growth of Gold Nanoparticles on the Capping Behavior of Surfactant at Ambient Conditions. *Cryst. Growth Des.* **2008**, *8*, 1713–1719.
- (122) Bakshi, M. S. A Simple Method of Superlattice Formation: Step-by-Step Evaluation of Crystal Growth of Gold Nanoparticles Through Seed–Growth Method. *Langmuir* **2009**, *25*, 12697–12705.
- (123) Bakshi, M. S.; Possmayer, F.; Petersen, N. O. Simultaneous Synthesis of Au and Cu Nanoparticles in Pseudo-Core-Shell Type Arrangement Facilitated by DMPG and 12–6–12 Capping Agents. *Chem. Mater.* **2007**, *19*, 1257–1266.
- (124) Personick, M. L.; Langille, M. R.; Zhang, J.; Harris, N.; Schatz, G. C.; Mirkin, C. A. Synthesis and Isolation of {110}-Faceted Gold Bipyramids and Rhombic Dodecahedra. *J. Am. Chem. Soc.* **2011**, *133*, 6170–6173.
- (125) Personick, M. L.; Langille, M. R.; Wu, J.; Mirkin, C. A. Synthesis of Gold Hexagonal Bipyramids Directed by Planar-Twinned Silver Triangular Nanoprisms. *J. Am. Chem. Soc.* **2013**, *135*, 3800–3803.
- (126) Personick, M. L.; Mirkin, C. A. Making Sense of the Mayhem Behind Shape Control in the Synthesis of Gold Nanoparticles. *J. Am. Chem. Soc.* **2013**, *135*, 18238–18247.
- (127) Langille, M. R.; Personick, M. L.; Zhang, J.; Mirkin, C. A. Defining Rules for the Shape Evolution of Gold Nanoparticles. *J. Am. Chem. Soc.* **2012**, *134*, 14542–14554.
- (128) Zhang, J.; Langille, M. R.; Personick, M. L.; Zhang, K.; Li, S.; Mirkin, C. A. Concave Cubic Gold Nanocrystals With High-Index Facets. *J. Am. Chem. Soc.* **2010**, *132*, 14012–14014.
- (129) Tao, A. R.; Habas, S.; Yang, P. Shape Control of Colloidal Metal Nanocrystals. *Small* **2008**, *4*, 310–325.
- (130) Millstone, J. E.; Métraux, G. S.; Mirkin, C. A. Controlling the Edge Length of Gold Nanoprisms via a Seed-Mediated Approach. *Adv. Funct. Mater.* **2006**, *16*, 1209–1214.
- (131) Ming, T.; Feng, W.; Tang, Q.; Wang, F.; Sun, L.; Wang, J.; Yan, C. Growth of Tetrahedral Gold-Nanocrystals with High-Index Facets. *J. Am. Chem. Soc.* **2009**, *131*, 16350–16315.
- (132) Ma, Y.; Kuang, Q.; Jiang, Z.; Xie, Z.; Huang, R.; Zheng, L. Synthesis of trisoctahedral gold nanocrystals with exposed high-index facets by a facile chemical method. *Angew. Chem., Int. Ed.* **2008**, *47*, 8901–8904.
- (133) Bratlie, K. M.; Lee, H.; Komvopoulos, K.; Yang, P.; Somorjai, G. A. Platinum Nanoparticle Shape Effects on Benzene Hydrogenation Selectivity. *Nano Lett.* **2007**, *7*, 3097–3101.
- (134) Manner, W. L.; Bishop, A. R.; Girolami, G. S.; Nuzzo, R. G. Platinum Nanoparticle Shape Effects on Benzene Hydrogenation Selectivity. *J. Phys. Chem. B* **1998**, *102*, 8816–8824.
- (135) Scarabelli, L.; Coronado-Puchau, M.; Giner-Casares, J. J.; Langer, J.; Liz-Marzan, L. M. Monodisperse Gold Nanotriangles: Size Control, Large-Scale Self-Assembly, and Performance in Surface-Enhanced Raman Scattering. *ACS Nano* **2014**, *8*, 5833–5842.
- (136) Huang, M. H.; Chiu, C.-Y. Achieving Polyhedral Nanocrystal Growth with Systematic Shape Control. *J. Mater. Chem. A* **2013**, *1*, 8081–8092.
- (137) DuChene, J. S.; Niu, W.; Abendroth, J. M.; Sun, Q.; Zhao, W.; Huo, F.; Wei, W. D. Halide Anions as Shape-Directing Agents for Obtaining High-Quality Anisotropic Gold Nanostructures. *Chem. Mater.* **2013**, *25*, 1392–1399.
- (138) Vautier-Giongo, C.; Bakshi, M. S.; Singh, J.; Ranganathan, R.; Hajdu, J.; Bales, B. L. Effects of Interactions on the Formation of Mixed Micelles of 1,2-Dihexanoyl-Sn-Glycero-3-Phosphocholine With Sodium Dodecyl Sulfate and Dodecyltrimethylammonium Bromide. *J. Colloid Interface Sci.* **2005**, *282*, 149–155.
- (139) Ranganathan, R.; Vautier-Giongo, C.; Bakshi, M. S.; Bales, B. L.; Hajdu, J. Phospholipid Containing Mixed Micelles: Characterization of Dihexanoyl Phosphatidylcholine (DHPC) and Sodium Dodecyl Sulfate and DHPC and Dodecyl Trimethylammonium Bromide. *Chem. Phys. Lipids* **2005**, *135*, 93–104.
- (140) Johansson, D.; Bergenstahl, B. Lecithins in oil-continuous emulsions. Fat crystal wetting and interfacial tension. *J. Am. Oil Chem. Soc.* **1995**, *72*, 205–211.
- (141) Sabra, M. C.; Jorgensen, K.; Mouritsen, O. G. Lindane suppresses the lipid-bilayer permeability in the main transition region. *Biochim. Biophys. Acta, Biomembr.* **1996**, *1282*, 85–92.
- (142) Lockwood, N. A.; Abbott, N. L. Self-assembly of surfactants and phospholipids at interfaces between aqueous phases and thermotropic liquid crystals. *Curr. Opin. Colloid Interface Sci.* **2005**, *10*, 111–120.
- (143) Caseli, L.; Zanielli, M. E. D.; Furriel, P. R. M.; Leone, F. A. Using phospholipid Langmuir and Langmuir–Blodgett films as matrix for urease immobilization. *Colloids Surf., B* **2003**, *30*, 273–279.
- (144) Ross, M.; Krol, S.; Janshoff, A.; Galla, H. J. Kinetics of phospholipids insertion into monolayers containing lung surfactants SP-B or SP-C. *Eur. Biophys. J.* **2002**, *31*, 52–61.
- (145) Wang, L.; Yamauchi, Y. Block Copolymer Mediated Synthesis of Dendritic Platinum Nanoparticles. *J. Am. Chem. Soc.* **2009**, *131*, 9152–9153.
- (146) Khullar, P.; Mahal, A.; Singh, V.; Banipal, T. S.; Kaur, G.; Bakshi, M. S. How PEO-PPO-PEO Triblock Polymer Micelles Control the Synthesis of Gold Nanoparticles: Temperature and Hydrophobic Effects. *Langmuir* **2010**, *26*, 11363–11371.
- (147) Khullar, P.; Singh, V.; Mahal, A.; Kumar, H.; Kaur, G.; Bakshi, M. S. Block Copolymer Micelles As Nanoreactors for Self-Assembled Morphologies of Gold Nanoparticles. *J. Phys. Chem. B* **2013**, *117*, 3028–3039.
- (148) Bakshi, M. S.; Sachar, S.; Singh, K.; Shaheen, A. Mixed Micelle Behavior of Pluronic L64 and Triton X-100 With Conventional and Dimeric Cationic Surfactants. *J. Colloid Interface Sci.* **2005**, *286*, 369–377.
- (149) Bakshi, M. S.; Sachar, S. Influence of Temperature on the Mixed Micelles of Pluronic F127 and P103 With Dimethylene-Bis-(Dodecyldimethylammonium Bromide). *J. Colloid Interface Sci.* **2006**, *296*, 309–315.
- (150) Bakshi, M. S.; Sachar, S. Influence of Hydrophobicity on the Mixed Micelles of Pluronic F127 and P103 Plus Cationic Surfactant Mixtures. *Colloids Surf., A* **2006**, *276*, 146–154.
- (151) Bakshi, M. S.; Singh, J.; Kaur, G. Antagonistic Mixing Behavior of Cationic Gemini Surfactants and Triblock Polymers in Mixed Micelles. *J. Colloid Interface Sci.* **2005**, *285*, 403–412.
- (152) Bakshi, M. S.; Sachar, S.; Yoshimura, T.; Esumi, K. Association Behavior of Poly(Ethylene Oxide)-poly(Propylene Oxide)-poly(Ethylene Oxide) Block Copolymers With Cationic Surfactants in Aqueous Solution. *J. Colloid Interface Sci.* **2004**, *278*, 224–233.
- (153) Narayanan, R.; El-Sayed, M. A. Shape-Dependent Catalytic Activity of Platinum Nanoparticles in Colloidal Solution. *Nano Lett.* **2004**, *4*, 1343–1348.
- (154) Lim, B.; Lu, X. M.; Jiang, M. J.; Camargo, P. H. C.; Cho, E. C.; Lee, E. P.; Xia, Y. N. Facile Synthesis of Highly Faceted Multioctahedral Pt Nanocrystals through Controlled Overgrowth. *Nano Lett.* **2008**, *8*, 4043–4047.
- (155) Mahmoud, M. A.; Tabor, C. E.; El-Sayed, M. A.; Ding, Y.; Wang, Z. L. A New Catalytically Active Colloidal Platinum Nanocatalyst: The Multiarmed Nanostar Single Crystal. *J. Am. Chem. Soc.* **2008**, *130*, 4590–4591.
- (156) Wang, L.; Wang, H.; Nemoto, Y.; Yamauchi, Y. Rapid and Efficient Synthesis of Platinum Nanodendrites With High Surface Area by Chemical Reduction With Formic Acid. *Chem. Mater.* **2010**, *22*, 2835–2841.
- (157) Song, Y.; Yang, Y.; Medforth, C. J.; Pereira, E.; Singh, A. K.; Xu, H.; Jiang, Y.; Brinker, C. J.; van Swol, F.; Shelnutt, J. A. Controlled Synthesis of 2-D and 3-D Dendritic Platinum Nanostructures. *J. Am. Chem. Soc.* **2004**, *126*, 635–645.
- (158) Song, Y.; Jiang, Y.-B.; Wang, H.; Pena, D. A.; Qiu, Y.; Miller, J. E.; Shelnutt, J. A. Platinum nanodendrites. *Nanotechnology* **2006**, *17*, 1300–1308.
- (159) Sanchez-Gaytan, B. L.; Qian, Z.; Hastings, S. P.; Reca, M. L.; Fakhraai, Z.; Park, S. J. Controlling the Topography and Surface

- Plasmon Resonance of Gold Nanoshells by a Templated Surfactant-Assisted Seed Growth Method. *J. Phys. Chem. C* **2013**, *117*, 8916–8923.
- (160) Sanchez-Gaytan, B. L.; Park, S.-J. Spiky Gold Nanoshells. *Langmuir* **2010**, *26*, 19170–19174.
- (161) Sanchez-Gaytan, B. L.; Swanglap, P.; Lamkin, T. J.; Hickey, R. J.; Fakhraai, Z.; Link, S.; Park, S.-J. Spiky Gold Nanoshells: Synthesis and Enhanced Scattering Properties. *J. Phys. Chem. C* **2012**, *116*, 10318–10324.
- (162) Hirsch, L.; Gobin, A.; Lowery, A.; Tam, F.; Drezek, R.; Halas, N.; West, J. Metal Nanoshells. *Ann. Biomed. Eng.* **2006**, *34*, 15–22.
- (163) Jana, N. R.; Gearheart, L.; Murphy, C. J. Wet Chemical Synthesis of High Aspect Ratio Cylindrical Gold Nanorods. *J. Phys. Chem. B* **2001**, *105*, 4065–4067.
- (164) Ha, T. H.; Koo, H. J.; Chung, B. H. Shape-Controlled Syntheses of Gold Nanoprisms and Nanorods Influenced by Specific Adsorption of Halide Ions. *J. Phys. Chem. C* **2007**, *111*, 1123–1130.
- (165) Garg, N.; Scholl, C.; Mohanty, A.; Jin, R. The Role of Bromide Ions in Seeding Growth of Au Nanorods. *Langmuir* **2010**, *26*, 10271–10276.
- (166) Qian, X. M.; Nie, S. M. Single-Molecule and Single-Nanoparticle SERS: From Fundamental Mechanisms to Biomedical Applications. *Chem. Soc. Rev.* **2008**, *37*, 912–920.
- (167) Lal, S.; Clare, S. E.; Halas, N. J. Nanoshell-Enabled Photothermal Cancer Therapy: Impending Clinical Impact. *Acc. Chem. Res.* **2008**, *41*, 1842–1851.
- (168) Huang, T.; Meng, F.; Qi, L. Controlled Synthesis of Dendritic Gold Nanostructures Assisted by Supramolecular Complexes of Surfactant With Cyclodextrin. *Langmuir* **2010**, *26*, 7582–7589.
- (169) Bakshi, M. S. Cationic Mixed Micelles in the Presence of β -Cyclodextrin: A Host–Guest Study. *J. Colloid Interface Sci.* **2000**, *227*, 78–83.
- (170) Valente, A. J. M.; Soderman, O. The Formation of Host-guest Complexes Between Surfactants and Cyclodextrins. *Adv. Colloid Interface Sci.* **2014**, *205*, 156–176.
- (171) Carvalho, R. A.; Correia, H. A.; Valente, A. J. M.; Soderman, O.; Nilsson, M. The Effect of the Head-Group Spacer Length of 12-s-12 Gemini Surfactants in the Host–guest Association With β -Cyclodextrin. *J. Colloid Interface Sci.* **2011**, *354*, 725–732.
- (172) Dharmawardana, U. R.; Christian, S. D.; Tucker, E. E.; Taylor, R. W.; Scamehorn, J. F. A Surface Tension Method for Determining Binding Constants for Cyclodextrin Inclusion Complexes of Ionic Surfactants. *Langmuir* **1993**, *9*, 2258–2263.
- (173) Mwakibete, H.; Cristantino, R.; Bloor, D. M.; Wyn-Jones, E.; Holzwarth, J. F. Reliability of the Experimental Methods To Determine Equilibrium Constants for Surfactant/cyclodextrin Inclusion Complexes. *Langmuir* **1995**, *11*, 57–60.
- (174) Liu, Y.; Yang, Y.-W.; Chen, Y. Thio[2-(benzoylamino)-ethylamino]- β -CD fragment modified gold nanoparticles as recycling extractors for [60]fullerene. *Chem. Commun.* **2005**, 4208–4210.
- (175) Bakshi, M. S.; Thakur, P.; Sachar, S.; Kaur, G.; Banipal, T. S.; Possmayer, F.; Petersen, N. O. Aqueous Phase Surfactant Selective Shape Controlled Synthesis of Lead Sulfide Nanocrystals. *J. Phys. Chem. C* **2007**, *111*, 18087–18098.
- (176) Bakshi, M. S.; Thakur, P.; Khullar, P.; Kaur, G.; Banipal, T. S. Surface Activity of Highly Hydrophobic Surfactants and Platelike PbSe and CuSe Nanoparticles. *Cryst. Growth Des.* **2010**, *10*, 1813–1822.
- (177) Kaur, G.; Bakshi, M. S. Nonideal Mixing of Se–Te in Aqueous Micellar Phase for Nanoalloys Over the Whole Mole Mixing Range With Morphology Control From Nanoparticles to Nanoribbons. *J. Phys. Chem. C* **2010**, *114*, 143–154.
- (178) Bakshi, M. S. 1D Flower-Like Morphologies of Palladium Nanoparticles Using Strongly Hydrophobic Surfactants. *J. Phys. Chem. C* **2009**, *113*, 10921–10928.
- (179) Bakshi, M. S.; Sharma, P.; Banipal, T. S.; Kaur, G.; Torigoe, K.; Petersen, N. O.; Possmayer, F. Lamellar Phase Supported Synthesis of Colloidal Gold Nanoparticles, Nanoclusters, and Nanowires. *J. Nanosci. Nanotechnol.* **2007**, *7*, 916–924.
- (180) Bolotin, I. L.; Asunskis, D. J.; Jawaaid, A. M.; Liu, Y.; Snee, P. T.; Hanley, L. Effects of Surface Chemistry on Nonlinear Absorption, Scattering, and Refraction of PbSe and PbS Nanocrystals. *J. Phys. Chem. C* **2010**, *114*, 16257–16262.
- (181) Talapin, D. V.; Black, C. T.; Kagan, C. R.; Shevchenko, E. V.; Afzali, A.; Murray, C. B. Alignment, Electronic Properties, Doping, and On-Chip Growth of Colloidal PbSe Nanowires. *J. Phys. Chem. C* **2007**, *111*, 13244–13249.
- (182) Hull, K. L.; Grebinski, J. W.; Kosel, T. H.; Kuno, M. Induced Branching in Confined PbSe Nanowires. *Chem. Mater.* **2005**, *17*, 4416–4425.
- (183) Schapotschnikow, P.; van Huis, M. A.; Zandbergen, H. W.; Vanmaekelbergh, D. I.; Vlugt, T. J. H. Morphological Transformations and Fusion of PbSe Nanocrystals Studied Using Atomistic Simulations. *Nano Lett.* **2010**, *10*, 3966–3971.
- (184) Imae, T.; Ikeda, S. Sphere-Rod Transition of Micelles of Tetradecyltrimethylammonium Halides in Aqueous Sodium Halide Solutions and Flexibility and Entanglement of Long Rodlike Micelles. *J. Phys. Chem.* **1986**, *90*, 5216–5223.
- (185) Lu, W.; Fang, J.; Ding, Y.; Wang, Z. L. Formation of PbSe Nanocrystals: A Growth toward Nanocubes. *J. Phys. Chem. B* **2005**, *109*, 19219–19222.
- (186) Talapin, D. V.; Yu, H.; Shevchenko, E. V.; Lobo, A.; Murray, C. B. Synthesis of Colloidal PbSe/PbS Core–Shell Nanowires and PbS/Au Nanowire–Nanocrystal Heterostructures. *J. Phys. Chem. C* **2007**, *111*, 14049–14054.
- (187) Wang, X.; Xi, G.; Liu, Y.; Qian, Y. Controllable Synthesis of PbSe Nanostructures and Growth Mechanisms. *Cryst. Growth Des.* **2008**, *8*, 1406–1411.
- (188) Cho, K. S.; Talapin, D. V.; Gaschler, W.; Murray, C. B. Designing PbSe Nanowires and Nanorings through Oriented Attachment of Nanoparticles. *J. Am. Chem. Soc.* **2005**, *127*, 7140–7147.
- (189) Xue, T.; Wang, X.; Kwak, S. K.; Lee, J. M. Synthesis of Mesoporous Polyaniline (PANI)-Se0.5Te0.5 Dual-Layer Film From Lyotropic Liquid Crystalline Template. *Ind. Eng. Chem. Res.* **2013**, *52*, 5072–5078.
- (190) Mayers, B.; Byron, G.; Yin, Y.; Xia, Y. Large-Scale Synthesis of Monodisperse Nanorods of Se/Te Alloys Through a Homogeneous Nucleation and Solution Growth Process. *Adv. Mater.* **2001**, *13*, 1380–1384.
- (191) Jeong, U.; Herricks, T.; Shahar, E.; Xia, Y. Amorphous Se: A New Platform for Synthesizing Superparamagnetic Colloids with Controllable Surfaces. *J. Am. Chem. Soc.* **2005**, *127*, 1098–1099.
- (192) Kaur, G.; Iqbal, M.; Bakshi, M. S. Biominerization of Fine Selenium Crystalline Rods and Amorphous Spheres. *J. Phys. Chem. C* **2009**, *113*, 13670–13676.
- (193) Liu, Z.; Hu, Z.; Liang, J.; Li, S.; Yang, Y.; Peng, S.; Qian, Y. Size-Controlled Synthesis and Growth Mechanism of Monodisperse Tellurium Nanorods by a Surfactant-Assisted Method. *Langmuir* **2004**, *20*, 214–218.
- (194) Yuan, J.; Gao, H.; Schacher, F.; Xu, Y.; Richter, R.; Tremel, W.; Müller, A. H. E. Alignment of Tellurium Nanorods via a Magnetization-Alignment–Demagnetization (“MAD”) Process Assisted by an External Magnetic Field. *ACS Nano* **2009**, *3*, 1441–1450.
- (195) Lin, Z.-H.; Yang, Z.; Chang, H.-T. Preparation of Fluorescent Tellurium Nanowires at Room Temperature. *Cryst. Growth Des.* **2008**, *8*, 351–357.
- (196) Ma, Y.; Qi, L.; Shen, W.; Ma, J. Selective Synthesis of Single-Crystalline Selenium Nanobelts and Nanowires in Micellar Solutions of Nonionic Surfactants. *Langmuir* **2005**, *21*, 6161–6164.
- (197) Xi, G.; Xiong, K.; Zhao, Q.; Zhang, R.; Zhang, H.; Qian, Y. Nucleation–Dissolution–Recrystallization: A New Growth Mechanism for T-Selenium Nanotubes. *Cryst. Growth Des.* **2006**, *6*, 577–582.
- (198) Wang, D.; Jakobson, H. P.; Kou, R.; Tang, J.; Fineman, R. Z.; Yu, D.; Lu, Y. Metal and Semiconductor Nanowire Network Thin Films With Hierarchical Pore Structures. *Chem. Mater.* **2006**, *18*, 4231–4237.
- (199) Ma, Y.; Qi, L.; Ma, J.; Cheng, H. Micelle-Mediated Synthesis of Single-Crystalline Selenium Nanotubes. *Adv. Mater.* **2004**, *16*, 1023–1026.
- (200) Pichon, B. P.; Leuvrey, C.; Ihiawakrim, D.; Tichit, D.; Gerardin, C. Films of Tunable ZnO Nanostructures Prepared by a Surfactant-

- Mediated Soft Synthesis Route. *J. Phys. Chem. C* **2011**, *115*, 23695–23703.
- (201) Jagadish, C.; Pearton, S. J. *Zinc Oxide Bulk, Thin Films and Nanostructures*; Elsevier: New York, 2006.
- (202) Beek, W. J. E.; Wienk, M. M.; Kemerink, M.; Yang, X.; Janssen, R. A. J. Hybrid Zinc Oxide Conjugated Polymer Bulk Heterojunction Solar Cells. *J. Phys. Chem. B* **2005**, *109*, 9505–9516.
- (203) Baxter, J. B.; Walker, A. M.; van Ommering, K.; Aydil, E. S. Synthesis and characterization of ZnO nanowires and their integration into dye-sensitized solar cells. *Nanotechnology* **2006**, *17*, S304–S312.
- (204) Xiang, B.; Wang, P.; Zhang, X.; Dayeh, S. A.; Aplin, D. P. R.; Soci, C.; Yu, D.; Wang, D. Rational Synthesis of p-Type Zinc Oxide Nanowire Arrays Using Simple Chemical Vapor Deposition. *Nano Lett.* **2007**, *7*, 323–328.
- (205) Khan, R.; Kaushik, A.; Solanki, P. R.; Ansari, A. A.; Pandey, M. K.; Malhotra, B. D. Zinc oxide nanoparticles-chitosan composite film for cholesterol biosensor. *Anal. Chim. Acta* **2008**, *616*, 207–213.
- (206) Li, C. C.; Du, Z. F.; Li, L. M.; Yu, H. C.; Wan, Q.; Wang, T. H. Surface-depletion controlled gas sensing of ZnO nanorods grown at room temperature. *Appl. Phys. Lett.* **2007**, *91*, 032101–032103.
- (207) Liu, J. F.; Ducker, W. A. Surface-Induced Phase Behavior of Alkyltrimethylammonium Bromide Surfactants Adsorbed to Mica, Silica, and Graphite. *J. Phys. Chem. B* **1999**, *103*, 8558–8567.
- (208) Griffiths, M. B. E.; Koponen, S. E.; Mandia, D. J.; McLeod, J. F.; Coyle, J. P.; Sims, J. J.; Giorgi, J. B.; Sirianni, E. R.; Yap, G. P. A.; Barry, S. T. Surfactant Directed Growth of Gold Metal Nanoplates by Chemical Vapor Deposition. *Chem. Mater.* **2015**, *27*, 6116–6124.
- (209) Hampden-Smith, M. J.; Kodas, T. T. Chemical Vapour Deposition of Metals: Part 1. An Overview of CVD Processes. *Chem. Vap. Deposition* **1995**, *1*, 8–23.
- (210) Zhukhovitskiy, A. V.; Mavros, M. G.; Van Voorhis, T.; Johnson, J. A. Addressable Carbene Anchors for Gold Surfaces. *J. Am. Chem. Soc.* **2013**, *135*, 7418–7421.
- (211) Hopkinson, M. N.; Richter, C.; Schedler, M.; Glorius, F. An overview of N-heterocyclic Carbenes. *Nature* **2014**, *510*, 485–496.
- (212) Jewell, A. D.; Sykes, E. C. H.; Kyriakou, G. Molecular-Scale Chemistry of a Common Metal Nanoparticle Capping Agent: Triphenylphosphine on Au (111). *ACS Nano* **2012**, *6*, 3545–3552.
- (213) Woehrle, G. H.; Brown, L. O.; Hutchison, J. E. Thiol-Functionalized, 1.5 nm Gold Nanoparticles Through Ligand Exchange Reactions: Scope and Mechanism of Ligand Exchange. *J. Am. Chem. Soc.* **2005**, *127*, 2172–2183.
- (214) Schmidbaur, H.; Shiotani, A. Organosilicon Compounds Containing Monovalent Gold. *J. Am. Chem. Soc.* **1970**, *92*, 7003–7004.
- (215) Woehrle, G. H.; Brown, L. O.; Hutchison, J. E. Thiol-Functionalized, 1.5 nm Gold Nanoparticles Through Ligand Exchange Reactions: Scope and Mechanism of Ligand Exchange. *J. Am. Chem. Soc.* **2005**, *127*, 2172–2183.
- (216) Bakshi, M. S. Solubilization of Various Organic Nitrogen Bases in O/W and W/O Microemulsions of Anionic and Cationic Surfactants. *Indian J. Chem., Sect. A: Inorg., Bio-inorg., Phys., Theor. Anal. Chem.* **1995**, *34*, 896–899.
- (217) Zhang, S.; Zhao, Y. Facile Preparation of Organic Nanoparticles by Interfacial Cross-Linking of Reverse Micelles and Template Synthesis of Subnanometer Au-Pt Nanoparticles. *ACS Nano* **2011**, *5*, 2637–2646.
- (218) Fendler, J. H. *Membrane Mimetic Chemistry: Characterizations and Applications of Micelles, Microemulsions, Monolayers, Bilayers, Vesicles, Host-Guest Systems, and Polyions*; Wiley: New York, 1982; pp 24–47.
- (219) Pileni, M. P. Nanosized Particles Made in Colloidal Assemblies. *Langmuir* **1997**, *13*, 3266–3276.
- (220) Pileni, M. P. The Role of Soft Colloidal Templates in Controlling the Size and Shape of Inorganic Nanocrystals. *Nat. Mater.* **2003**, *2*, 145–150.
- (221) Ganguli, A. K.; Ganguly, A.; Vaidya, S. Microemulsion-Based Synthesis of Nanocrystalline Materials. *Chem. Soc. Rev.* **2010**, *39*, 474–485.
- (222) Carroll, N. G.; Pylypenko, S.; Atanassov, P. B.; Petsev, D. N. Microparticles with Bimodal Nanoporosity Derived by Microemulsion Templating. *Langmuir* **2009**, *25*, 13540–13544.
- (223) Lin, J.-C.; Dipre, J. T.; Yates, M. Z. Microemulsion-Directed Synthesis of Molecular Sieve Fibers. *Chem. Mater.* **2003**, *15*, 2764–2773.
- (224) Johnson, C. J.; Li, M.; Mann, S. Seed-Assisted Synthesis of BaCrO₄ Nanoparticles and Nanostructures in Water-in-Oil Microemulsions. *Adv. Funct. Mater.* **2004**, *14*, 1233–1239.
- (225) Eastoe, J.; Hollamby, M. J.; Hudson, L. Recent Advances in Nanoparticle Synthesis with Reversed Micelles. *Adv. Colloid Interface Sci.* **2006**, *128*–130, 5–15.
- (226) Jung, H. M.; Price, K. E.; McQuade, D. T. Synthesis and Characterization of Cross-Linked Reverse Micelles. *J. Am. Chem. Soc.* **2003**, *125*, 5351–5355.
- (227) Price, K. E.; McQuade, D. T. A Cross-Linked Reverse Micelle-Encapsulated Palladium Catalyst. *Chem. Commun.* **2005**, 1714–1716.
- (228) Park, Y. S.; Chae, H. K. Geometric Control and Intense Plasmon Resonances of Colloidal Truncated Triangular Copper Nanoplates in Nonionic Microemulsions Containing Tetrabutylammonium Hydroxide. *Chem. Mater.* **2010**, *22*, 6280–6290.
- (229) Mao, J.; Li, X. L.; Qin, W. J.; Niu, K. Y.; Yang, J.; Ling, T.; Du, X. W. Control of the Morphology and Optical Properties of ZnO Nanostructures Via Hot Mixing of Reverse Micelles. *Langmuir* **2010**, *26*, 13755–13759.
- (230) Pileni, M. P.; Zemb, T.; Petit, C. Solubilization by reverse micelles: solute localization and structure perturbation. *Chem. Phys. Lett.* **1985**, *118*, 414–420.
- (231) Xi, L.; Lam, Y. M.; Xu, Y. P.; Li, L. J. Synthesis and Characterization of One-Dimensional CdSe by a Novel Reverse Micelle Assisted Hydrothermal Method. *J. Colloid Interface Sci.* **2008**, *320*, 491–500.
- (232) Zhang, X. H.; Ho, K. M.; Wu, A. H.; Wong, K. H.; Li, P. Hydrothermal Microemulsion Synthesis of Oxidatively Stable Cobalt Nanocrystals Encapsulated in Surfactant/Polymer Complex Shells. *Langmuir* **2010**, *26*, 6009–6014.
- (233) Lin, X. M.; Sorensen, C. M.; Klabunde, K. J.; Hadjipanayis, G. C. Temperature dependence of morphology and magnetic properties of cobalt nanoparticles prepared by an inverse micelle techniques; the limited influence of inverse micelles. *Langmuir* **1998**, *14*, 7140–7146.
- (234) Lisiecki, I.; Pileni, M. P. Synthesis of well-defined and low size distribution cobalt nanocrystals. *Langmuir* **2003**, *19*, 9486–9489.
- (235) Singh, N. B.; Middendorf, B. Calcium Sulphate Hemihydrate Hydration Leading to Gypsum Crystallization. Progress in Crystal Growth and Characterization. *Prog. Cryst. Growth Charact. Mater.* **2007**, *53*, 57–77.
- (236) Woo, K. M.; Yu, B.; Jung, H. M.; Lee, Y. K. Comparative Evaluation of Different Crystal-Structured Calcium Sulfates as Bone-Filling Materials. *J. Biomed. Mater. Res., Part B* **2009**, *91B*, 545–554.
- (237) Jung, H. M.; Song, G. A.; Lee, Y. K.; Baek, J. H.; Ryoo, H. M.; Kim, G. S.; Choung, P. H.; Woo, K. M. Modulation of the Resorption and Osteoconductivity of α -Calcium Sulfate by Histone Deacetylase Inhibitors. *Biomaterials* **2010**, *31*, 29–37.
- (238) Park, Y.; Dziak, R.; Genco, R.; Swihart, M.; Perinpanayagam, H. Calcium Sulfate Based Nanoparticles. US Patent 7767226B2, 2010.
- (239) Wang, P.; Lee, E.; Park, C.; Yoon, B.; Shin, D.; Kim, H.; et al. Calcium Sulfate Hemihydrate Powders with a Controlled Morphology for Use as Bone Cement. *J. Am. Ceram. Soc.* **2008**, *91*, 2039–2042.
- (240) Kong, B.; Guan, B.; Yates, M. Z.; Wu, Z. Control of α -Calcium Sulfate Hemihydrate Morphology Using Reverse Microemulsions. *Langmuir* **2012**, *28*, 14137–14142.
- (241) Bezou, C.; Nonat, A.; Mutin, J. C.; et al. Investigation of the Crystal Structure of γ -CaSO₄, CaSO₄·0.5H₂O, and CaSO₄·0.6·H₂O by Powder Diffraction Methods. *J. Solid State Chem.* **1995**, *117*, 165–176.
- (242) Ballirano, P.; Maras, A.; Meloni, S.; Caminiti, R. The Monoclinic I2 Structure of Bassanite, Calcium Sulphate Hemihydrate (CaSO₄·0.5H₂O). *Eur. J. Mineral.* **2001**, *13*, 985–993.
- (243) Kim, D. S.; Gösele, U.; Zacharias, M. Surface-Diffusion Induced Growth of ZnO Nanowires. *J. Cryst. Growth* **2009**, *311*, 3216–3219.
- (244) Yu, J.; Xiang, Q.; Ran, J.; Mann, S. One-Step Hydrothermal Fabrication and Photocatalytic Activity of Surface-Fluorinated TiO₂ Hollow Microspheres and Tabular Anatase Single Micro-crystals with High-Energy Facets. *CrystEngComm* **2010**, *12*, 872–879.

- (245) Nagy, J. B. Multinuclear NMR Characterization of Microemulsions: Preparation of Monodisperse Colloidal Metal Boride Particles. *Colloids Surf.* **1989**, *35*, 201–220.
- (246) Takenaka, S.; Hirata, A.; Tanabe, E.; Matsune, H.; Kishida, M. Preparation of supported Pt-Co alloy nanoparticle catalysts for oxygen reduction reaction by coverage with silica. *J. Catal.* **2010**, *274*, 228–238.
- (247) Shimazaki, Y.; Hayasaka, S.; Koyama, T.; Nagao, D.; Kobayashi, Y.; Konno, M. A durable PtRu/C catalyst with a thin protective layer for direct methanol fuel cells. *J. Colloid Interface Sci.* **2010**, *351*, 580–583.
- (248) Shimazaki, Y.; Kobayashi, Y.; Sugimasa, M.; Yamada, S.; Itabashi, T.; Miwa, T.; Konno, M. *J. Colloid Interface Sci.* **2006**, *300*, 253–258.
- (249) Matsumori, H.; Takenaka, S.; Matsune, H.; Kishida, M. Preparation of carbon nanotubes supported by Pt catalysts covered by silica layers; application to cathode catalyst for PEFC. *Appl. Catal., A* **2010**, *373*, 176–185.
- (250) Dahlberg, K. A.; Schwank, J. W. Synthesis of Ni@SiO₂ Nanotube Particles in a Water-in-Oil Microemulsion Template. *Chem. Mater.* **2012**, *24*, 2635–2644.
- (251) Tornblom, M.; Henriksson, U. Effect of Solubilization of Aliphatic Hydrocarbons on Size and Shape of Rodlike C₁₆ TABr Micelles Studied by ²H NMR Relaxation. *J. Phys. Chem. B* **1997**, *101*, 6028–6035.
- (252) Zhang, J.; Ge, Z.; Jiang, X.; Hassan, P. A.; Liu, S. Stopped-flow kinetic studies of sphere-to-rod transitions of sodium alkyl sulfate micelles induced by hydrotropic salt. *J. Colloid Interface Sci.* **2007**, *316*, 796–802.
- (253) Shrestha, L. K.; Shrestha, R. G.; Varade, D.; Aramaki, K. Tunable Parameters for the Structural Control of Reverse Micelles in Glycerol Monoisostearate/Oil Systems: A SAXS Study. *Langmuir* **2009**, *25*, 4435–4442.
- (254) Shrestha, L. K.; Sato, T.; Acharya, D. P.; Iwanaga, T.; Aramaki, K.; Kunieda, H. Phase Behavior of Monoglycerol Fatty Acid Esters in Nonpolar Oils: Reverse Rodlike Micelles at Elevated Temperatures. *J. Phys. Chem. B* **2006**, *110*, 12266–12273.
- (255) Teng, F.; Tian, Z.; Xu, J.; Xiong, G.; Lin, L. Synthesis of the high-surface-area Ce_xBa_{1-x}MnAl₁₁O_y catalyst in reverse microemulsions using inexpensive inorganic salts as precursors. *Stud. Surf. Sci. Catal.* **2004**, *147*, 493–498.
- (256) Zhao, Y.; Frost, R. L.; Yang, J.; Martens, W. N. Size and Morphology Control of Gallium Oxide Hydroxide GaO(OH), Nano- to Micro-Sized Particles by Soft-Chemistry Route Without Surfactant. *J. Phys. Chem. C* **2008**, *112*, 3568–3579.
- (257) Xiang, G.; Zhuang, J.; Wang, X. Morphology-Controlled Synthesis of Inorganic Nanocrystals Via Surface Reconstruction of Nuclei. *Inorg. Chem.* **2009**, *48*, 10222–10230.
- (258) Dong, J. Y.; Hsu, Y. J.; Wong, D. S.-H.; Lu, S. Y. Growth of ZnO Nanostructures With Controllable Morphology Using a Facile Green Antisolvent Method. *J. Phys. Chem. C* **2010**, *114*, 8867–8872.
- (259) Wei, L.; Fan, Y. J.; Tian, N.; Zhou, Z. Y.; Zhao, X. Q.; Mao, B. W.; Sun, S. G. Electrochemically Shape-Controlled Synthesis in Deep Eutectic Solvents: A New Route to Prepare Pt Nanocrystals Enclosed by High-Index Facets With High Catalytic Activity. *J. Phys. Chem. C* **2012**, *116*, 2040–2044.
- (260) Bakshi, M. S. Nanoshape Control Tendency of Phospholipids and Proteins: Protein–Nanoparticle Composites, Seeding, Self-Aggregation, and Their Applications in Bionanotechnology and Nanotoxicology. *J. Phys. Chem. C* **2011**, *115*, 13947–13960.
- (261) Bakshi, M. S.; Jaswal, V. S.; Kaur, G.; Simpson, T. W.; Banipal, P. K.; Banipal, T. S.; Possmayer, F.; Petersen, N. O. Biominerization of BSA-Chalcogenide Bioconjugate Nano- and Microcrystals. *J. Phys. Chem. C* **2009**, *113*, 9121–9127.
- (262) Singh, V.; Khullar, P.; Dave, P. N.; Kaur, G.; Bakshi, M. S. Ecofriendly Route To Synthesize Nanomaterials for Biomedical Applications: Bioactive Polymers on Shape-Controlled Effects of Nanomaterials Under Different Reaction Conditions. *ACS Sustainable Chem. Eng.* **2013**, *1*, 1417–1431.
- (263) Mahal, A.; Khullar, P.; Kumar, H.; Kaur, G.; Singh, N.; Jelokhani-Niaraki, M.; Bakshi, M. S. Green Chemistry of Zein Protein Toward the Synthesis of Bioconjugated Nanoparticles: Understanding Unfolding, Fusogenic Behavior, and Hemolysis. *ACS Sustainable Chem. Eng.* **2013**, *1*, 627–639.